FLOW OF R-12 THROUGH CAPILLARY TUBES OF VARIOUS CONFIGURATIONS

by

NITAI KRUSHNA GIRI

DEPARTMENT OF MECHANICAL ENGINEERING

INDIAN INSTITUTE OF TECHNOLOGY KANPUR

JUNE, 1976

FLOW OF R-12 THROUGH CAPILLARY TUBES OF VARIOUS CONFIGURATIONS

A Thesis Submitted
in partial Fulfilment of the Requirements
for the Degree of
DOCTOR OF PHILOSOPHY

by

NITAI KRUSHNA GIRI

to the

DEPARTMENT OF MECHANICAL ENGINEERING

INDIAN INSTITUTE OF TECHNOLOGY KANPUR

JUNE, 1976

To

my beloved

FATHER

who is no more

ME-1976-D-GIR-FLO

CERTIFICATE

This is to certify that this doctoral work on FLOW OF R-12 THROUGH CAPILLARY TUBES OF VARIOUS CONFIGURATIONS has been carried out under our supervision and it has not been submitted elsewhere for a degree.

P.N. Kaul
Assistant Professor
Dept. of Mech. Engineering
I.I.T. Kanpur

H.C. Agrawal
Professor
Dept. of Mech. Engineering
I.I.T. Kanpur

ACKNOWLEDGEMENTS

The author wishes to place on record, with a deep sense of gratitude, his sincere thanks to:

His thesis supervisors - Dr. H.C. Agarwal and Dr. P.N. Paul for their able guidance, keen interest, constant help and encouragement throughout the course of this work.

Dr. V. Kadambi, whom the author has been associated with in the initial stages of his graduate program.

Dr. V.K. Stokes for making available the necessary funds and laboratory facilities so essential for the successful execution of the present work.

Mr. Manohar Prasad for his enormous help in every possible manner during all the phases of this work, but for which this work would have remained incomplete.

Mr. P.N. Misra for his immense technical help not only with the setting up of the experimental rig, but also with the running of the tests.

His friends Messrs Keshav Kant, N. Ravichandran, M. Prasad, K.A. Narayan, R.K. Shah, K. Prasad, R.K. Sehgal, S.C. Patra, N.K. Banthiya and Anil Nigam for their direct and indirect help towards the completion of this thesis.

Members of the technical staff particularly Messrs Bakshish Singh, Nihal Singh, Mushtaq Ali, A.S. Parihar, B.L. Sharma, I. Samson, R.A. Sharma, Shambhu Sharma, S.L. Yadav and others for their timely help whenever needed.

Mr. J.D. Varma for his excellent typing, Mr. R.N. Bajpai for the beautiful tracings and Mr. D.P. Sarkar for the nice photographs.

Last but not the least to his wife Indu who stoically and steadfastly shared his joys and sorrows and to his daughter Luna for her neglected years.

TABLE OF CONTENTS

LIST OF FIGURES

NOMENCLATURE

A	Area of cross section of the tube, m^2
c	Velocity of sound, m/s
C	Term related to quality of refrigerant
d	Internal diameter of capillary tube, m
D	Diameter of curvature of helical section, m
f	Friction factor
f_g	Gas phase friction factor
f_l	Liquid phase friction factor
f_{TP}	Two-phase friction factor
g	Acceleration due to gravity, m/s^2
g_c	Conversion factor, kg-m / kgf-s^2
G	Mass velocity, kg/hr-m^2
h_l	Enthalpy of liquid refrigerant, kcal/kg
h_g	Enthalpy of refrigerant vapour, kcal/kg
l	Length of capillary tube, m
$\dot{m}$	Mass flow rate of refrigerant, kg/hr
p	Pressure of refrigerant, kgf/cm^2 (ata)
p_i	Pressure of refrigerant at the inlet to test section, kgf/cm^2
P	Pitch of the Archimedian spiral section, m
q	Heat transfer, kcal/kg
Q	Heat equivalent of electric energy input, kcal/min-^oC
R_i	Minimum radius of Archimedian spiral, m
R_o	Maximum radius of Archimedian spiral, m

x	Quality
Re_{TP}	Two-phase Reynolds number
s	Entropy of refrigerant, kcal/kg-^{o}K
t_a	Ambient temperature, ^{o}C
t_l	Liquid refrigerant temperature ^{o}C
t_s	Saturated temperature of refrigerant, ^{o}C
T	Temperature ^{o}K
v	Specific volume of refrigerant, m^3/kg
v_g	Specific volume of refrigerant vapour, m^3/kg
v_l	Specific volume of refrigerant liquid, m^3/kg
V	Velocity of refrigerant, m/s
w	Weight, kg
ρ	Density, kg/m^3
θ	Helix angle, degree
ϕ	Diameter of tube, m
μ	Viscosity of refrigerant, kg/m-hr
μ_g	Viscosity of refrigerant vapour, kg/m-h
μ_l	Viscosity of refrigerant liquid, kg/m-hr
μ_{TP}	Two-phase viscosity of refrigerant, kg/m-hr

Subscripts:

i	Inlet condition
o	Outlet condition
fr	Due to friction
ac	Due to acceleration
gr	Due to gravitation
TP	Two-phase flow
l	Liquid phase
g	Gas phase

SYNOPSIS

An experimental and theoretical investigation has been made for the flow of Refrigerant-12 through capillary tubes of straight, helical and Archimedian - spiral configurations. Test specimens of different sizes have been studied under saturated and subcooled refrigerant inlet conditions. The experimental data are presented in the form of graphs and charts which can be used for the design of expansion devices for various applications within the limits of the present investigation.

Comparison of the performance of the different capillary configurations in a system establishes the superiority of the spiral shape over the helical and the straight, not only from the operational view point, but from the economic view point too.

A theoretical expression has been developed for each configuration for the two-phase flow of R-12 within the temperature range -35 °C to 50 °C, to determine the capillary length for a given pressure drop. Two-phase flow friction factor correlation has also been derived for each capillary configuration using the present experimental data. The theoretical and experimental results are compared and the agreement is found satisfactory. The proposed theoretical expression is, therefore, considered

CHAPTER I

INTRODUCTION

1.1 Capillary Tube as a Flow Control Device

Control of refrigerant flow is an essential feature of all refrigeration systems. All the mechanical refrigerating units have a pressure reducing arrangement or a throttling device which meters the flow of refrigerant to the low pressure side in accordance with the demands placed on the system. This constitutes one of the four basic components of a refrigeration system, viz. the compressor, the condenser, the expansion valve or the throttling device and the evaporator. The thermostatic expansion valve has proved to be a successful throttling device (excluding the case of flooded evaporators), but it is quite costly and complicated. However, with the advent of hermetic-type compressor and the halocarbon refrigerants, the capillary tube flow control became practicable and popular. This has been used commonly with small units like house hold refrigerators, food freezers, water coolers, dehumidifiers and room air conditioners. More recently, it has also been used with large units, upto 10 tons capacity (17).

The capillary tube is placed between the condenser and the evaporator. The restriction through this tube is sufficient to hold back high pressure in the condenser and, at the same time, it allows liquid to bleed through to the evaporator. The passage of liquid refrigerant through the capillary tube is much more easy, than the refrigerant vapour, due to its higher density. In fact, a cubi centimeter of liquid refrigerant weighs 20 to 40 times as compared to that of a cubic centimeter of its vapour depending upon the pressure (21).

The most efficient operation of the capillary tube occurs only at one particular combination of condenser and evaporator pressures. In a properly sized capillary tube, subcooled liquid enters the tube giving a liquid seal at the entrance. This liquid is forced through the tube due to condenser pressure. There is a pressure drop along the length of the tube. When the pressure drops to a point where the refrigerant becomes saturated, flash gas forms. The formation of flash gas increases as the liquid moves further. This mixture of refrigerant liquid and vapour is delivered to the evaporator at a pressure slightly above that of the evaporator (6). The part of the capillary tube containing only the liquid refrigerant is called the liquid length. The point at which the first bubble of flash gas forms is called the bubble point. The remaining

part of the tube which contains both liquid and vapour is called the two-phase length. All the two-phase flow patterns occur in this portion of the capillary tube (15).

If the condenser pressure increases, or the evaporator pressure decreases, the flow in the capillary is increased and there occurs a little or no subcooling at all. As a result, the bubble point moves closer to the entrance of the tube, which increases the overall restriction and decreases the flow. Such self-regulating characteristics enable the capillary tube to work so well under a variety of operating conditions.

The most outstanding advantages of a capillary tube are the following (3):

(i) it is inexpensive and simple in construction,

(ii) it has no moving parts, and

(iii) it allows the high side pressure to unload or balance out the low side pressure during the off-cycle, when used in a system having a hermetically sealed compressor. This permits the compressor to start in an unloaded condition, allowing the use of a low starting torque motor. The need for a separate unloading device on the compressor which is complicated, costly, and troublesome is, thus, eliminated. It is evident, therefore, that the use of a capillary tube

results in a considerable saving in the manufacturing cost of a refrigerating system.

The successful operation of a well-designed capillary system is dependent upon:

(i) keeping the system fully charged with refrigerant over its working life,

(ii) maintenance of high standards of internal cleanliness and dehydration,

(iii) the efficacy of the compressor to mix the oil at a uniform rate with the refrigerant.

In a hermetically sealed compressor with a capillary tube, all the above conditions are fulfilled. The same, however, is not true with an open-type compressor, which may lose sufficient refrigerant by leakage past the shaft seals, thereby, requiring occasional field servicing.

The following factors influence the flow of refrigerant through a capillary tube:

1. Capillary factors:

(i) diameter

(ii) length

(iii) entrance restrictions

(iv) internal finish, roughness etc.

2. System Factors:

(i) velocity at the capillary entrance

(ii) pressure difference across the capillary

(iii) condition of refrigerant entering the capillary (subcooled or saturated)

(iv) heat flow along the capillary (from outside or from heat exchanger)

(v) refrigerant properties (density and viscosity)

(vi) lubricant properties (oil circulation rate, oil viscosity, and miscibility of oil with refrigerant).

It is, thus, obvious that despite the capillary tube's physical simplicity, it is essential that a refrigerating system employing a capillary tube be carefully designed to obtain satisfactory operation. Not only should the capillary and the heat exchanger assembly be properly matched for capacity balance, but both the high and low pressure sides should also be properly designed for optimal performance.

1.2 Review of the Previous Work

The first noticeable work available in literature in connection with capillary tubes is due to Staebler (4). Based on his experimental results he has provided few charts and tables to help selection of a capillary tube for use with R-12 and R-22. Use of this information reduced the preliminary testing work thereto necessary in the proper design of a capillary tube for a refrigerating system.

The work due to Lathrop (5) is based on the compilation of the experimental results on refrigerating equipment at Philo Corporation. The paper deals with a straight forward approach to capillary tube design and provides information for a more accurate solution of problems pertaining to capillary restrictor tubes. The data are presented in a graphical form to depict relations between different parameters like, flow rates and degrees of subcooling of refrigerants, diameter and length of capillary tubes, and pressure differences at inlet and outlet of capillary tubes. The author has also attempted the problem of matching the tube characteristics with the compressor characteristics.

Bolstad and Jordon (6) studied the case of an adiabatic flow in a capillary tube theoretically and experimentally. Capillary tubes of diameters ranging

from 0.026 to 0.055" (five nos.), and lengths 6, 12 and 18 ft using R-12, at inlet pressures of 120, 140 and 160 psia, were tested. It was found that, for adiabatic flow through a given tube with a given inlet pressure and temperature, there exists a critical pressure just before the tube outlet below which the pressure can not fall. Any pressure in the evaporator below this critical pressure can not affect the flow rate through the tube. The flow rate is dependent upon inlet pressure, temperature and the oil content of the refrigerant. The presence of oil in the liquid refrigerant increases the flow rate.

A theoretical analysis has also been made by the authors for the first time as an attempt to have a better understanding of the problem. One dimensional flow in a horizontal tube of circular cross section was assumed and the following equation was derived to estimate the capillary length

$$dl = (Tds - dq)J / \left((fv^2 / 2gd) \left(\dot{m} / A \right)^2 \right).$$

While direct integration of the above equation was not possible, a graphical method was presented whereby the factor $(2gd/f)\ (A / \dot{m})^2\ (T / v^2)$ was plotted against entropy. The area under the curve plotted as above, is equal to the accumulated tube length for a given flow rate and set of inlet conditions.

Marcy (7) developed an ingenious method of computing the length of a capillary tube for the adiabatic expansion of a refrigerant. The method also enables one to determine the flow rate of refrigerant through a given tube. The author's analysis involves graphical integration of the Fanning equation and the solution, therefore, does not depend upon empirical factors. Within the limited range of conditions of the investigation a good agreement with the test data is obtained. The paper is a useful addition to the literature on capillary tubes as it constitutes a successful venture by the author of attackings the problem by other than the experimental method. However, the work does not take care of capacity balance, roughness of capillary tube and effects of oil entrainment on the rate of flow through the capillary. Further, the method can only be applied to adiabatic flow conditions.

The second paper by Bolstad and Jordon (8) presents test data on capillary tube expansion devices using heat exchangers. The authors carried out test runs on 15 different diameter-length combinations of capillary tubes with diameters ranging from 0.026 to 0.055" and lengths from 6 to 18 ft at different inlet pressures, varying from 120 to 160 psia. They presented their results as plots between various parameters, employing the bubble point temperature concept. All through their tests, they

maintained the evaporator pressure constant at approximately 15 psia. They have also presented a correlation between friction factor and Reynolds number based on their experimental data on two diameters, 0.031 and 0.055" using water as the test fluid. Although, the authors carried out a large number of tests but, their correlated friction factor values were based upon the data yielded by one such test only. The value of f varies from 0.0242, for the liquid portion of the flow where Re = 23,470, to an average value of about 0.039 for the two-phase portion of the flow.

Hopkins (9) studied in detail the flow ratings of the capillary tubes using R-12 and R-22 as the working fluids. The ratings provided therein are the results of a study based upon an analysis using the basic fluid flow data in a manner similar in many respects to that of Bolstad and Marcy for refrigerants and Benjamin (2) for steam. These ratings enable one to determine the diameter and approximate length of the capillary before any tests are carried out.

Whitesel (10) studied simultaneous flow of gas and liquid through capillaries and developed two general formulae analytically for slug flow conditions. The first formula was derived for flow of a non-condensable gas and a non-volatile liquid while the second one was developed on the same lines for R-12. The author carried

out an experimental investigation using air and water for the first formula and R-12 for the second. The R-12 formula according to the author is applicable at all inlet qualities, all inlet and outlet pressures, all capillary dimensions and in the temperature range - 40 °F to 140 °F. The author also obtained a secondary empirical formula for computing the two-phase flow friction factors for R-12. The formula is as given below:

$$f_{TP} = 1.5 \left(f_l (1 - x) + f_g x \right)$$

where, f_l and f_g are the values of Fanning friction factors for liquid and gas respectively, evaluated at the average velocity of mixture at the capillary entrance with the assumption of unit slip ratio. The 1.5 multiplier gives the increase in the friction factor due to two-phase flow over single phase value.

Cooper et al (11) made a comprehensive study of capillary tube performance using mathematical technique. They have also presented an experimental correlation for their data yielding a simple and useful means for capillary tube selection. With the help of charts and equations presented, a complete performance of a vast number of tube lengths and diameters can be determined over wide operating ranges. In their experiments, they studied capillaries of lengths, 12, 18, 24, 30 and 36" and I.D., 0.1 and 0.036"

making four samples of each size. Inlet pressures used, were 151, 196, 240 and 285 psia corresponding to 76, 94, 109 and 122 ^{o}F inlet temperatures, respectively. Four flow visualisation tests were also performed using a glass tube capillary. As seen by the naked eye, the mixture could best be described as 'fog flow'. No 'slug' or 'bubble flow' was observed.

Whitesel (12) in another paper developed a two-phase flow formula for R-22 in a manner similar to that for R-12 vide his first paper (10). He also modified his earlier two-phase flow friction factor formula in the light of the additional tests conducted by him covering a wider range of capillary tube parameters. His modified formula can be applied with ease to both R-12 and R-22. He has also presented a relation for computing critical discharge pressure for maximum flow through the capillary tube. To facilitate calculations, tables and charts have been provided. Unlike previous workers, the work of Whitesel is unique in the sense that his theoretical prediction does not require step-wise integration.

Mikol (15) studied adiabatic, single and two-phase flow of R-12 and R-22 in capillary tubes both theoretically and experimentally. He conducted experiments on 0.055509" I.D. drawn copper tube of 6 ft length.

Visual and photographic studies of two-phase flow phenomenae of R-12 were also conducted in a glass tube of 0.049" I.D. and 6 ft length. The results led to the following conclusions:

(1) Drawn copper tubings of small diameters, in general, can not be considered smooth for purposes of friction factor estimation.

(2) Fluid flow through small diameter tubes conforms to continuum flow condition as established for large diameter tubes and pipes.

(3) The author maintains that friction factor correlation of Moody and of others consistent with Moody's correlation, is applicable to single-phase flow in small diameter tubes.

(4) The phenomenon of metastability, which can be described as the persistence of the liquid state to pressures less than the saturation pressures corresponding to their temperatures, was observed in all test runs and during all visual flow observations. This means that it is a phenomenon which must be considered in refrigerant capillary design.

Mikol observed two distinct modes of flow in the capillary. The first one was a sharply pulsating mode comprising large bubbles separated by slugs of

liquid. In each case, liquid surrounded the bubble and was in contact with the capillary wall all-around. The second mode was a stable mode and consisted sequentially, of subcooled liquid flow, metastable liquid flow, a 'flash point', a sinuous thread of vapour flowing as a central core surrounded by liquid and a fog or spray flow close to the end of the tube. The author recommends that the refrigerant capillary should be designed according to the stable mode.

For the two-phase portion of the flow, a tentative correlation as suggested by the author for the apparent friction factor is as follows:

$$f_{TP_{(apparent)}} / f_l \simeq 0.95.$$

This value agrees within $\pm$ 10% with integrated average two-phase friction factor value computed from his test data.

The author has also discussed the phenomenon of choking flow in two-phase flow. He holds that choking in two-phase flow occurs in the same way and for the same reasons as in the case of gaseous flow. Sonic velocity occurs at the tube exit with expansion to higher velocities occurring beyond the tube exit. The paper also includes curves for getting the speed of sound in homogeneous two-phase mixtures of R-12 based on the following formula:

$$c = \left(g_c \left(dp / d\rho \right)_{s=const.} \right)^{0.5}.$$

Niaz and Davis (18) conducted experiments with drawn copper tubes, 0.03, 0.05 and 0.068" I.D. and 7 ft long, using R-12. They developed an equation for two-phase pressure drop, using a single phase friction factor relation obtained on the basis of their experimental results. It has been found that the capillary lengths yielded by their equation for a given pressure drop, are 10% greater than those obtained experimentally. The authors have, therefore, suggested further work for a better correlation of the two-phase flow friction factor.

1.3 Motivation and Scope of the Present Work

Reviewing the contributions made by the previous workers, so far, it seems that a significant amount of experimental work, on capillary tube refrigerant flows, was carried out during the period 1948 to 1966. A considerable amount of data have since been published in the form of curves and tables to assist in determining the overall performance of capillary expansion tubes. However, none of these data cover all the possible conditions of capillary tube applications. On the other hand, rigorous mathematical analysis of two-phase flow of refrigerant in capillary tubes presents difficulties, which, if not impossible, are rather hard to surmount. The few attempts that have been made in the past in obtaining an analytical formulation of the phenomenon are by no means complete. These formulations have yet to take into consideration the following factors:

(i) correct determination of two-phase flow friction factor and

(ii) development of a suitable theoretical expression pertaining to the actual flow situation in the capillary tube restrictor.

It is to be further noted that all the previous data on capillary tubes pertain to straight tube configuration only. Configurations other than straight (viz.

helical, spiral etc.) which, undoubtedly, are economical and compact have not yet been analysed. In some applications, particularly, domestic refrigerators, capillary tubes are generally used in helical forms, as a matter of convenience, to accommodate long lengths and not as a factor of design. However, due consideration should be given to their design aspect also. This is because of the fact that due to secondary flows in curved sections, the pressure drops will be higher than those in the straight sections, resulting, thereby, in a considerable saving of length of capillary tube in the design of a refrigeration system. This important aspect of capillary tube design has been overlooked so far and needs investigation.

The present work has been undertaken with a view to overcome the above shortcomings related to refrigerant flow through capillary tubes. The work comprises both experimental and theoretical study of adiabatic, two-phase flow in capillary tubes of three configurations - straight, helical and Archimedian spiral - using R-12*. Archimedian spiral is chosen because it is easier to fabricate.

Table 1.1, given below, presents all the relevant information regarding the size and nature of various specimens tested under this study alongwith the thermodynamic conditions of the refrigerant used.

---

*Mafron-12 is the trade name given to R-12 by the Indian manufacturers.

TABLE - 1.1

(a) Condition of refrigerant at the inlet of each test section:

Pressure, p (kgf/cm^2 abs.)	Saturated/Subcooled (^oC)
8	Saturated, 5 subcooling
	10 subcooling
10	Saturated, 5 subcooling
	10 subcooling
	15 subcooling
12	Saturated, 5 subcooling
	10 subcooling
	15 subcooling

(b) Geometry* of the test sections under study:

(i) Straight:

No. of test sections.	Diameter of tube, d (m)	Length of tube, l (m)
3	0.00106408	2.4, 1.8 & 1.2
5	0.0017657	3.6, 3.0, 2.4 1.8, & 1.2

* The basis of selection of the dimensions of the capillary specimens has been explained in Chapter II.

(ii) Helical :

No. of test sections	Diameter of tube, d (m)	Diameter of curvature, D (m)	D/d ratio	Helix angle, θ (degree)	Pitch P (m)	Length of tube, l (m)
2	0.00106408	0.0106408	10	6.8233	0.004	1.8, & 1.2
3	0.00106408	0.0159612	15	5.6943	0.005	2.4, 1.8 & 1.2
5	0.0017657	0.0264855	15	4.1244	0.006	3.6, 3.0, 2.4, 1.8 & 1.2
5	0.0017657	0.035314	20	3.6103	0.007	3.6, 3.0, 2.4, 1.8 & 1.2

(iii) Spiral :

No. of test sections	Diameter, d (m)	Pitch, p (m)	R_i, (m)	R_o, (m)	Length, l (m)
3	0.00106408	0.005	0.005	0.0625	2.4
				0.0535	1.8
				0.0435	1.2
5	0.0017657	0.005	0.005	0.0775	3.6
				0.069	3.0
				0.0625	2.4
				0.0535	1.8
				0.0435	1.2

A theoretical expression for two-phase flow pressure drop for the flow of R-12 in a capillary tube has been developed for all the configurations studied. Curve-fit expressions for two-phase flow friction factors required in these formulations are obtained from the experimental data for each configuration, separately. These friction factor expressions also take care of the geometry of the test specimens. The theoretical predictions compare well with the experimental observations. The results of the present theoretical model are found to be in good agreement with the experimental work of Niaz and Davis (18).

Experimental data have been presented in the form of charts to facilitate selection of suitable capillary sizes and configurations for various applications. Method of using these charts is also discussed.

CHAPTER II

EXPERIMENTAL SET-UP AND TEST PROCEDURE

1.1 Experimental Set-up

The experimental set-up comprises, basically, a 2-ton capacity vapour-compression refrigeration system, designed and fabricated as per I.S.I. (20) specifications for the testing of compressors (24). Added on to this basic structure, are the various instruments designed to make measurements on capillary tubes. The set-up is flexible enough to enable the testing of different types and sizes of test specimens.

A schematic diagram of the set-up is shown in Fig. 2.1. Photographic view of the experimental set-up is presented in Figs. 2.2 (a) through 2.2 (d). Mixture of oil and R-12 vapour, delivered from an open type compressor, is passed through an oil separator. The R-12 vapour from the oil separator is passed through a water cooled condenser. The liquid refrigerant from the condenser passes into one of the flowmeter tubes, connected in parallel, after which it goes to a drier. From the drier, the refrigerant flows to the calorimeter through either of the two different routes — one containing the valve DV_4 and a thermostatically controlled expansion

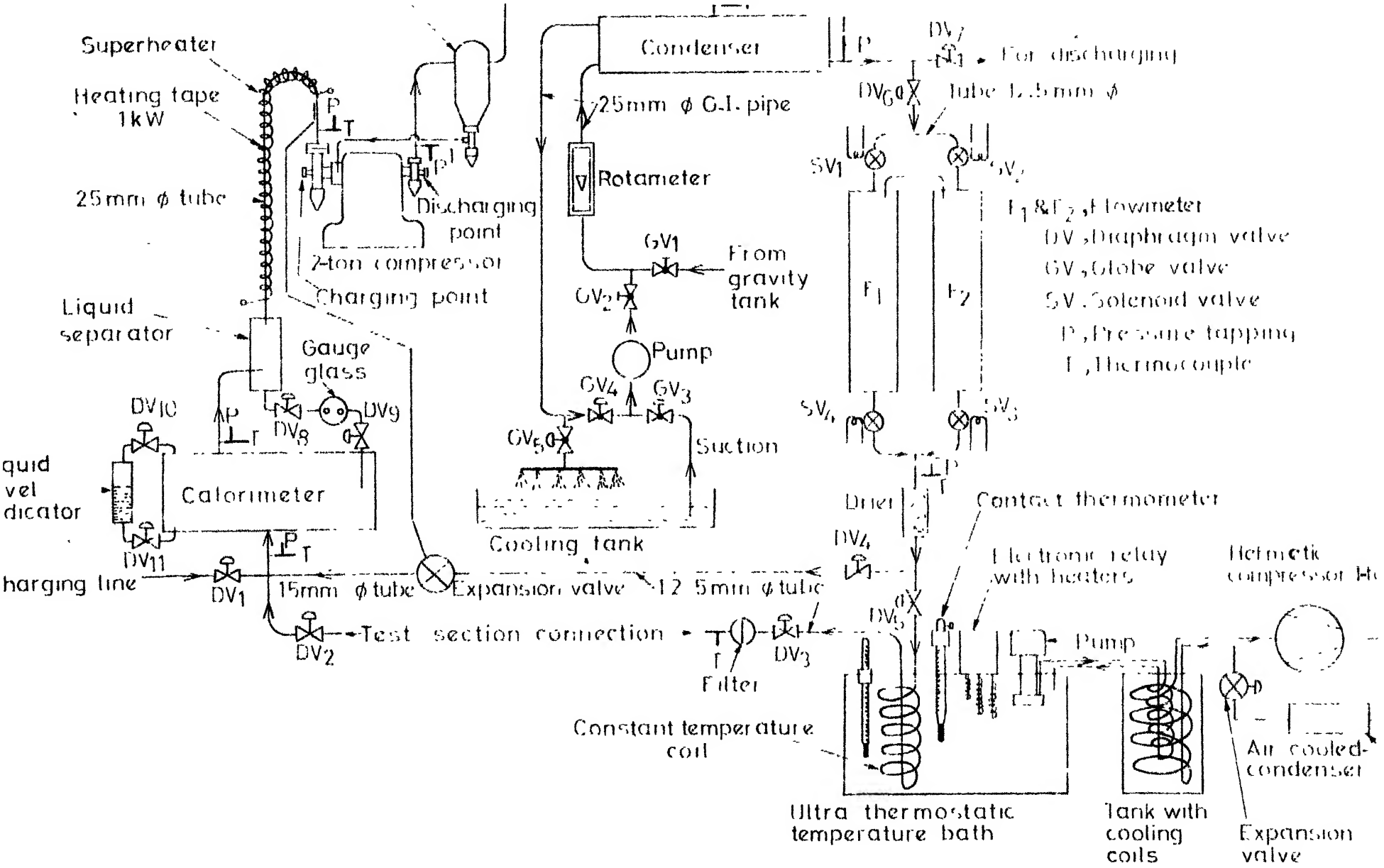

Fig. 2.1 Schematic diagram of the set-up

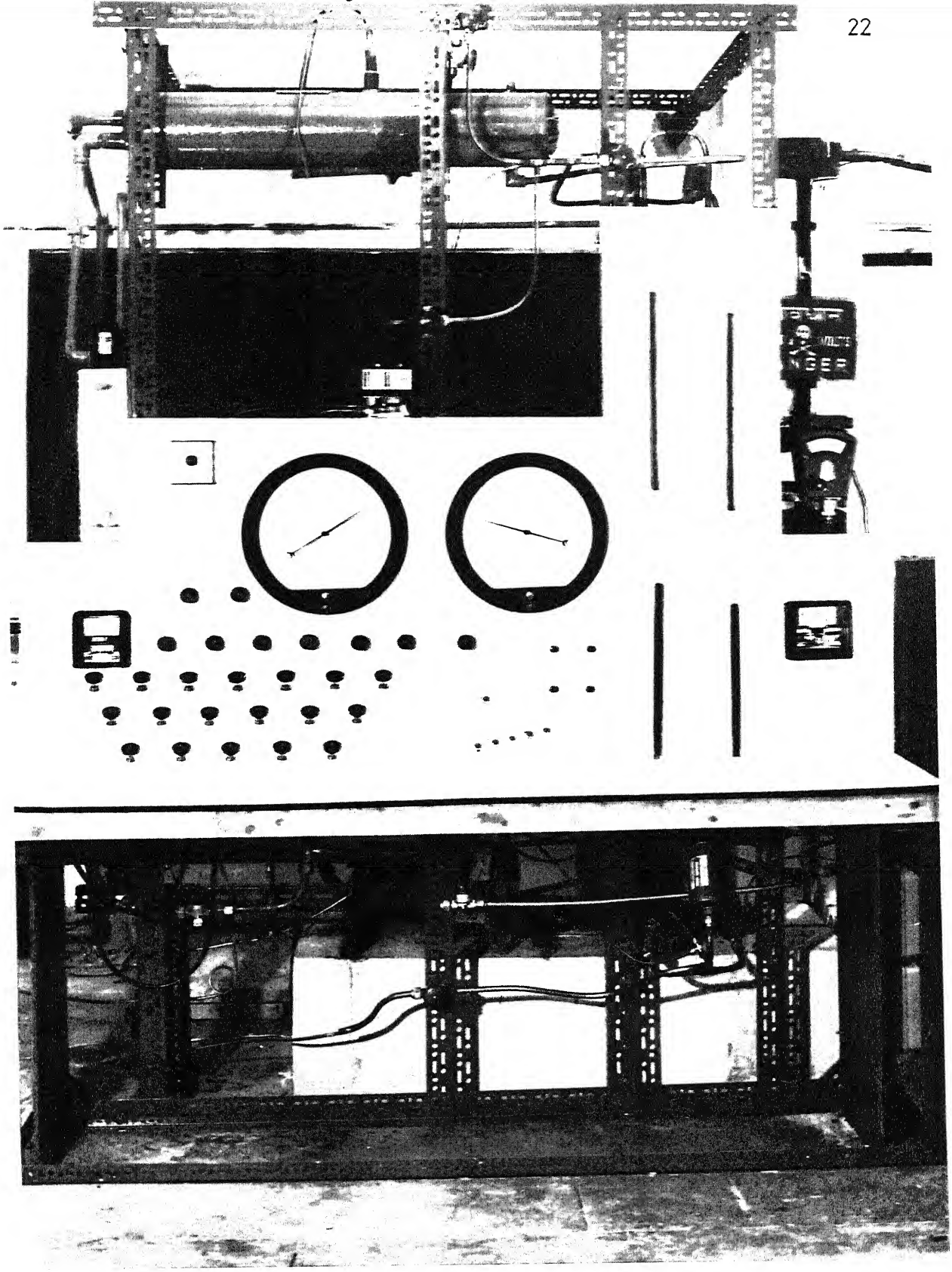

Fig. 2.2(a) Front view of the rig without insulation

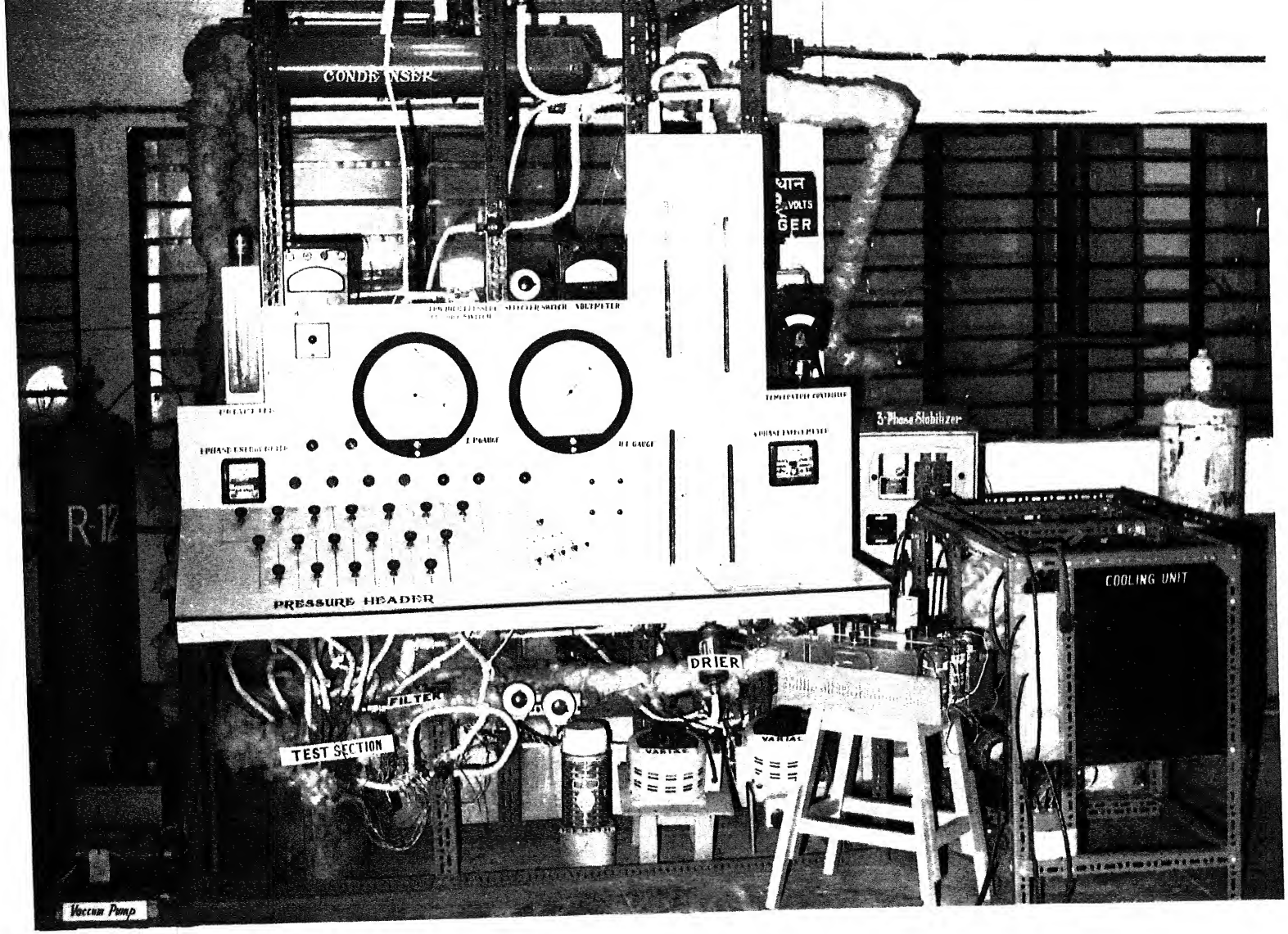

Fig. 2.2(b) Front view of the rig with insulation

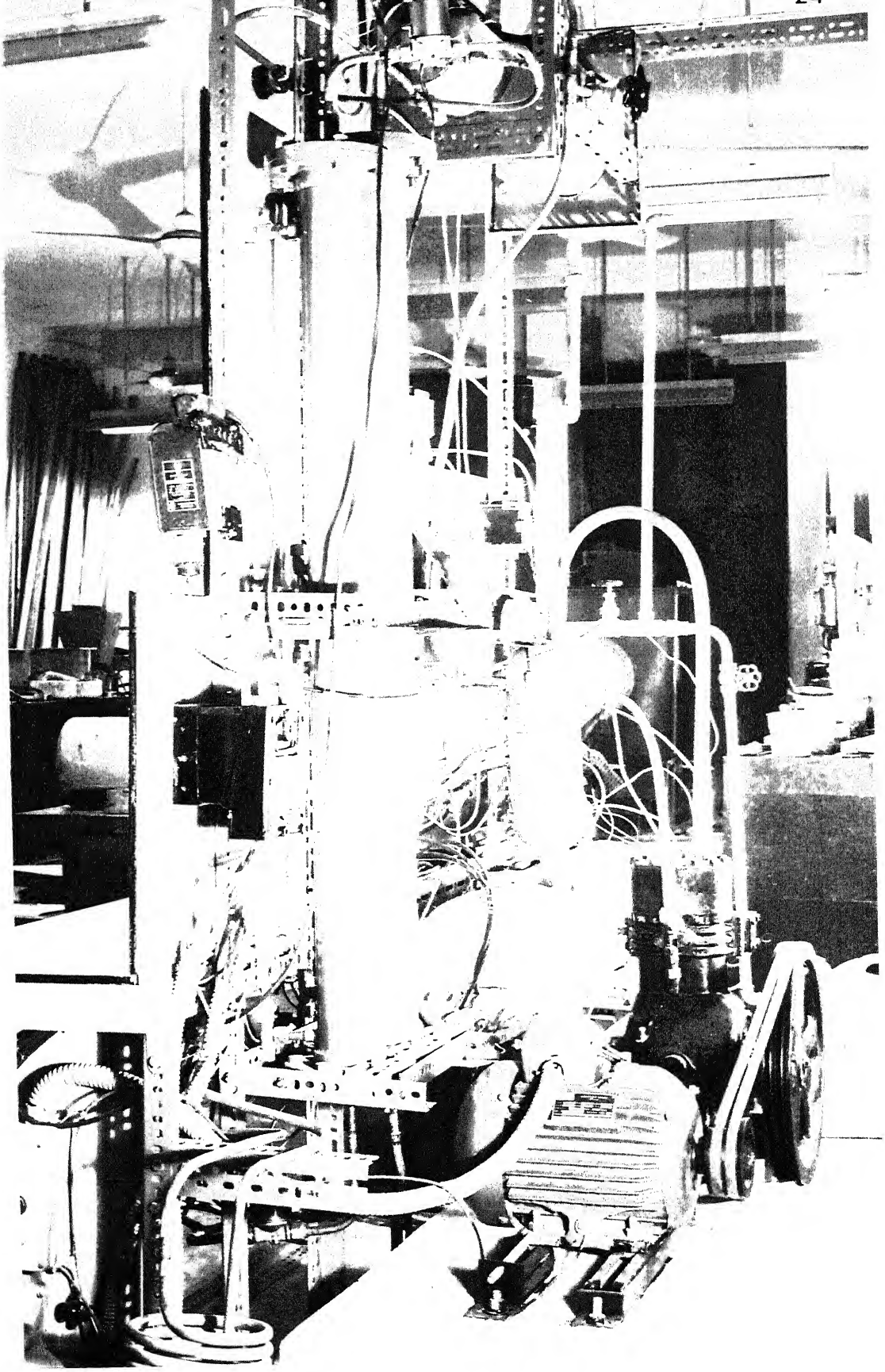

Fig. 2.2(c) Back view of the rig without insulation

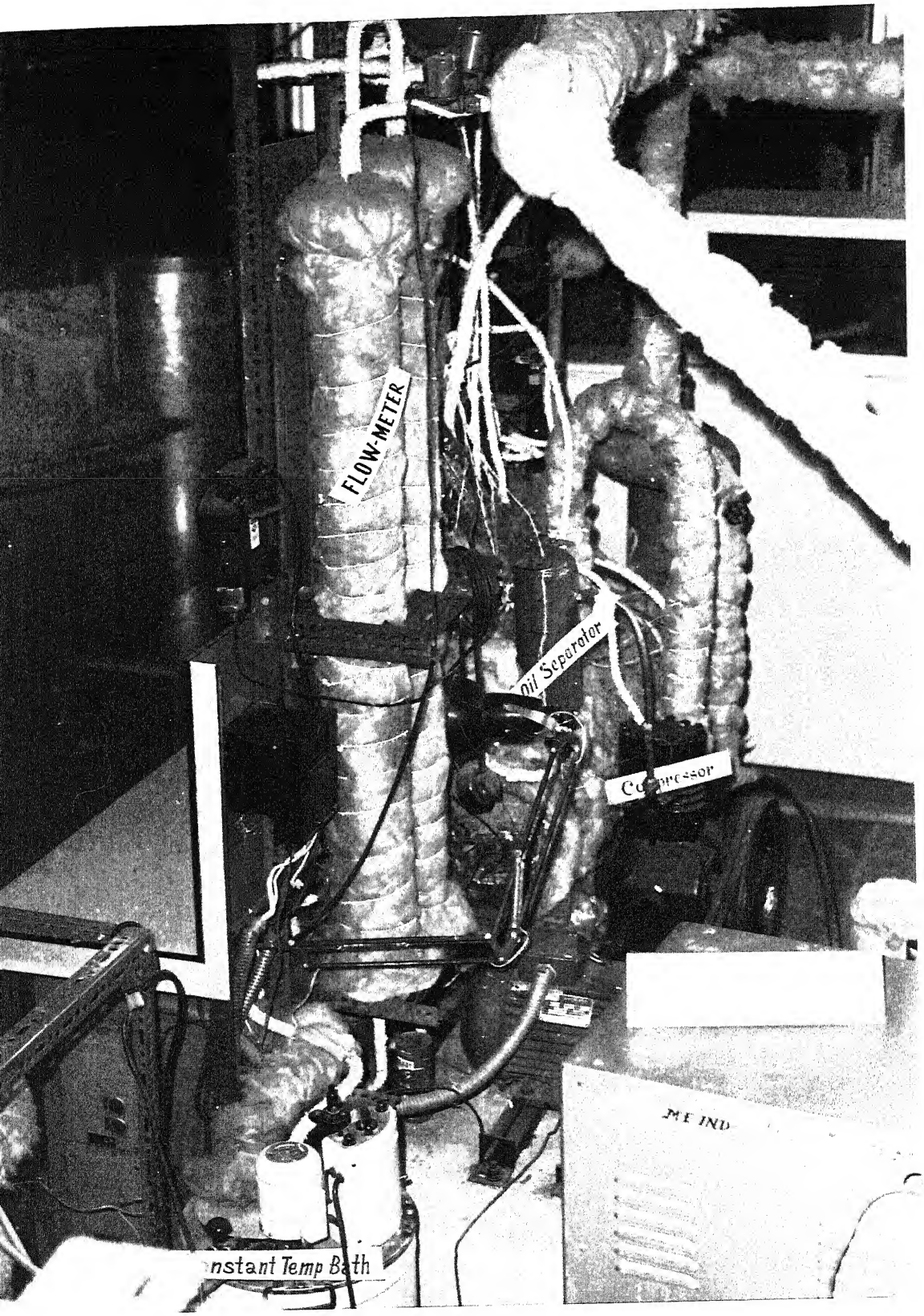

Fig. 2.2(d) Back view of the rig with insulation

valve and the other via the valve DV_5, constant temperature coil (placed inside a constant temperature bath), valve DV_3, filter, test section and the valve DV_2, as shown in Fig. 2.1. The saturated vapour of R-12, from the calorimeter, is further made to pass through a liquid separator and a superheater before being delivered to the compressor.

A detailed description of the various components of the experimental set-up is as follows:

(i) Compressor: An open type, positive displacement compressor of 2-ton capacity for R-12, manufactured by Freez King India Ltd., has been used in the set-up. Both the inlet and outlet valves of the compressor have got provision for an additional opening. These additional openings at the inlet and the outlet are used for charging and discharging the system, respectively. The open type compressor has been used because no sealed unit of this capacity is available in India.

(ii) Oil Separator: Since R-12 is completely miscible with oil, an oil separator has been incorporated into the system to separate the oil from the refrigerant vapour.

(iii) Condenser: A two-pass water cooled condenser of approximately 3-ton capacity, manufactured by the

American Refrigeration Company, India, has been used to condense the refrigerant vapour coming from the oil separator. The capacity of the condenser is such that it can deliver subcooled liquid refrigerant at various operating conditions of the plant. Ordinary tap water is used for the condenser cooling.

(iv) Drier: A silica-gel drier, of Danfoss make, is fitted in the system to absorb moisture, if any, mixed with the refrigerant. The moisture, if not removed, can choke the capillary tube partially or completely.

(v) Thermostatic Expansion Valve: A 2-ton capacity thermostatic expansion valve made by FLICA, Germany, has been used for throttling the refrigerant as shown in Fig. 2.1. The sensing bulb of the expansion valve is attached to the wall of the suction pipe at the compressor inlet.

(vi) Filter: A micro-filter, made by Hokes, U.S.A., is also included in the system to arrest any suspended impurities which may block the capillary passage. The filter capable of separating very tiny particles is located upstream of the test section.

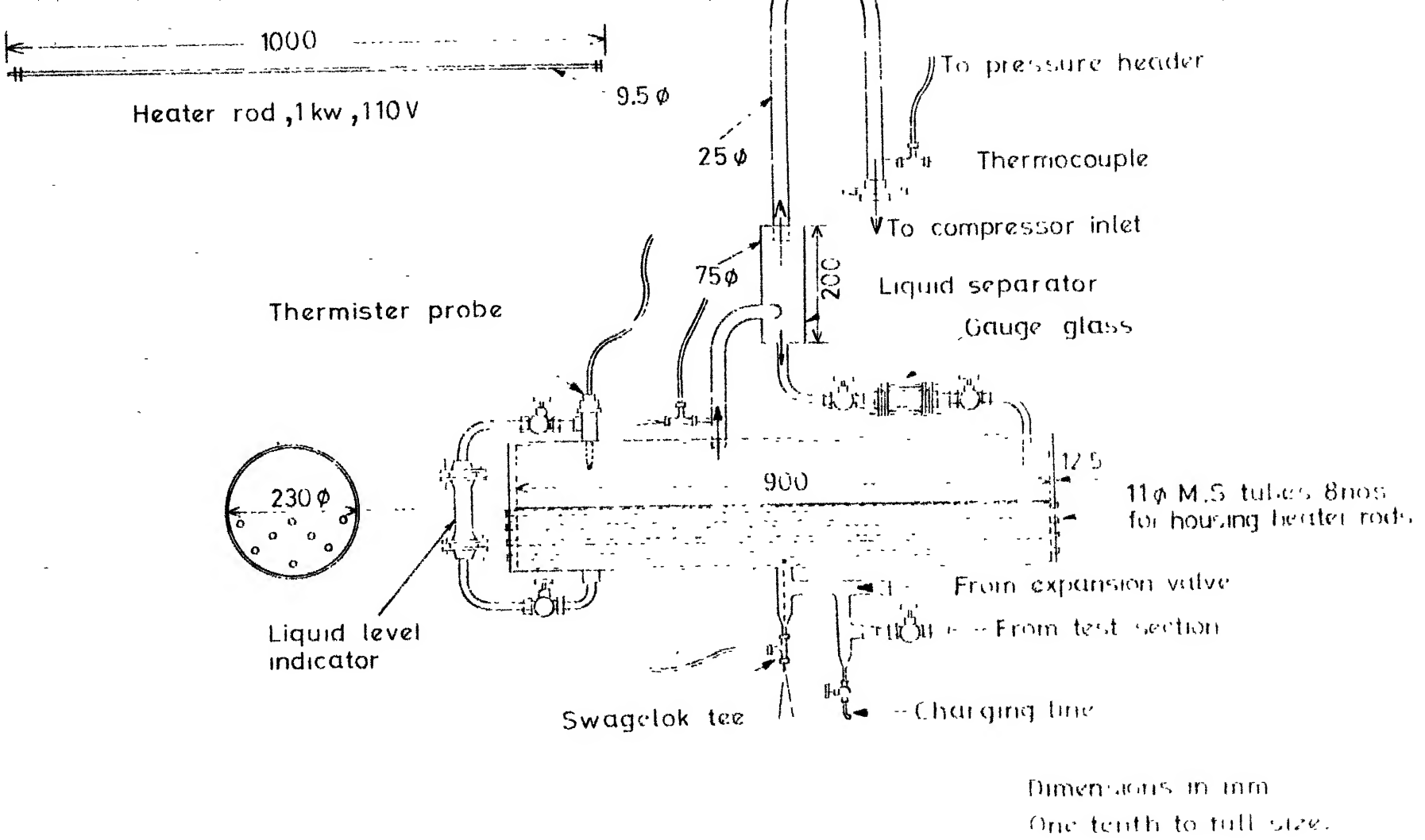

Fig. 2.3 Calorimeter assembly

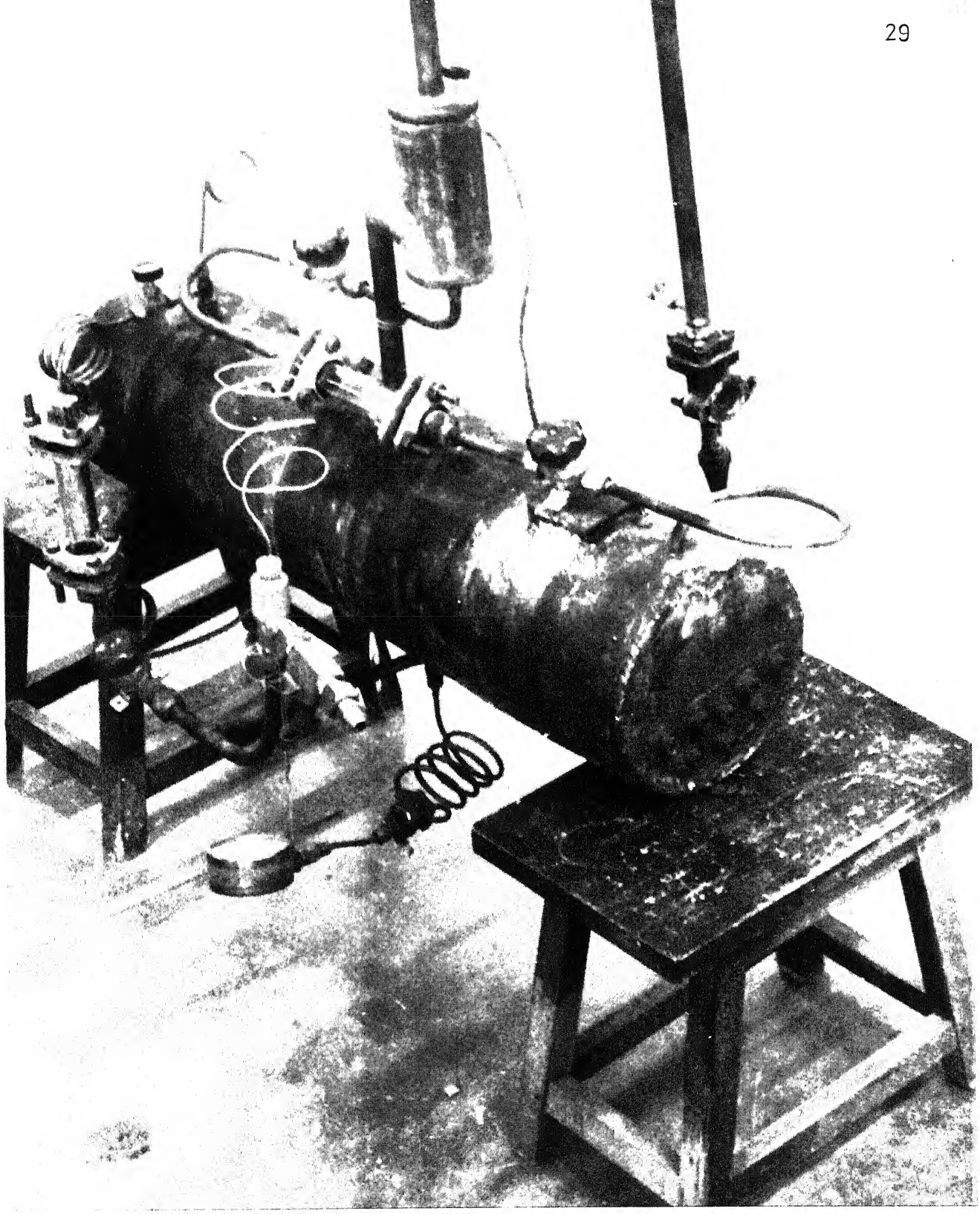

Fig. 2.4 Calorimeter assembly

(vii) Calorimeter: The purpose of the calorimeter is to help finding the refrigerating capacity of the compressor at different test conditions. Also, it acts as a refrigerant reservoir. No additional reservoir has therefore been provided in the system. The calorimeter has been fabricated in the Institute Workshop. It is a cylindrical shell of 230 mm I.D. and 900 mm length, fabricated from a 6 mm thick brass sheet. The brazed end covers of the shell are made of 12.5 mm thick M.S. plate. Eight M.S. pipes of 11 mm I.D. are placed axially in the lower half of the calorimeter shell as shown in Fig. 2.3 to house eight 1 kW, electric heater rods, 1.0 m long and 9.5 mm O.D. The M.S. pipes are welded at both the ends to the end covers. The heater rods are made in U.S.A. Fig. 2.4 gives a photographic view of the calorimeter.

A thick wall pyrex glass tube of 25 mm I.D. and 150 mm length is used as a refrigerant liquid-level indicator. Connections to the indicator are taken through a 12.5 mm copper tubing with special fittings at both the ends. The main line copper tubing is connected to the calorimeter through two valves, one at the top and the other at the bottom as shown in Fig. 2.3. A

16 mm copper tee is brazed at the bottom of the calorimeter to permit the inflow of refrigerant liquid into the calorimeter and also to allow the measurements of pressure and temperature of the liquid. The refrigerant vapour generated in the calorimeter leaves through a 25 mm diameter copper tube, brazed at the top, to enter the liquid separator, tangentially. The method of calibration of the calorimeter is discussed in detail in Appendix-A.

(viii) Liquid Refrigerant Separator: A separator of swirling flow type has been constructed and incorporated in the compressor suction line just above the calorimeter (Fig. 2 .3) to separate any liquid refrigerant droplets, carried by the saturated vapour. The separator consists of M.S. pipe of 7.5 cm I.D. and 200 mm length, with 3 mm thick M.S. end plates brazed to it. The pipe line connections to the separator are as shown in Fig. 2.3. The wet vapour from the calorimeter flows tangentially into the separator through a 25 mm copper tube at a point approximately 50 mm above its bottom end. The swirling vapour flows upward and out through the top of the separator. The liquid separated from the vapour collects at

the bottom of the separator from where it flows back into the calorimeter through the 12.5 mm copper tube. To observe the drainage of liquid refrigerant from the separator to the calorimeter a sight glass is fitted in the line complete with an inlet and an outlet valve.

(ix) Superheater: The 25 mm diameter and approximately 900 mm long copper suction line, from the separator outlet to the compressor inlet, is used to superheat the vapour coming out of the separator. The superheating is achieved by wrapping a 1 kW heating tape around the suction line.

(x) Valves and Pipe Lines: All the main line valves are of Danfoss make diaphragm type with flared connections. All the piping consists of copper tubings of different diameters as shown in Fig. 2.1. Use of fittings has been avoided in the set-up except for the incorporation of valves and the test sections, in order to minimize the possibility of leakage.

1.2 Test Sections

Commercially drawn copper tubings of two internal diameters 0.00106408 m and 0.0017657 m are used for the making of capillary tube test specimens. These diameters are arrived at, by the procedure described in Appendix-B. The following numbers of test specimens of different geometries are fabricated from each diameter copper tubing:

(a) one of straight configuration,

(b) two of helical configuration of different D/d ratios, and

(c) one of spiral configuration.

For each configuration, specimens of the largest length studied are first made. The lengths are then gradually reduced to obtain test sections of the sizes mentioned in Table - 1.1 (Chapter I). In deciding the maximum starting length for the test sections, due note is taken of the capacity, of both the flowmeter and the calorimeter. This is necessitated by the fact that the flow rate invariably decreases with increase in the length of the capillary tube, for a particular diameter. This decrease in flow rate, creates a capacity balance problem which, in our case, would be characterised by a slow fall in the level of the refrigerant in one of the flowmeter tubes and a sharp rise in the level of the refrigerant in the other. This would

finally result in the flow of the refrigerant from one tube of the flowmeter into the other. Another serious problem arising out of the ensuing reduction in the flow of the refrigerant, as a result of increased capillary length, would be the denudation of some of the heater rods fitted in the calorimeter and their subsequent failure by overheating. The maximum lengths of the test sections in the present studies are, therefore, arrived at, after actual testing of the capillary specimens.

(i) Straight Configuration: Initially, two straight test sections of 2.4 m and 3.6 m length and of 0.00106408 m and 0.0017657 m I.D., respectively, are made. Holes of 0.5 and 0.75 mm diameter at 0.3 m spacing are drilled along the test section lengths of the above two diameter tubes, respectively, for pressure measurement purposes. To make sure that the holes drilled are free from burrs, a soft G.I. wire of a diameter slightly less than the bore of the capillary tube is slowly pushed through the tube a number of times. In addition to this, a small needle is used to clean the holes individually. This method of removing burrs, which is found to be quite effective, has been perfected by carrying out tests on a number of small pieces of capillary tubings, then breaking them open at the holes and examining them under a magnifying glass.

Pressure tappings of 50 mm length and 4 mm diameter, are fixed by copper eutectic to the test

specimens at the pressure holes. To ensure that the pressure holes do not get chocked by molten copper during the above process, high pressure air was made to flow through the capillary tubes. The pressure tappings are next joined to the 6 mm diameter connecting lines of the pressure header through short pieces, approximately 50 mm long, of the same diameter tubing using flare fittings. The test specimens, likewise, are connected to the main line through small lengths of 6 mm diameter tubing, at either end, followed by 12.5 mm diameter tubing with the help of flare fittings.

i) Helical Configuration: To start with, four specimens of helical configuration are made with the following specifications:

No.	Length, l (m)	Capillary tube diameter I.D. (m)	O.D. (m)	D/d ratio
1	1.8	0.00106408	0.0021	10
2	2.4	0.00106408	0.0021	15
3	3.0	0.0017657	0.00315	15
4	3.6	0.0017657	0.00315	20

The D/d ratio for the specimen Nos. 2 and 3 has been kept identical with a view to study its effect on the performance of capillary tubes of different diameters.

For the drilling of burr-free pressure holes the same procedure and precautions are followed as for the straight test sections. Helical shapes are obtained by rolling the capillary tubes of required diameters over wooden mandrils. These wooden mandrils are turned to the proper size and shape on a lathe machine. Keeping in mind, the outer diameters of the capillary tubes which are 0.00315 m and 0.0021 m the diameters of the wooden mandrils are computed. However it is not possible to keep the above theoretically derived values due to the machining inaccuracy of the lathe used. Hence, the wooden mandril sizes actually used in the making of the specimens are as given in the following table:

D/d ratios	∅ 10	∅ 15	∅ 15	∅ 20
Diameter of mandril (mm) (theoretical)	8.5408	13.8612	23.3355	32.164
Diameter of mandril (mm) (actual)	8.5	13.9	23.3	32.2

The end connections for the test specimens and the pressure tapping connections are the same as for the straight test section. The pitch and the helix angles for the various test specimens are as given in Table 1.1.

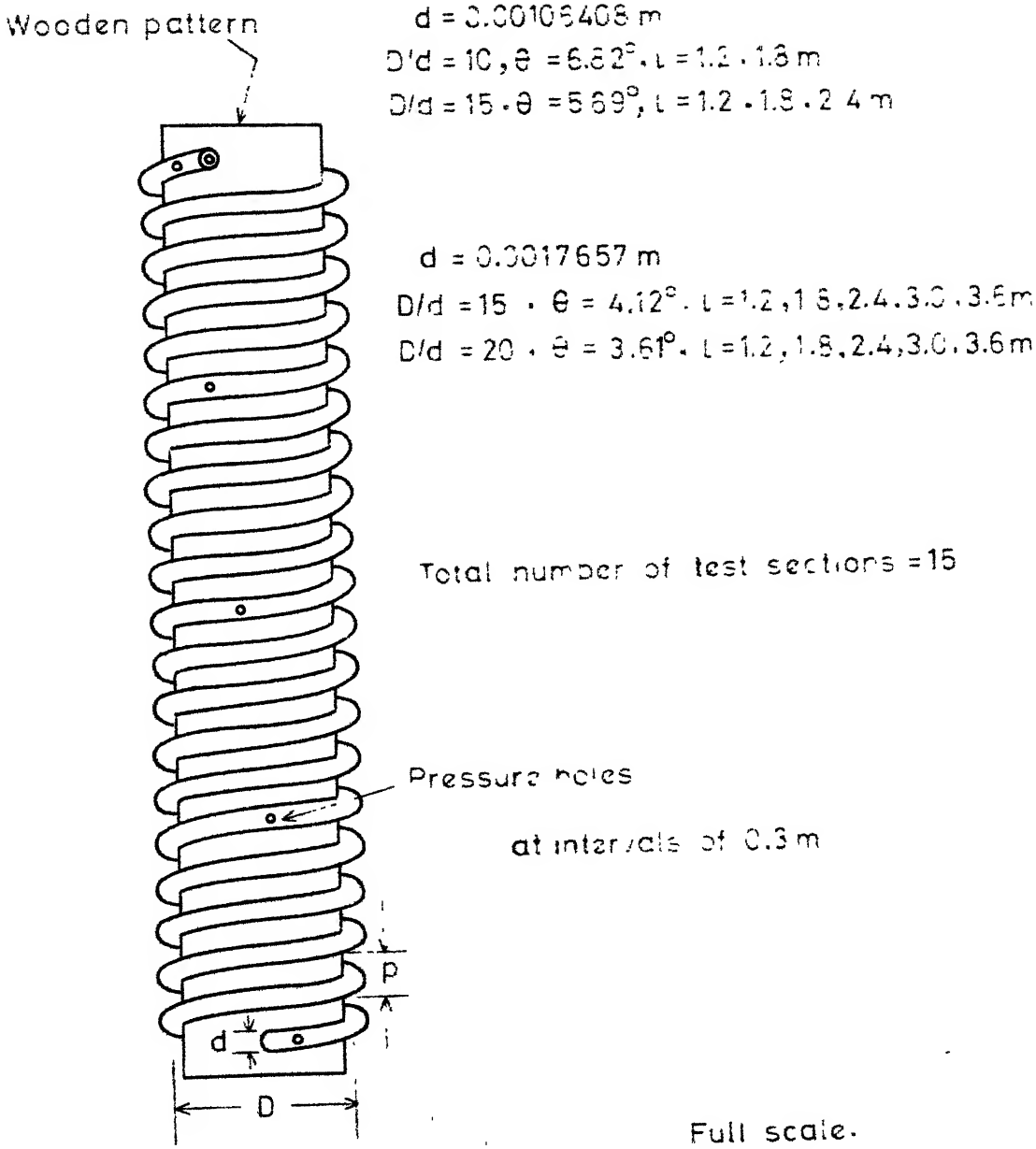

Fig. 2.5 Helical test section

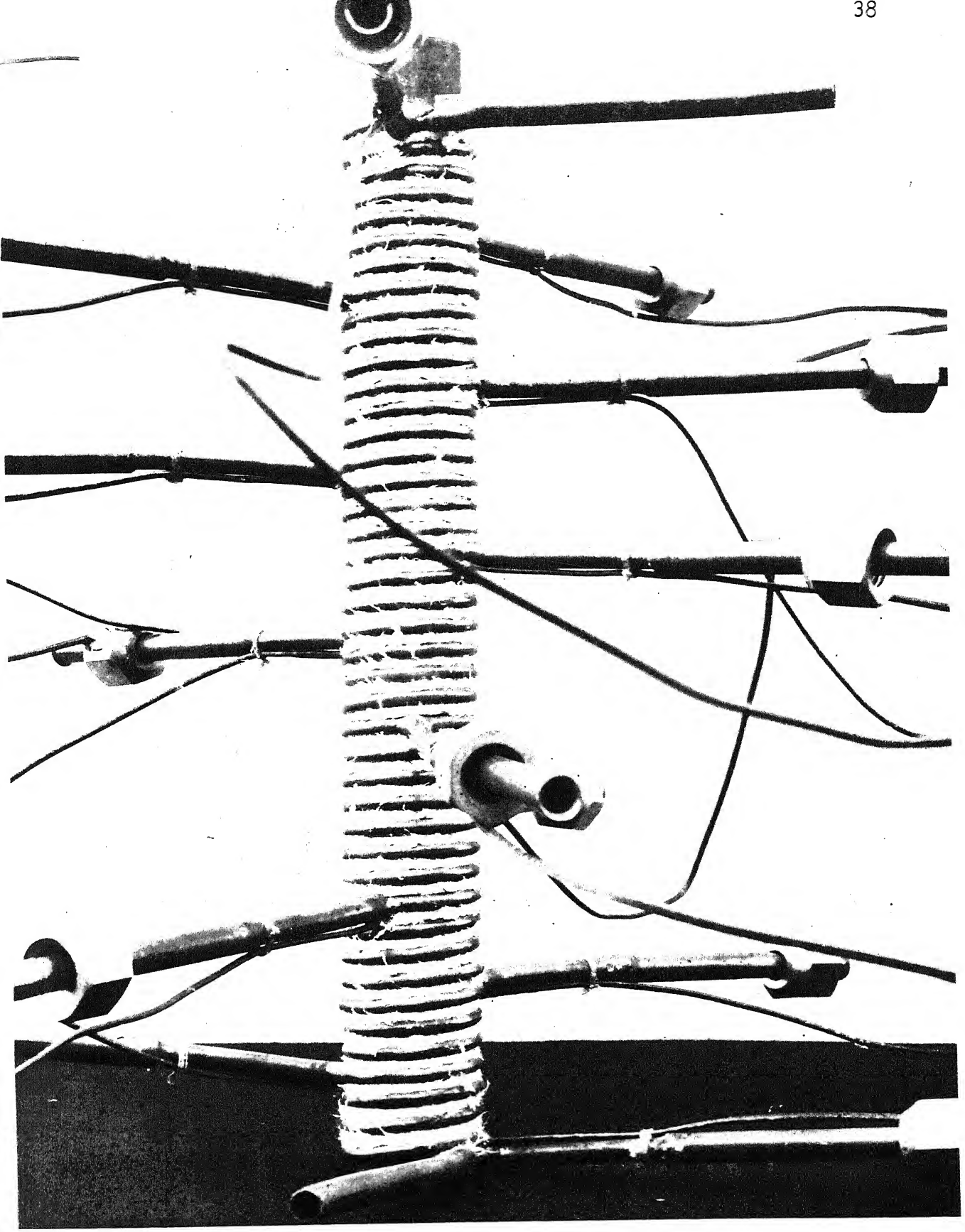

Fig. 2.6 Helical test section

Figure 2.5 shows the schematic diagram of a helical test configuration and Fig. 2.6, the photograph of one of the test specimens. The helical test sections are kept vertical during the experimental investigation and the refrigerant flow maintained from top to bottom. This flow scheme is adopted purely for convenience since the calorimeter occupies the lowest position in the set-up.

(iii) Spiral Configuration: The starting test lengths and diameters of the capillary tubings in this case are the same as for the straight test specimens viz., 3.6 m and 2.4 m lengths of 0.0017657 m and 0.00106408 m diameter, respectively. For the drilling of burr-free pressure holes, and making of pressure tapping connections and end connection for the specimens, the procedures followed are the same as for the case of straight configuration.

Archimedian spiral shaped specimens are made with the help of two wooden patterns. To obtain the desired shapes, grooves of diameters and depths equal to outside diameters of the respective capillary tubings are cut in a piece of Shisham wood on a lathe machine. A pitch of 5 mm for the spiral is choosen because of the ease and convenience of making the patterns rigid. The minimum practicable radius at the centre for these specimens is 5 mm.

b = 0.005 m

R_i = 0.005 m

R_o = 0.0435 0.0535 0.0625 m for d = 0.0018408 m
L = 1.2 1.8 2.4 m

R_o = 0.0435 0.0535 0.0625 0.069 0.0755 m for d = 0.0017667 m
L = 1.2 1.8 2.4 3.0 3.6 m

Total number of test sections = 8

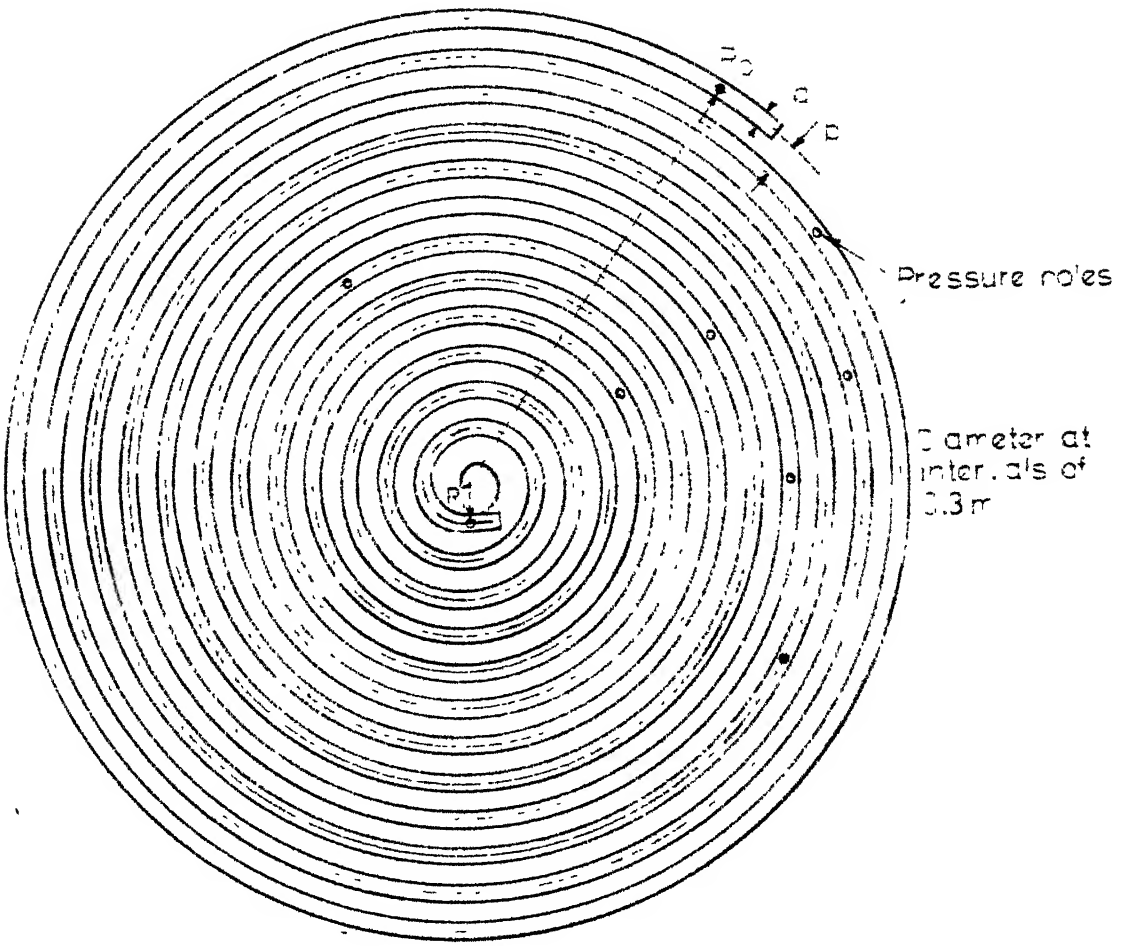

Fig. 2.7 Spiral test section

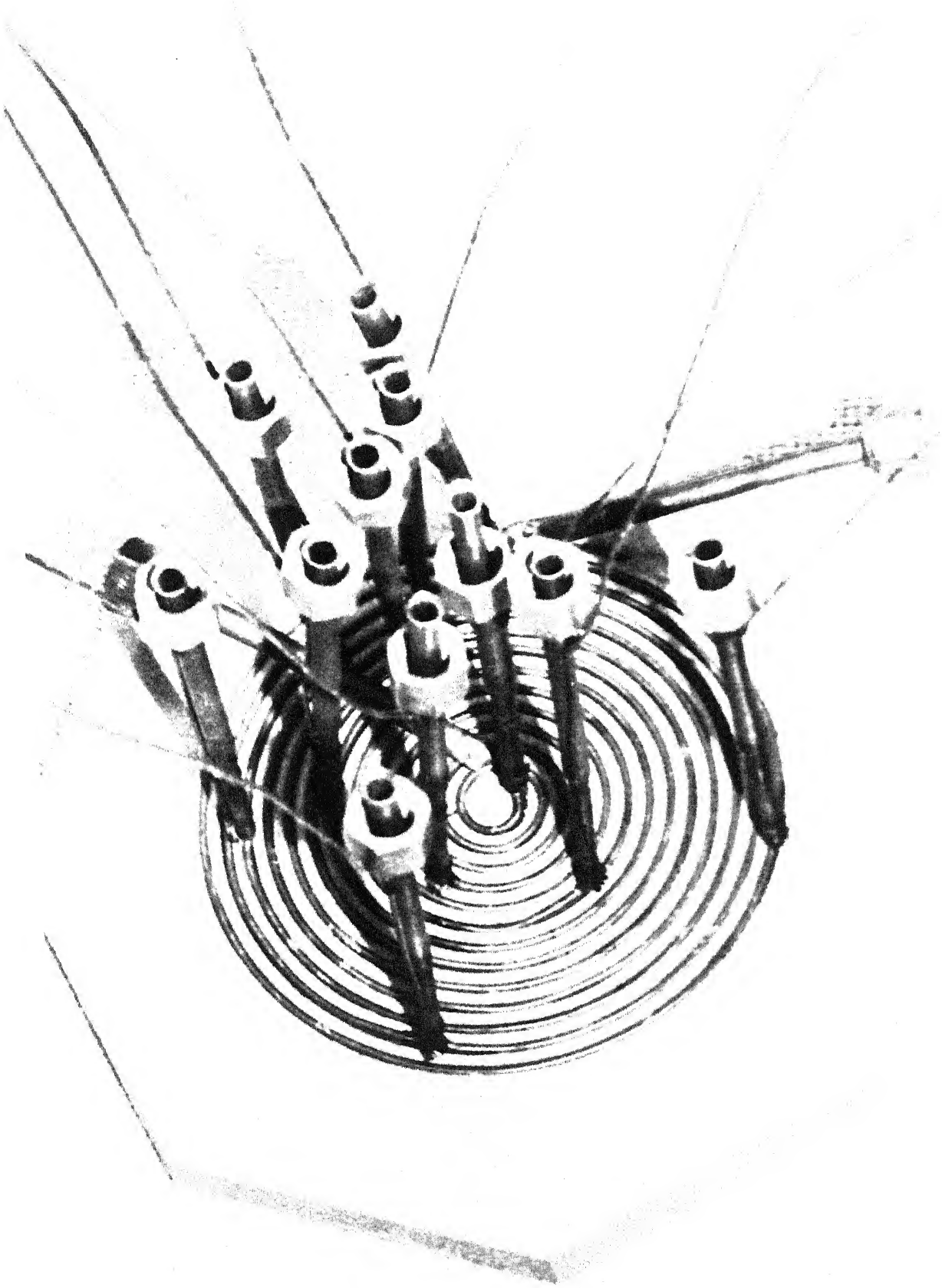

Fig. 2.8 Spiral test section

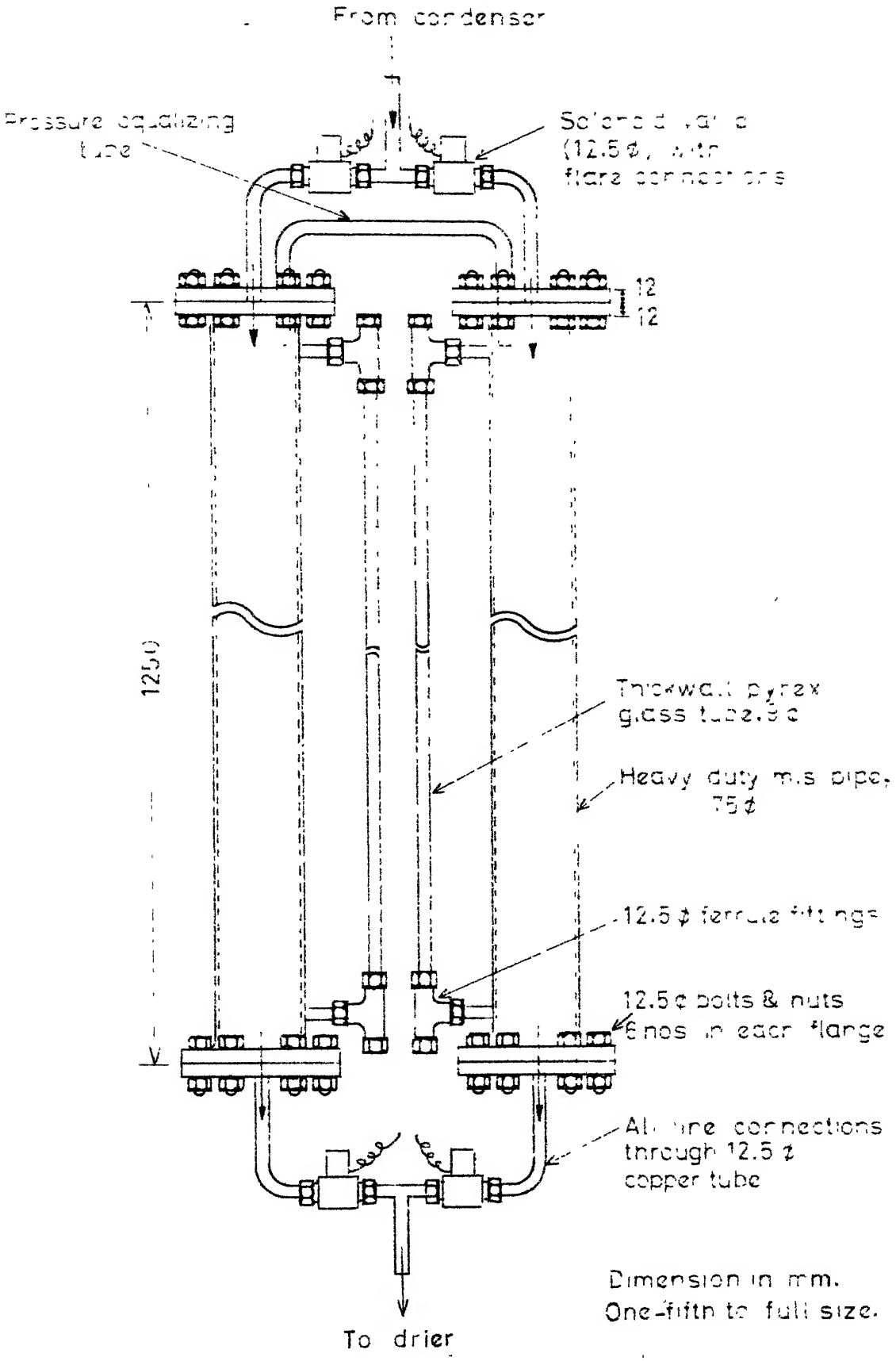

Fig. 2.9 Flowmeter assembly

The direction of flow of refrigerant in these spirals is maintained from the periphery towards the centre, in order to achieve higher pressure drops. During experimental studies, the spiral test sections are placed in a horizontal position. Fig. 2.7 shows the diagramatic view of an Archimedian spiral and Fig. 2.8, the photograph of a test spiral section.

2.3 Instrumentation and Control

(i) Measurement of Refrigerant Flow Rate: The refrigerant flow is measured by means of a flowmeter, shown in Fig. 2.9. The flowmeter consists of two identical limbs of heavy duty M.S. pipe, 75 mm I.D. and 1.0 m long, with flanged ends. Four, 12.5 mm thick M.S. end plates are fixed to the flanges of the flowmeter limbs at both the ends with a bolt and nut arrangement. High pressure jointing and selac solution are used to make these joints leakproof. Holes of diameter 12.5 mm are drilled and copper tubes of the same diameter brazed at the centre of each of the end plates to provide inlet and outlet connections to the flowmeter. Further, both the limbs of the flowmeter are connected through a 12.5 mm diameter copper tube, at the top for pressure equalization purposes. The refrigerant lines coming out of the flowmeter both at the top and the bottom, are joined to the main line through tee-junctions. Solenoid valves are incorporated into each of

the lines going into and coming out of the flowmeter limbs between the tee-junctions and the end plates.

Thick walled pyrex glass tubes in two pieces (for purposes of safety) are incorporated in parallel with each of the flowmeter limbs (Fig. 2.9) for the graduation of the flowmeter. To fix the pyrex gauge glass tubes in position, four thickwalled copper tubes of 12.5 mm diameters and 50 mm lengths are brazed to each limb of the flowmeter along its length as shown in the above figure. Connections to the gauge glass tubes are taken through the copper tubes using 12.5 mm ferrule tees and synthetic rubber sealing rings.

Both the limbs of the flowmeter are used simultaneously during experimentation; while one supplies a measured quantity of refrigerant through a drier to the expansion device, the other limb keeps on collecting the condensate at the same time. The calibration of the flowmeter is described in Appendix-A.

(ii) Test Section Inlet Pressure Control: The pressure at the inlet to the test section is controlled by regulating the flow rate and the temperature of the condenser cooling water. The schematic diagram of the arrangement is shown in Fig. 2.1, which includes the connections to supply water to the condenser from a gravity tank and also from a cooling tank, using a pump. Water

from the condenser outlet is either cooled through a spraying arrangement fitted in the cooling tank or, alternatively, heated by recirculating it again and again through the condenser, depending upon the pressure required at the inlet to the test section. The exact control of temperature of water in the condenser is achieved by adjusting the flow rate of water by the globe valves placed in the circuit.

(iii) Refrigerant Temperature Control at the Inlet to the Test Section: The required refrigerant temperature is attained by passing the refrigerant through a constant temperature coil placed in a constant temperature distilled water bath, made by Colora, Germany. The constant temperature helical coil consists of 6 turns of 12.5 mm diameter copper tube with a mean coil diameter of approximately 150 mm. The distilled water is heated or cooled to attain the desired temperature in the bath. Immersion heaters of variable capacity (0.5, 1.0 and 1.5 kW) are used for heating the water. Cooling is achieved by circulating the bath water through a cooling coil placed in a separate tank of distilled water, submerged in which is the evaporator coil of a 1-ton R-12 refrigerating unit. This refrigeration unit has been fabricated in the laboratory and is shown in Fig. 2.1. A thermostatic switch has been put in the circuit for controlling the refrigeration unit. The temperature of water in the bath is controlled

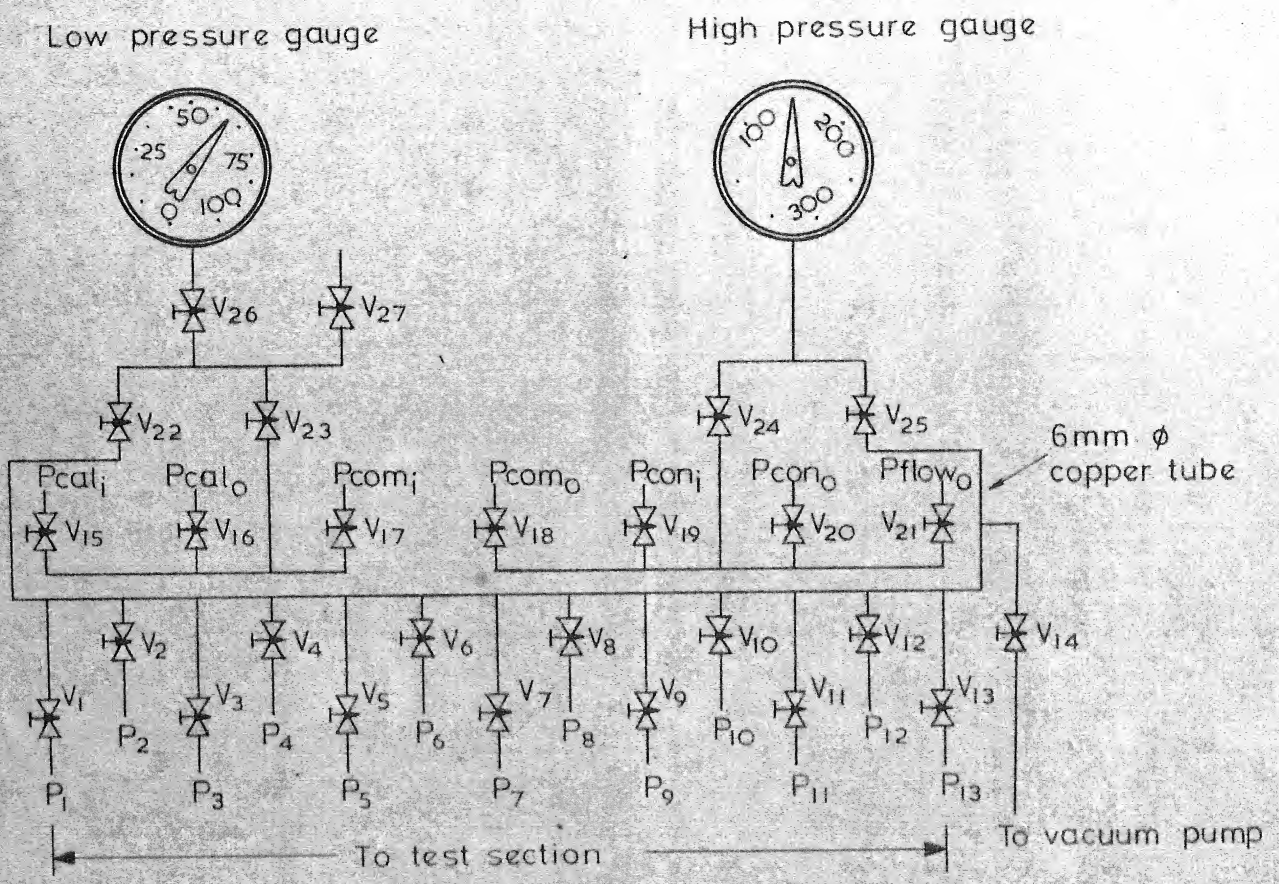

Pcal$_i$ & Pcal$_o$ – Calorimeter inlet & outlet

Pcom$_i$ & Pcom$_o$ – Compressor inlet & outlet

Pcon$_i$ & Pcon$_o$ – Condenser inlet & outlet

Pflow$_o$ – Flowmeter outlet

Fig. 2.10 Schematic diagram of pressure tappings

with the help of a mercury contact thermometer. A mercury-in-glass thermometer with graduation of 0.1 ^{o}F has been used for accurate recording of water temperature in the bath.

(iv) Pressure Measurement: The pressure measurement is done through Heise pressure gauges of two different ranges appropriate to high and low pressures in the system and the test section.

Calibration of the pressure gauges is described in Appendix-A. Since only two gauges are used for pressure measurement of both the system and the test section, a suitable header has been constructed as shown in Fig. 2.10. A Hoke's needle valve is fitted in the line of each pressure tapping as shown in the above figure. Valves V_1 to V_{13} are used for the test section pressure tappings and valve V_{14} connects the test section to a vacuum pump for purposes of flushing the specimens before testing.

Pressure is measured in the system at seven different locations as shown in Figs. 2.1 and 2.10. The valves V_{15} to V_{17} are used on low-pressure side and V_{18} to V_{21} on high-pressure side. The test section pressure tappings and the low-pressure side of the system are connected to the low-pressure gauge through valve V_{22} and V_{23}, respectively. Similarly, the high-pressure side of the system and the test section pressure points are

connected to high pressure gauge through valves V_{24} and V_{25}, respectively. Although,space for the inclusion of one more pressure gauge has been provided in the set-up, through valves V_{26} and V_{27}, it is, however, left unutilized in the present study.

All the connections of the valves and pressure gauges are through 6 mm copper tubing using 6 mm swagelok fittings. The test section pressure tappings are connected with their respective pressure lines in the header using 6 mm flare unions and brass nuts. This enables to make or break the connections easily from the header whenever required.

(v) Temperature Measurement: The temperature is measured at the same locations where pressure is also measured. In addition to this, the atmospheric temperature and the temperature of the refrigerant at the inlet to the test section are also recorded. Copper constantan thermocouples of 24 gauge have been used. Calibration of the thermocouples is discussed in Appendix-A.

For measurement of temperature in the system, at seven different locations, copper tubes of approximately 30 mm length and 6 mm diameter are brazed to the main-line. A 6 mm swagelok tee is fitted to the copper tubes. A thermocouple is then inserted through the limb of the tee (Figs. 2.1 and 2.3), vertical to the main line, such that

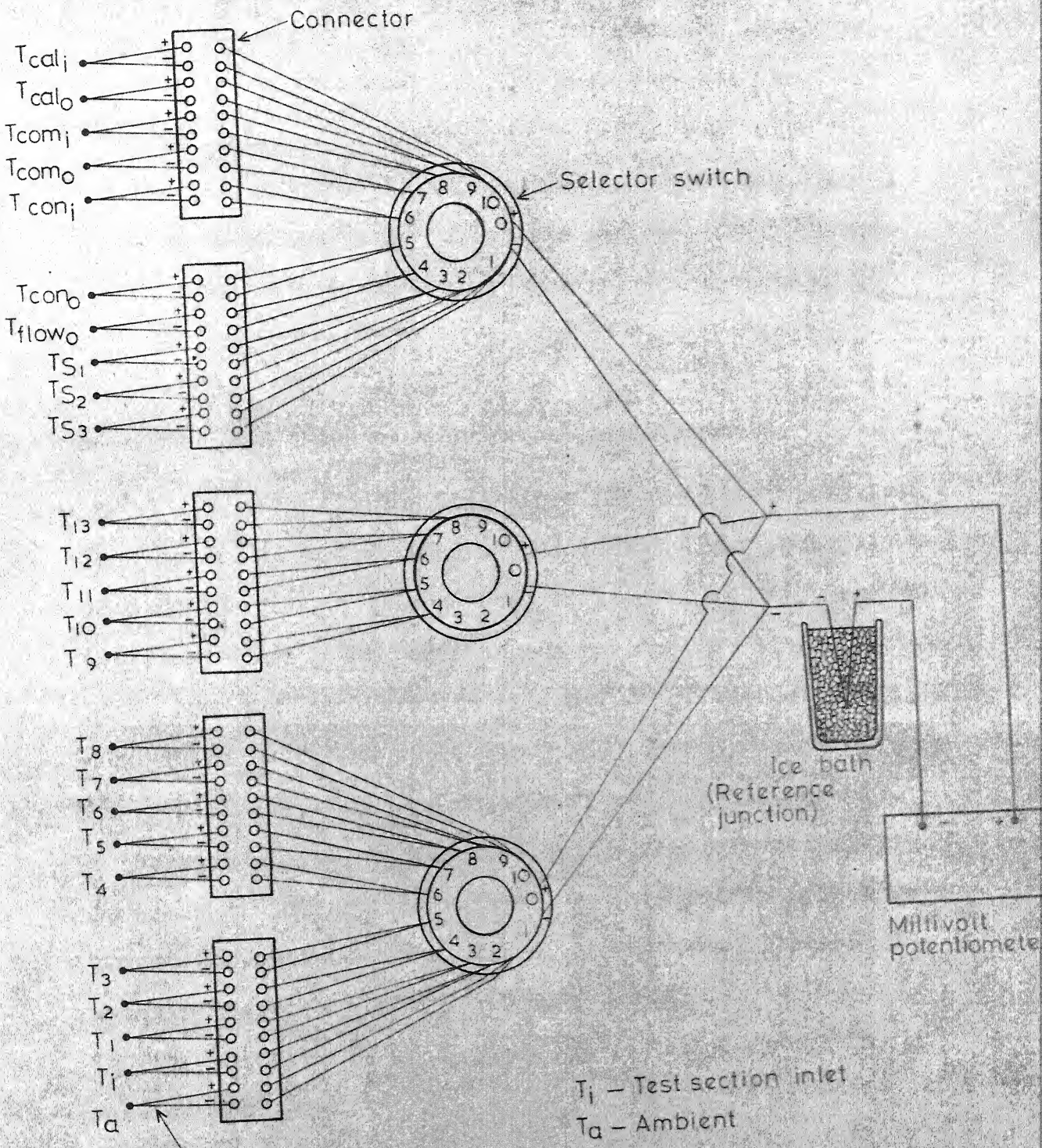

T_i – Test section inlet
T_a – Ambient
$T_1, T_2 \ldots T_{13}$ – Test section
$T_{S1} \ldots T_{S3}$ – Calorimeter surface
T_{cal_i} & T_{cal_o} – Calorimeter inlet & outlet
T_{com_i} & T_{com_o} – Compressor inlet & outlet
T_{con_i} & T_{con_o} – Condenser inlet & outlet
T_{flow_o} – Flowmeter outlet

Fig. 2.11 Schematic diagram of thermocouple connection

the bead is approximately at the centre of the flow. In order to form a leak proof joint a teflon cone with two small holes adequate to accommodate thermocouple wires is used. The teflon cone, during the process of tightening of the nut, is pressed against the wall of the swagelok tee and the thermocouple wires, thus rendering a leak proof joint. The horizontal limb of the swagelok tee has been used for the system pressure measurement.

However, for temperature measurement of the test section, it is not desirable to insert the thermocouple bead inside the capillary tube, as it will almost block the capillary bore. The beads of the thermocouples have, therefore, been soft soldered to the surface of the capillary tube close to the pressure tappings. Thermocouples T_1 [redacted] T_{13}, in Fig. 2.11., have been provided for this purpose. A thermocouple, T_i is inserted in the flow, immediately upstream of the capillary inlet, for indicating the refrigerant temperature. The ambient temperature is measured using a thermocouple, T_a. Thermocouples, Ts_1, Ts_2 and Ts_3 are fixed on to the surface of the calorimeter with a view to determine its rate of heat loss.

All thermocouple-connections to selector switches are made through suitable connectors as shown in Fig. 2.11. The output terminals of selector switches are connected to a Leeds and Northrup millivolt potentiometer (least count 0.005 mV) through an ice bath reference junction.

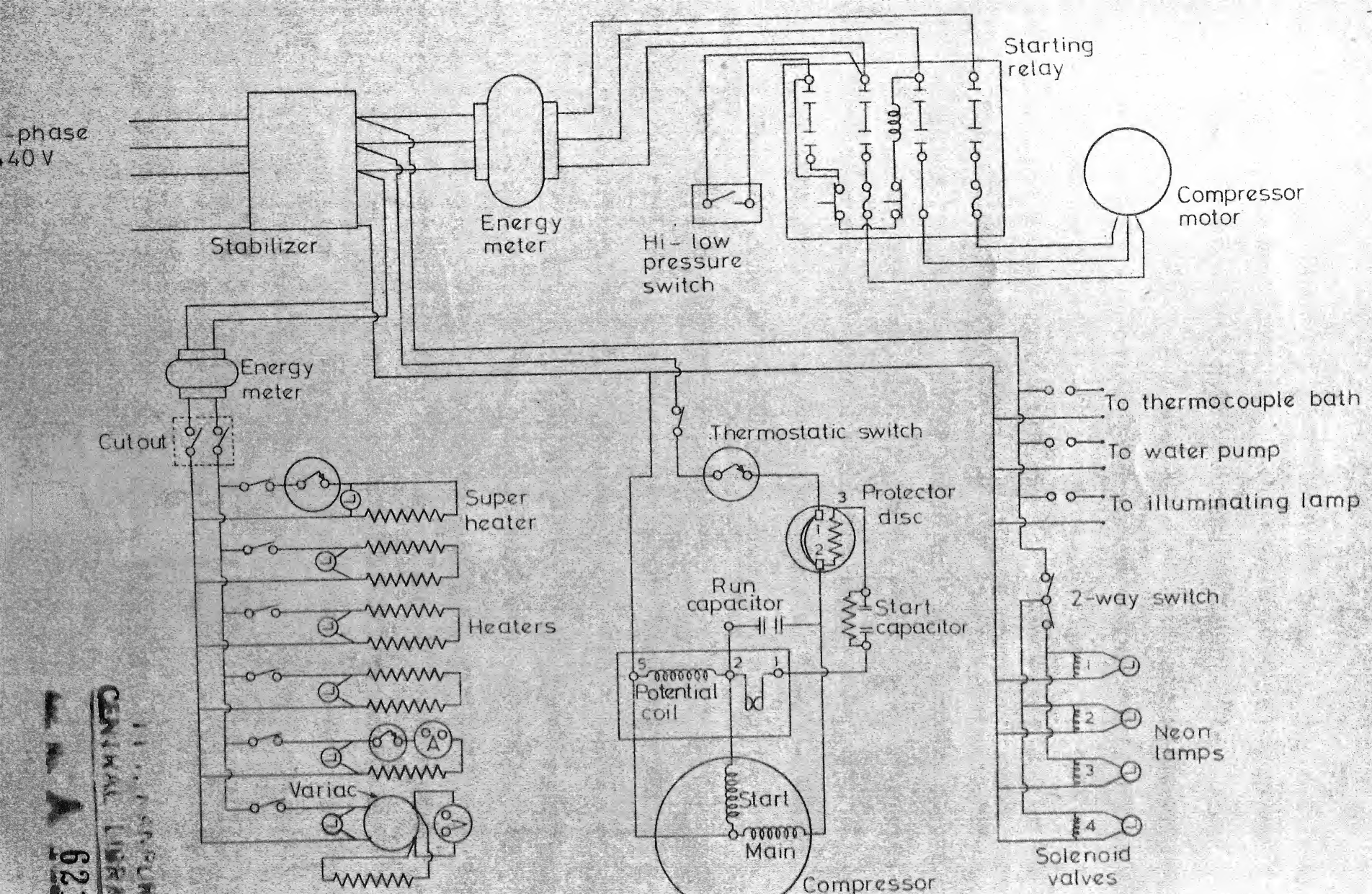

Fig.2.12 Electrical circuit diagram

(vi) Power Supply: The power supply is taken from a 440 Volts 50 cycles/sec, 3-phase mains, through a 3-phase voltage stabilizer made by Automatic Electric Co., Bombay, with an accuracy of ± 1%. The stabilized output is fed to the 3-phase compressor motor via an energy-meter, a starter and an off-and-on switch as shown in Fig. 2.12. All the heaters are energized by connecting them across one of the stabilized phases. Indicating neon lamps, one for each heater rod and the energy-meter have been included in the circuit. The cooling unit and the other energy consuming devices viz., constant temperature bath, water pump, illuminating lamp for flowmeter and the four solenoid valves, complete with indicating neon lamps, are connected across the other two phases, respectively.

(vii) Calorimeter Pressure and Temperature Control: Pressure and hence, temperature in the calorimeter, is controlled by regulating the energy input to the heater rods through a coarse and fine adjustment controls. Coarse adjustment control consisted of a 1 kW heater rod connected in parallel with a variac. For finer adjustments an Aplab temperature controller is connected in series with another 1 kW heater rod. The thermister of the controller is inserted directly into the calorimeter as shown in Fig. 2.3. The electric circuit of heaters is shown in Fig. 2.12.

(viii) Refrigerant Superheating Control: The input to the superheater is taken through a thermostatic switch, the sensing bulb of which is fixed to the last portion of the suction pipe just ahead of the compressor inlet. An indicating neon lamp is also fitted in this circuit.

(ix) Energy Measurement: The energy input to the heater rods in the calorimeter and to the superheater is monitored by a calibrated single phase energy-meter. Similarly, a calibrated 3-phase energy-meter is used to measure the input to the motor driving the two-ton, open type compressor. The electric circuit is shown in Fig. 2.12. Calibration of energy meter is discussed in Appendix-A.

(x) Water Flow Measurement: A Brook's rotameter is connected at the inlet to the condenser for the measurement of the flow rate of cooling water. However, in the present study, the rotameter has been used only to control the cooling water flow rate.

2.4 Leak Proofing of the System

The calorimeter, the flowmeter and the condenser are individually made leak proof before incorporating them into the system. For the calorimeter, leaks are detected employing soap solution technique, at 10 ata pressure (17), using compressed air, and 50 micron vacuum successively.

Any leaks observed in the calorimeter while being tested, both under pressure and vacuum conditions, are properly sealed and the component made leak proof. This is further ratified by the steady indication of the respective gauge readings over a period of 24 hours. The flowmeter and the condenser are tested for leaks under water at a pressure of 20 ata (17), using high pressure Nitrogen. Any leaks noticed in the components are mended and the components put under 24 hour test, as mentioned earlier.

The entire system excluding the test section and the cooling unit is, then, checked for leaks at 10 ata, using soap solution. After sealing all the leaks at this pressure, the high and the low-pressure sides of the system are separated by closing the compressor inlet and outlet valves, and the valve DV_4. The low pressure side is now alternately evacuated and pressurized using the same technique as was used for the leak testing of the calorimeter. The high-pressure side is checked for leaks at 20 ata pressure.

Next, the cooling unit, is made leak proof, following the same procedure as for the main system. Each test section, fitted with all the pressure tappings, are also checked for leaks at 20 ata pressure, under water, before being installed into the system.

2.5 Charging of the System

The system is first evacuated to 50 micron vacuum, then filled with carbon dioxide gas till the pressure increases to approximately 1 atm and then again evacuated and refilled with CO_2. This process of flushing is repeated thrice with CO_2 gas and twice with R-12 vapour. The system, after the flushing is over, is ready for charging. A cylinder containing R-12 is connected to the charging port provided at the inlet to the compressor (Fig. 2.1). Next, the inlet valve to the compressor, is completely closed and the charging port is left fully opened. The compressor is now run. The cooling water is supplied to the condenser. The system is charged slowly with refrigerant. Charging is continued till (i) the liquid level in the calorimeter is approximately 25 mm above the topmost heater tube fitted therein and (ii) atleast one of the flowmeter limb gets filled with the refrigerant. The compressor is then stopped and the charging line disconnected. The cooling unit is also, similarly, charged with the required amount of R-12.

2.6 System Insulation

The calorimeter is wrapped first with 6 mm thick asbestos belt. Its surface and the connected lines (going to the gauge glass) are then covered with, 100 mm thick glass wool. The suction line, the separator and the

flowmeter are all insulated with, 75 mm thick, glass wool. All the lines in the system including pressure header connections are insulated with 6 mm diameter asbestos rope. In addition, the lines from the flowmeter outlet to the test section inlet, from the test section outlet to the calorimeter inlet and the pressure header connections are all covered with glass wool, 50 mm thick.

The straight test section is first insulated with 6 mm diameter asbestos rope and then covered with glass wool. The spacing between the turns of the helical coil is first insulated by winding asbestos rope around the wooden mandril and then the whole coiled specimen including the spacing is further insulated with glass wool. Since, the spiral test section is made on a wooden pattern, it is covered with glass wool insulation after incorporating it in the set-up.

In the cooling unit, the cooling tank is insulated with glass wool upto 75 mm thickness. The portion of the evaporator line exposed to ambient is also covered with glass wool. The recirculation line for the condenser cooling water is heavily insulated with glass wool.

2.7 Experimental Procedure

Test sections of straight, helical and spiral configurations have been studied. As mentioned earlier, experiments are initiated using the longest lengths for each test section, which are subsequently reduced in stages to yield a number of test samples (Table 1.1). All the samples are tested at three inlet pressures (12, 10 and 8 kgf/cm^2 absolute) and four inlet temperatures of the refrigerant (saturated and 5 ^oC, 10 ^oC and 15 ^oC subcooling) for each inlet pressure. However, for 8 kgf/cm^2 absolute pressure, it is not feasible to test the samples at 15 ^oC subcooling due to the limitations of the cooling unit.

After mounting a particular test section into position, the system is switched on. Before taking down any measurements, the system is run till such time as the desired inlet conditions (pressure and temperature) at the test section are obtained. This invariably takes about half an hour duration. The procedure followed to attain the required inlet conditions is as follows:

The constant temperature bath and the cooling unit are switched on. The bath temperature, which is controlled by a mercury contact thermometer installed in the bath heater circuit, is maintained at a temperature slightly higher than that desired at the test section inlet, to take care of any heat losses between the

constant temperature bath and the inlet to the test section. The valve DV_4 in the by-pass line is closed to ensure the flow of refrigerant through the test section. The mercury contact thermometer is further adjusted to attain the desired temperature at the inlet to the test section as indicated by the thermocouple T_i.

The pressures at the inlet to the calorimeter and the test section are indicated by the low and high pressure gauges, respectively. The heaters in the calorimeter and the superheater at the compressor inlet, to superheat the refrigerant to about 10 ^{o}C, are switched on. To maintain the temperature constant in the calorimeter use is made of the thermostatic switch fitted in the circuit of one of the calorimeter heater rods.

In order to obtain the required pressure at the test section inlet, the flow rate of cooling water through the condenser is controlled by means of the valve GV_1. As mentioned before, 8 kgf/cm^2 absolute pressure at the test section is achieved by circulating water through the condenser from either the gravity tank or the cooling tank, or both. The remaining pressures are obtained by recirculating the condenser water and held constant by mixing the condenser water with the gravity tank water.

The refrigerant flow is measured by recording the time of fall of a particular volume of refrigerant in

the flowmeter limbs and the final reading is taken as the mean of the two. A double way switch fitted in the solenoid valve circuit is operated manually to connect either of the flowmeter limbs alternatively with the test section. Pressure and temperature at various locations in the test section and of the calorimeter are then recorded. Also, the temperature of refrigerant at the inlet to the test section and both at the inlet and outlet of the flowmeter are noted. The above data alongwith the ambient temperature and the pressure constitute one set of readings. Similar set of readings are recorded for various combinations of test section inlet pressures and temperatures. Steps delineated above are repeated in sequence for other test section lengths, diameters and configurations. It is to be noted that each time a new test section is incorporated into the system, it is duly checked for any leaks and properly flushed.

During the course of experimentation, especially with small diameter capillaries, the capacity balance problem is observed. This is combated by draining the accumulated fluid from high-pressure side to the low-pressure side via the thermostatic expansion valve line. In order to ensure the reliability of the data, readings are repeated at random and found reproducible

CHAPTER III

THEORETICAL ANALYSIS AND DATA REDUCTION

3.1 Governing Equations

It is well known that two phase gas-liquid flow is amenable to theoretical analysis by the use of either the "homogeneous model" or the separated flow model" the assumptions on which the "homogeneous model" is based, are:

(a) one-dimensional, steady state, adiabatic flow with equal vapour and liquid linear velocities (i.e. slip ratio unity)

(b) attainment of thermodynamic equilibrium between the phases and

(c) the two phases considered to flow as a single phase, possessing mean fluid properties.

The "separated flow model", on the other hand, considers the phases to be artificially segregated into two separate streams, each travelling at a different velocity.

The "homogeneous model" which is also known as the "friction factor" or "fog-flow" model has been more commonly used in the refrigeration applications for a considerable time because of its simplicity.

Unlike the "separated flow model", the "homogeneous flow model" does not require the evaluation of the two-phase multiplier and the void fraction which is quite complicated and cumbersome. It is to be further noted that while the "separated flow model" provides accurate pressure drop estimates in the low mass-velocity range, $G = 1360$ kg/m^{2}s, the "homogeneous model" gives better agreement in the higher mass-velocity range, $G > 2000 - 2500$ kg/m^{2}s (23).

In the present study, however, the "homogeneous model" has been adopted for the reasons that, apart from being simple and tractable in its analysis, it has been highly recommended for use with high mass-velocity, flows, which were invariably encountered in this investigation.

Using the momentum balance approach, the pressure change in the tube is given by,

$$dp/dl = (dp/dl)_{fr} + (dp/dl)_{ac} + (dp/dl)_{gr} \qquad (3.1)$$

where,

$(dp/dl)_{fr}$ = pressure gradient due to friction

$$= - f_{TP}\, \rho\, V^2 / 2\, g_c\, d$$

$$= - f_{TP}\, G^2\, v / 2\, g_c\, d \qquad (3.2)$$

$(dp/dl)_{ac}$ = the pressure gradient due to acceleration, brought about by area and phase change

$$= - (\dot{m} / A g_c) (dV/dl)$$

$$= - (G^2 / g_c) (dv/dl) \text{ (the area being constant in the present study)} \quad (3.3)$$

$$(dp/dl)_{gr} = \text{pressure gradient due to gravity}$$

$$= - (g / g_c) \rho \sin \theta$$

$$= - (g / g_c) (\sin \theta / v) \quad (3.4)$$

$$v = x v_g + (1 - x) v_l \quad (3.5)$$

$$\text{and } V = G / \rho = Gv \quad (3.6)$$

Substituting relations (3.2) - (3.6) in the equation (3.1), we get,

$$(dp/dl) = - f_{TP} G^2 v / 2 g_c d - (G^2 / g_c) (dv/dl) - (g / g_c) (\sin \theta / v)$$

$$= - f_{TP} G^2 v / 2 g_c d - (G^2 / g_c) (dv/dp)(dp/dl) - (g/g_c) (\sin \theta / v)$$

The various parameters appearing in the above expressions have the following units:

p (pressure): kgf / cm^2

v (specific volume): m^3/kg

G (mass velocity): kg/m^2-h

g (acceleration due to gravity): 9.81 m^2/s

g_c (conversion factor): 9.81 (kg-m) / (kgf-s^2)

l (length): m

d (diameter): m

$$(dp/dl)\ (1 + (G^2 / g_c)\ (dv/dp)) = - f_{TP}\ G^2 v / 2 g_c d - (g / g_c)\ (\sin\theta / v)$$

$$(dp/dl) = - (f_{TP}\ G^2 v / 2 g_c d + (g / g_c)\ (\sin\theta / v)) / (1 + (G^2 / g_c)\ (dv / dp))$$

$$= - (f_{TP}\ v / 2d + g \sin\theta / G^2 v) / ((g_c / G^2) + (dv / dp)) \qquad (3.7)$$

Taking account of units as defined in the foot note on page 62 the Eq. (3.7) becomes,

$$(dp/dl) = - (f_{TP}\ v / 2d + 9.81\ (3600)^2 \sin\theta / v\ G^2) / (9.81\ (3600)^2\ 10^4 / G^2 + (dv / dp)) \qquad (3.8)$$

To obtain the solution for l as a function of p, the specific volume, v, has to be substituted as a function of pressure. The expressions for v_f and v_g in Eq. (3.5) to estimate the specific volume, v, are obtained by the curve fitting technique, employing the data available on saturated R-12 (13), as follows:.

$$v_g = 0.16375321 / p^{0.9529} \qquad (3.9)$$

$$v_l = 0.00066633 + 0.00002638\ (p - 0.84136132)^{0.731} \qquad (3.10)$$

The expressions (3.9) and (3.10) are valid in the temperature range - 30 °C to 50 °C with curve-fit errors of 1.552% and 0.2798%, respectively.

Substituting for v_g and v_J in Eq. (3.5), we get;

$$v = (0.00066633 + 0.00002638\ (p - 0.8436132)^{0.371}\ (1 - x) + 0.16375321\ x\ /\ p^{0.9529} \qquad (3.11)$$

with 1.5521% error over the temperature range - 35 °C to 50 °C.

An equation similar to Eq. (3.11) was derived by Niaz and Davis (18), as follows:

$$v = 0.00074906\ (1 - x) + 35.95509\ x\ /\ p \qquad (3.11a)$$

which has an error of 5% over the temperature range - 5 °C to 50 °C. It is obvious, therefore, that Eq. (3.11) is more accurate than that given by Niaz and Davis and covers a much wider temperature range.

Differentiating Eq. (3.11) and rearranging, it gives,

$$(dv/dp) = 1.928378 * 10^{-5}\ (1 - x)(p - 0.8436132)^{-0.269} - (6.6633 * 10^{-4} + 2.638 * 10^{-5}\ (p - 0.8436132)^{0.731})\ (dx\ /\ dp) + 0.16375321\ p^{-0.9529}\ (dx\ /\ dp) - 0.1560403\ p^{-1.9529}\ x \qquad (3.12)$$

The quality, x increases as the fluid flows through the capillary tube. The expression for x, given by Whitesel (10) has been used in the present formulation, i.e.;

$$x = 1.8 - (1.8 - x_i) \exp (0.11541 (p^{0.5} - p_i^{0.5})) \quad (3.13)$$

where, the subscript, i, denotes inlet conditions. This equation was derived by Whitesel under the assumption that the fluid flowed isenthalpically. The enthalpy falls slightly as the velocity and, hence the kinetic energy, increases with the increase of dryness fraction. However, in the region of present interest, the error introduced by Eq. (3.13) is only of the order of 1% (18). This error being small in magnitude however, outweighs the advantages gained from a more rigorous analysis based on true adiabatic conditions which is very involved and tedious.

Differentiating Eq. (3.13),

$$(dx/dp) = -0.057705\, p^{-0.5}\, C$$

where,

$$C = (1.8 - x_i) \exp (0.11541 (p^{0.5} - p_i^{0.5})) \quad (3.14)$$

Hence, expression (3.13) may be written in a simplified form as,

$$x = 1.8 - C \quad (3.14\ a)$$

Substituting Eqs. (3.13), (3.14) and (3.14 a) into Eq. (3.12),

$$(dv/dp) = 1.928378 * 10^{-5} (C - 0.8) (p - 0.8436132)^{-0.269}$$
$$+ 0.38450601 * 10^{-4} C p^{-0.5}$$
$$+ 0.1522259 * 10^{-5} C p^{-0.5} (p - 0.8436132)^{0.731}$$
$$- 0.94493858 * 10^{-2} C p^{-1.4529}$$
$$- 0.1560403 (1.8 - C) p^{-1.9529} \qquad (3.15)$$

Further, substituting Eqs. (3.11), and (3.15) into Eq. (3.8), the equation for pressure drop becomes:

$$(dp/dl) = - ((f_{TP} / 2d)((6.6633 * 10^{-4}$$
$$+ 2.638 * 10^{-5} (p - 0.8436132)^{0.731})(C - 0.8)$$
$$+ 0.16375321 (1.8 - C) p^{-0.9529})$$
$$+ 1.271376 * 10^{8} \sin\theta / (G^2 (6.6633 * 10^{-4}$$
$$+ 2.638 * 10^{-5} (p - 0.8436132)^{0.731})(C - 0.8)$$
$$+ 0.16375321 (1.8 - C) p^{-0.9529})) /$$
$$(1.271376 * 10^{12} G^{-2}$$
$$+ 1.928378 * 10^{-5} (C - 0.8)(p - 0.8436132)^{-0.269}$$
$$+ 0.38450601 * 10^{-4} C p^{-0.5}$$
$$+ 0.1522259 * 10^{-5} C p^{-0.5} (p - 0.8436132)^{0.731}$$
$$- 0.9449358 * 10^{-2} C p^{-1.4529}$$
$$- 0.1560403 (1.8 - C) p^{-1.9529}) \qquad (3.16)$$

For helical test sections, Eq. (3.16) remains valid except that the gravity terms will be negative as in the

present study, the direction of refrigerant flow in the helical test specimens is from top to bottom. For the straight and spiral configurations, however, the pressure gradient terms due to gravity will be zero, since θ is zero. Therefore, the governing equation for the pressure gradient, for these two cases, (i.e. straight and spiral) reduces to

$$\begin{aligned}(dp/dl) = &- (f_{TP} / 2d)((6.6633 * 10^{-4} \\ &+ 2.638 * 10^{-5} (p - 0.8436132)^{0.731} (C - 0.8) \\ &+ 0.16375321 (1.8-C) p^{-0.9529})/ (1.271376 * 10^{12} G^{-2} \\ &+ 1.928378 * 10^{-5} (C - 0.8) (p - 0.8436132)^{-0.269} \\ &+ 0.38450601 * 10^{-4} C p^{-0.5} \\ &+ 0.1522259 * 10^{-5} C p^{-0.5} (p - 0.8436132)^{0.731} \\ &- 0.9449358 * 10^{-2} C p^{-1.4529} \\ &- 0.1560404 (1.8 - C) p^{-1.9529})\end{aligned} \qquad (3.17)$$

Niaz and Davis (18) also developed an expression similar to Eq. (3.17) as follows:

$$\begin{aligned}(dp/dl) = &(fp / 2d) (0.84372 * 10^{3} p (C - 0.8) \\ &+ 40.5 (1.8 - C)) / \\ &(1.3392 * 10^{8} p^{2} / G^{2} + 0.335574 * 10^{5} C p^{1.5} \\ &- 0.1610853 C p^{0.5} + 40.5 C - 72.9)\end{aligned} \qquad (3.17a)$$

After making appropriate substitutions for f_{TP} in Eqs (3.16) and (3.17), one gets (dp/dl) as a function of d, G, p and C. These expressions for dp/dl can be easily integrated to determine the capillary length for a particular pressure drop or vice versa, for the desired configuration.

3.2 Friction Factor and Reynolds Number

(i) Straight Test Section

The findings of Mikol (15) revealed that the viscosity of the liquid phase was much more significant than that of the vapour phase. This has also been pointed out by Marcy (7). Further, Mikol suggested that, in the two-phase region of flow through a capillary, an apparent friction factor could be used which is related to the Moody friction factor for the flow of a pure liquid, by:

$$f_{TP_{(apparent)}} / f_l \simeq 0.95.$$

On the otherhand, Whitesel (10) recommended that the friction factor should be calculated using an average viscosity found from the values for the liquid and gas phases, weighted according to their respective mass fractions.

According to Niaz and Davis (18), the friction factor is considerably more complex than indicated by

either of the above approaches. They, however, found experimentally the single phase liquid friction factor, as follows:

$$f_l = 0.324 / Re^{0.25} \qquad (3.18)$$

They also expressed viscosity of liquid R-12 as

$\mu_l = 3.3962151 / p^{0.18}$, with 1% error over the temperature range -20 °C to 50 °C. Substituting the above expression for μ_l in Eq (3.18), they obtained,

$$f_l = 0.43984 / (G d p^{0.18})^{0.25} \qquad (3.19)$$

They solved Eq (3.17a) using Eq (3.19) for friction factor and found that the length calculated for a given pressure drop is approximately 10% greater than that obtained experimentally by them. They have also pointed out that the value of f used by them was too low.

In the present investigation, the Eq (3.18) has been modified and substituted for f_{TP} in Eq (3.17). Therefore, more accurate curve fit expression for μ_l and μ_g have been obtained as follows:

$$\mu_l = 1.29924141 / p^{0.277} \qquad (3.20)$$

$$\mu_g = 0.03909286\ p^{0.07721914} \qquad (3.21)$$

The expressions (3.20) and (3.21) are valid in the temperature range - 40 °C to 50 °C with curve fit errors of 0.4064% and 0.8556%, respectively.

From Eqs (3.18) and (3.20) one gets,

$$f_l = 0.3459134 7 / (Gd)^{0.25} p^{0.06925} \qquad (3.22)$$

Using Eq (3.22) for f_{TP} , the Eq (3.17) has been solved. The results are presented in Chapter IV.

The two-phase flow friction factor, f_{TP}, has also been obtained as a function of two-phase flow Reynolds number, Re_{TP} , from the experimental results. R_{TP} is defined as,

$$Re_{TP} = Gd / \mu_{TP} \qquad (3.23)$$

where, μ_{TP}, according to McAdams (1), is given by the expression;

$$1 / \mu_{TP} = x / \mu_g + (1 - x) \mu_l \qquad (3.24)$$

where, μ_l and μ_g are substituted from Eqs (3.20) and (3.21), respectively.

The relation between f_{TP} and Re_{TP} has been obtained in the same form as Eq (3.18) for single phase flow. This is consistent with the suggestions of Collier (23). The local two-phase flow friction factor values are obtained using Eq (3.17) in the following form:

$$f_{TP} = - 2d (dp/dl) (1.271376 * 10^{12} G^{-2}$$
$$+ 1.928378 * 10^{-5} (C - 0.8) (p - 0.8436132)^{-0.269}$$
$$+ 0.38450601 * 10^{-4} C p^{-0.5}$$

$$+ 0.1522259 * 10^{-5} C p^{-0.5} (p - 0.8436132)^{0.731}$$
$$- 0.9449358 * 10^{-2} C p^{-1.4529}$$
$$- 0.1560403 (1.8 - C) p^{-1.9529}) /$$
$$((6.6633 * 10^{-4} + 2.638 * 10^{-5} (p - 0.8436132)^{0.731}) (C - 0.8)$$
$$+ 0.16375321 (1.8 - C) p^{-0.9529}) \qquad (3.25)$$

The value of f_{TP} is obtained at the pressure points along the length of the test section. In order to evaluate pressure gradient (dp/dl), a polynomial is fitted using the observed pressure data, for each set of readings. The polynomial, thus obtained, is differentiated, with respect to length to yield the value of (dp/dl). This value of (dp/dl) is then substituted in Eq. (3.25) along with other parameters to obtain the value of f_{TP}. The local values of Re_{TP} are also obtained using Eqs. (3.23) and (3.24). Using the set of values for f_{TP} and Re_{TP}, derived above, the step-wise linear regression program* is used to determine the constants in the following relation:

$$f_{TP} = A\, Re_{TP}^{B} . \qquad (3.26)$$

The exact form of this equation using the data of the present investigation, is given in Chapter IV.

---

*The program was developed by

Dr. Potluri Rao
Professor of Econommetric
University of Chicago
U.S.A.

(ii) Helical Test Section

For this configuration, no two-phase flow friction factor correlation is available in literature, not even for large diameter tubes. However, for single phase turbulent flow in coils, Mori and Nakayama (19) present the following relation for evaluating the friction factor:

$$f_l = 0.3\,(d/D)^{0.5} / (Re\,(d/D)^2)^{0.2} * (1.0 + 0.112 / (Re\,(d/D)^2)^{0.2} \quad (3.27)$$

In the present study, a two-phase flow friction factor correlation has been developed for the helical configuration in a manner similar to that for the straight test section by using the experimental data on helical test sections. The local two-phase flow friction factor values are first obtained using the Eq. (3.16) in the following form:

$$\begin{aligned} f_{TP} = -\,2d\,(dp/dl)\,((& 1.271376 * 10^{12}\,G^{-2} \\ & + 1.923878 * 10^{-5}\,(C - 0.8)\,(p - 0.8436132)^{-0.269} \\ & - 0.1560304\,(1.8 - C)\,p^{-1.9529} \\ & + 0.1522259 * 10^{-5}\,C * p^{-0.5}\,(p - 0.8436132)^{0.731} \\ & + 38450601 * 10^{-4}\,C * p^{0.5} \\ & - 0.9449358 * 10^{-2}\,C * p^{-1.4529} \\ & - 1.271376 * 10^{8} \sin\theta / (G^2 * (6.6633 * 10^{-4} \end{aligned}$$

$$+ 2.638 * 10^{-5} (p - 0.8436132)^{0.731})$$
$$(C - 0.8) + 0.16375321 (1.8 - C) p^{-0.9529})) /$$
$$((6.6633 * 10^{-4} + 2.638 * 10^{-5} (p - 0.8436132)^{0.731})$$
$$(C - 0.8) + 0.16375321 (1.8 - C) p^{-0.9529})$$

(3.28)

Step-wise linear regression technique is then used for obtaining a curve-fit expression of the form :

$$f_{TP} = A' (Re_{TP})^{B'} (D / d)^{C'} \qquad (3.29)$$

The evaluation of constants (A', B', C') for the above equation is discussed in Chapter IV.

(iii) Spiral Test Section

The most recent work on this configuration is due to Ali and Seshadri (22). They have studied the flow of water in polythene Archimedian spirals; the direction of flow being from the centre towards the periphery. The turbulent, single phase friction factor expression, developed by them, is :

$$f = 0.65 * Re^{-0.18} (d (P 1)^{-0.5})^{0.5} (R_o (P 1)^{-0.5})^{0.75}$$
$$((R_o - R_i) (P 1)^{-0.5})^{0.75} \qquad (3.30)$$

In the present work, two-phase flow friction factor correlation has been developed for spiral

configuration, using the experimental data. The local values of two-phase flow friction factor are obtained from the Eq. (3.25). Step-wise linear regression program is employed to obtain a curve fit expression of the form:

$$f_{TP} = A'' \, Re^{B''} \, (d / (P\ \ 1)^{0.5})^{C''} \, (R_o / (P\ 1)^{0.5})^{D''} \, ((R_o - R_i) / (P\ 1)^{0.5})^{E''} \qquad (3.31)$$

The evaluation of constants appearing in the above equation is discussed in Chapter IV.

CHAPTER IV

RESULTS AND DISCUSSION

As mentioned earlier, capillary tubes of straight, helical and spiral configurations of various sizes have been tested to study their relative performance for the flow of refrigerant-12, under various inlet conditions. The results for each configuration are presented and discussed, separately.

4.1 Straight Section

In the experimental investigation relating to straight test specimens, the following parameters have been varied:

(i) diameter and length of the capillary tube

(ii) temperature and pressure at the inlet to the test section.

This, automatically, results in the variation of the mass-flow rate of the refrigerant during experimentation. The mass-flow rate also is, therefore, considered as an additional variable.

Eight test sections of different sizes have been tested under various inlet conditions as stated in Table 1.1 (Chapter I). All the recorded data are analysed

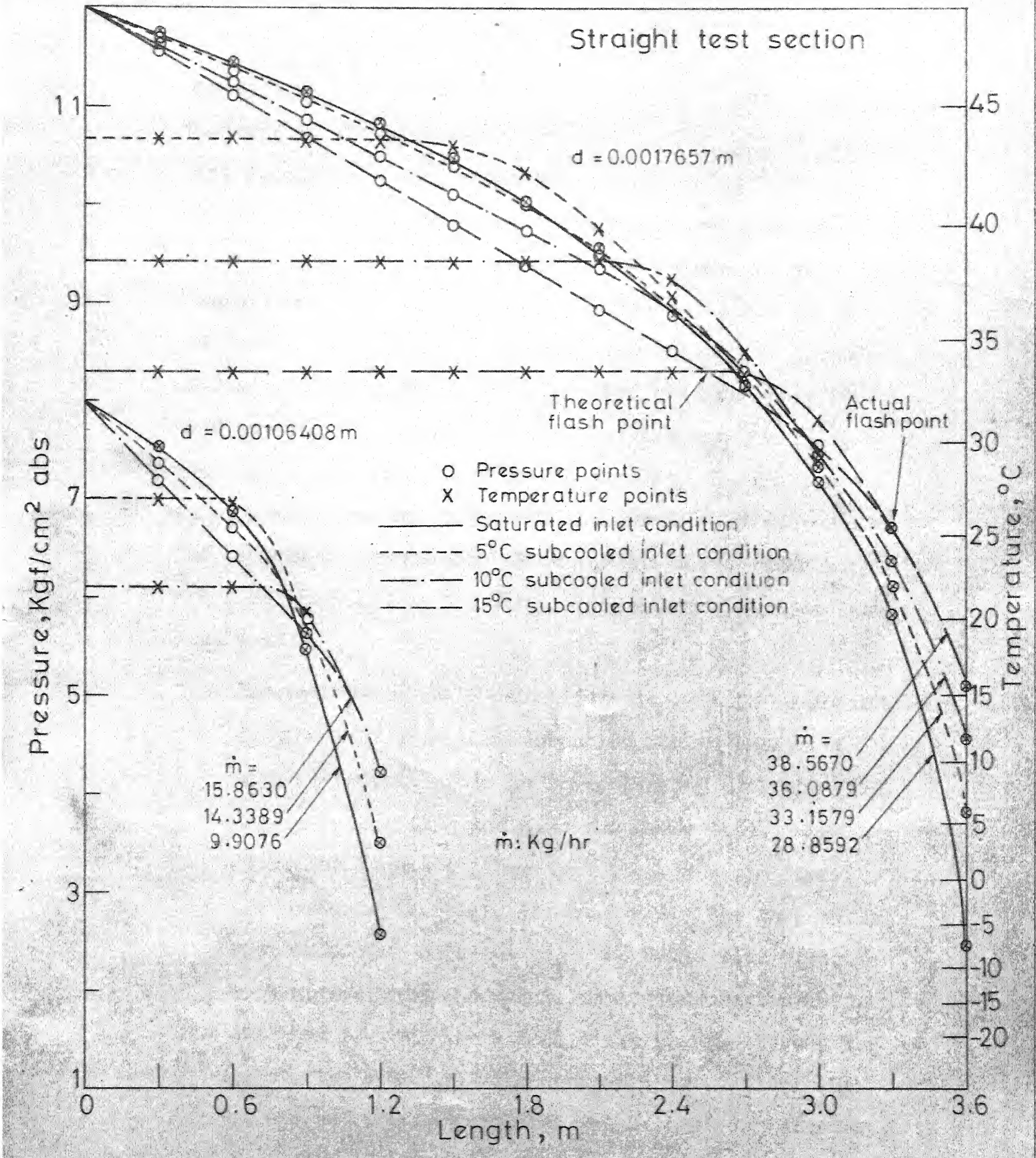

Fig.4.1 Pressure-temperature variation with capillary length for different inlet temperatures at a particular inlet pressure

and plotted for various parameters. When pressure and temperature are plotted against length for particular sized test specimens, under saturated and subcooled conditions of the refrigerant at a specified inlet pressure, it is observed that the trend of the pressure-temperature vs length curves is similar in nature for all other inlet pressures. Therefore, it is felt unnecessary to include all the plots in this work. However, data for only two test specimens of sizes, the largest and the smallest, are plotted in Fig. 4.1. for the highest and the lowest inlet pressures, respectively, for purposes of discussion. The flow rates corresponding to various inlet conditions are also shown. The following observations are made from Fig. 4.1:

(i) The phenomenon of metastability is seen to occur in all the test runs when subcooled liquid enters the test specimens. This is in conformity with the findings of Mikol (15) and Niaz and Davis (18). When subcooled liquid is throttled through a capillary tube, the pressure decreases linearly while the temperature remains almost constant till the saturation pressure corresponding to subcooled liquid temperature is attained at the theoretical flash point. Beyond this point, the pressure decreases at a rate faster than before and the temperature, which is so far constant,

starts falling, rather, slowly initially, thereby, causing the liquid refrigerant to remain at a metastable - superheated state. This state persists in the flow upto the actual flash point where the degree of superheat is sufficient enough to cause bubble nucleation. In the case of saturated liquid entry, on the other hand, a thermodynamic equilibrium exists and, hence, nucleation takes place as soon as the pressure starts decreasing.

Further, it is noticed from the figure that the metastable length* decreases with the increase of the degree of subcooling. This is because the slope of the pressure curve at the theoretical flash point decreases with the increase of the degree of subcooling. The tendency of the temperature to lag behind is, thus, reduced, which results in the reduction of the metastable length.

ii) For a particular sized specimen, at a given inlet pressure, the exit pressure and the flow rate increase as the inlet temperature changes from saturated to subcooled conditions. Also, it is noticed that the higher the degree of subcooling, the lower the rise in the exit pressure. The above observations may be explained as follows:

---

*metastable length is defined as the capillary length between the theoretical and the actual flash points as shown in Fig. 4.1 for 15 ^{o}C subcooled inlet condition, as an illustration.

Under two-phase flow conditions, the resistance to flow in the capillary is greater than that for the single phase flow situation. This is supposed to be due to

(i) the change of phase from liquid to vapour and

(ii) the irreversible mixing of the liquid and the vapour phases.

This increase in resistance causes the flow rate through the capillary to decrease, with the result that the pressure at the exit of the capillary reduces to a value lower than that observed under single phase flow conditions. The figure, however, shows that both the exit pressure and the flow rate increase with an increase in the degree of subcooling. This is due to the fact that the two-phase flow length (i.e. the length from the actual flash point to the capillary exit), where greater resistance to the flow and hence a higher pressure drop occurs, gradually decreases as one moves from the saturated towards the subcooled conditions. As expected, the two-phase flow length for the 15 ^{o}C subcooled condition is seen to be the minimum. From the figure 4.1, it can also be seen that the two-phase flow portions of the curves become much steeper as the subcooling at the inlet to the capillary decreases. This explains the lower rate of rise in the inlet pressures with increased subcooling.

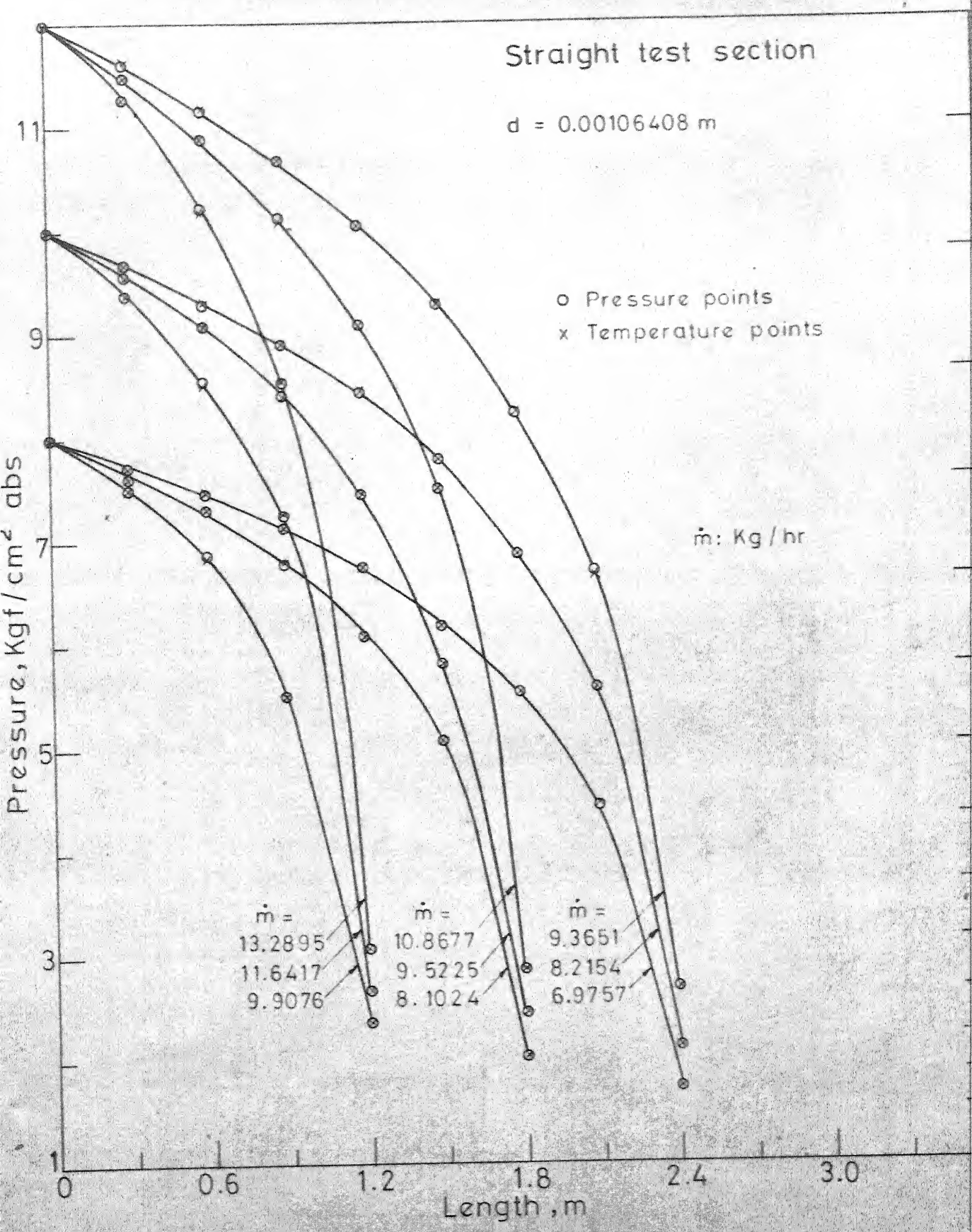

Fig.4.2(a) Pressure and temperature vs. capillary length for saturated liquid at different inlet pressures

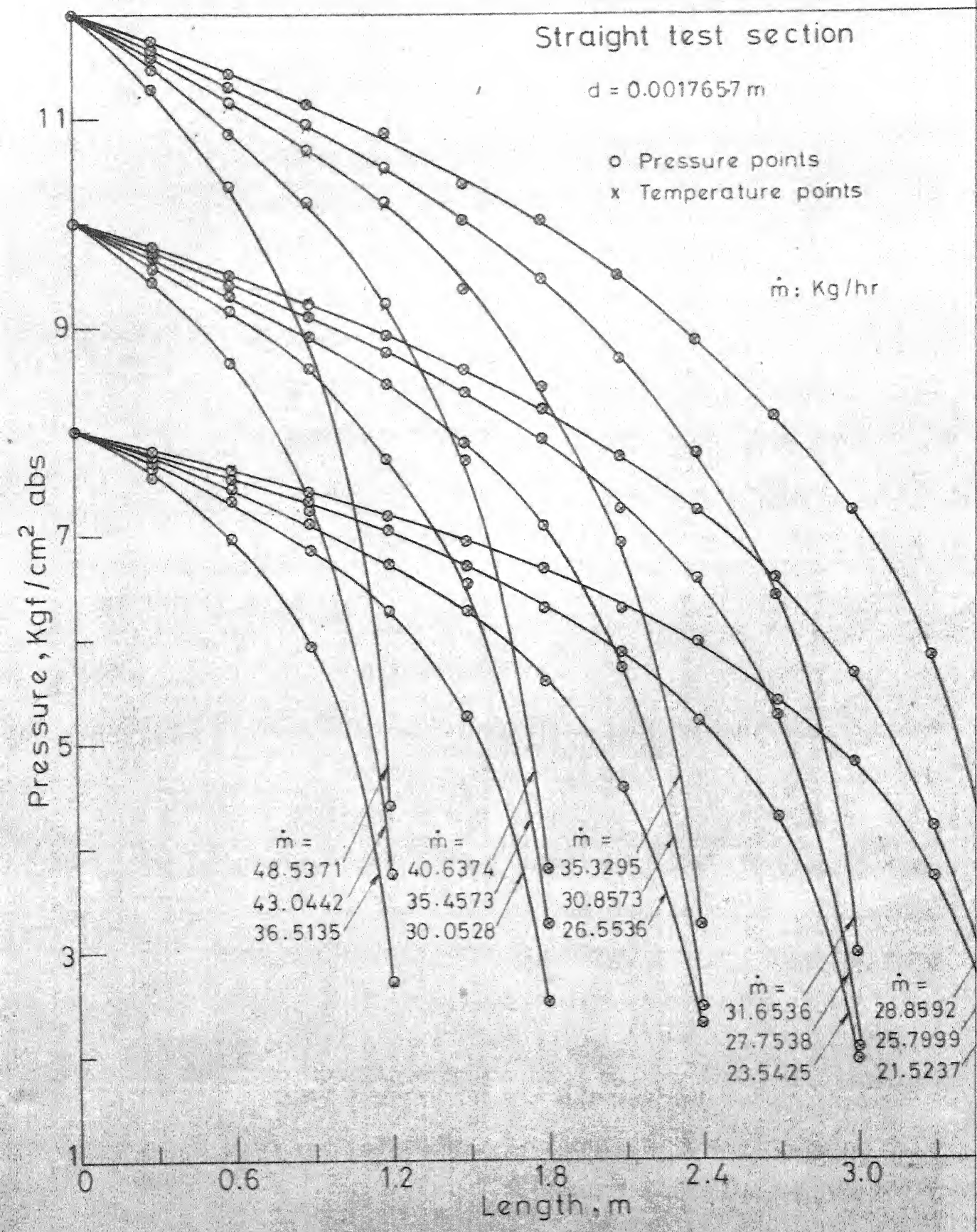

Fig.4.2(b) Pressure and temperature vs. capillary length fo
saturated liquid at different inlet pressures

Figures 4.2 (a) and 4.2 (b) show pressure-temperature variation with the capillary length for saturated liquid at different inlet pressures for the capillary-tube diameters of 0.0010640 m and 0.0017657 m, respectively. Refrigerant flow rates, $\dot{m}$, corresponding to various test section lengths and inlet pressures are also shown in the figures. The following observations are made about the plots:

(i) For saturated inlet conditions, no metastability occurs and the pressure and temperature behave, as expected, in accordance with the saturation relationship. This confirms the accuracy of the test observations.

(ii) For the same initial pressure and temperature conditions, the exit pressure and the flow rate are seen to decrease non-linearly with increased length of the capillary. This is explained by the fact that as the capillary length increases, the resistance to flow increases non-linearly. This situation is also encountered in the case of single-phase flow.

(iii) Comparing figures 4.2 (a) and 4.2 (b), it is observed that for the same inlet state of the refrigerant and the capillary length, the flow rate decreases appreciably for the case of the

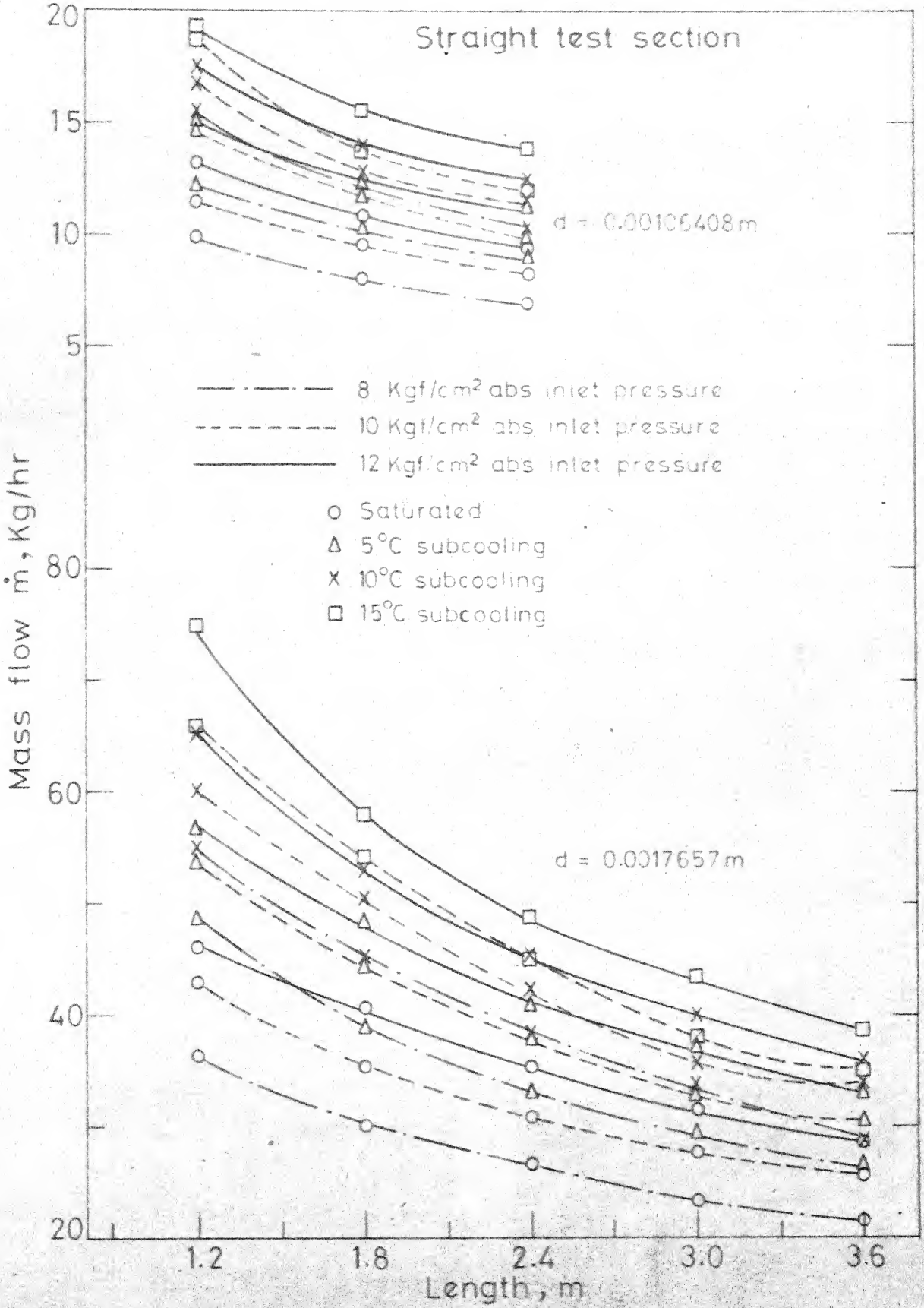

Fig 4.3 Mass flow rate of R-12 vs. length of capillary

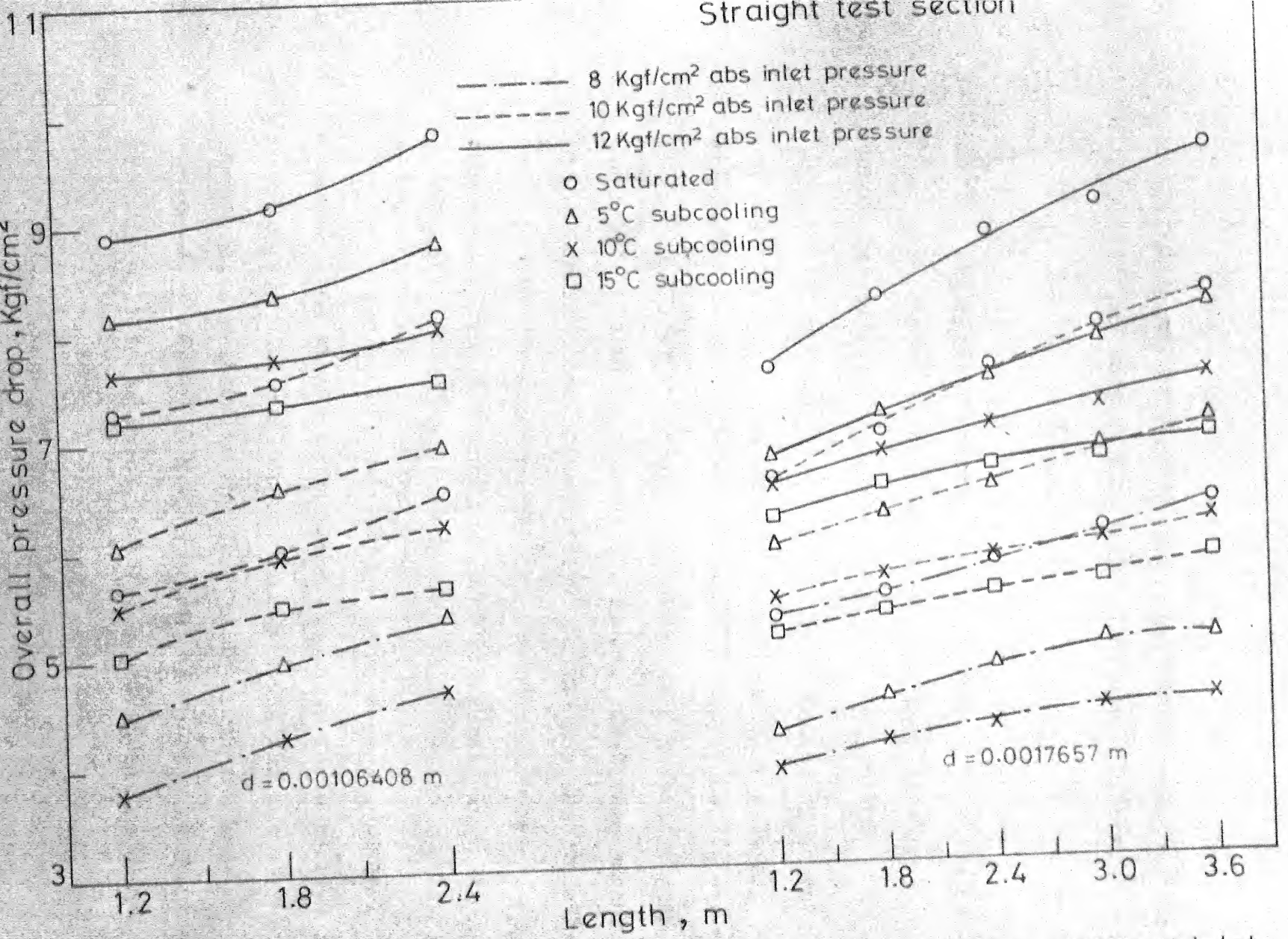

Fig. 4.4 Overall pressure drop vs. length of capillary tube for different inlet conditions and diameters

small diameter capillary tube, as expected. The exit pressure is also observed to be lower for the case of the small diameter capillary.

In Fig. 4.3, the variation of the mass flow rate with capillary length is shown for all inlet conditions and the two capillary tube-diameters. As expected, the mass flow rate is seen to decrease with increased capillary length, due to the increase in resistarce.

Figure 4.4, represents the variation of overall pressure drop with the length of the capillary tube for different inlet conditions and the two capillary-diameters. It is found that the overall pressure drop increases with the length of the capillary tube and is relatively higher for the small diameter capillary. It is also observed that for a particular sized capillary, the overall pressure drop decreases with the decreasing inlet pressure. This is as it should be.

Figures 4.3 and 4.4 may be used as charts to determine the straight capillary tube size for a refrigeration system. The method demonstrating the use of these charts for a particular application is presented and discussed in detail in Appendix - D. Referring to the Appendix - D, it is found that for a refrigeration unit of 0.3175 ton capacity operating between 0 ^{o}C and 41 ^{o}C, the capillary tube length required to give the desired

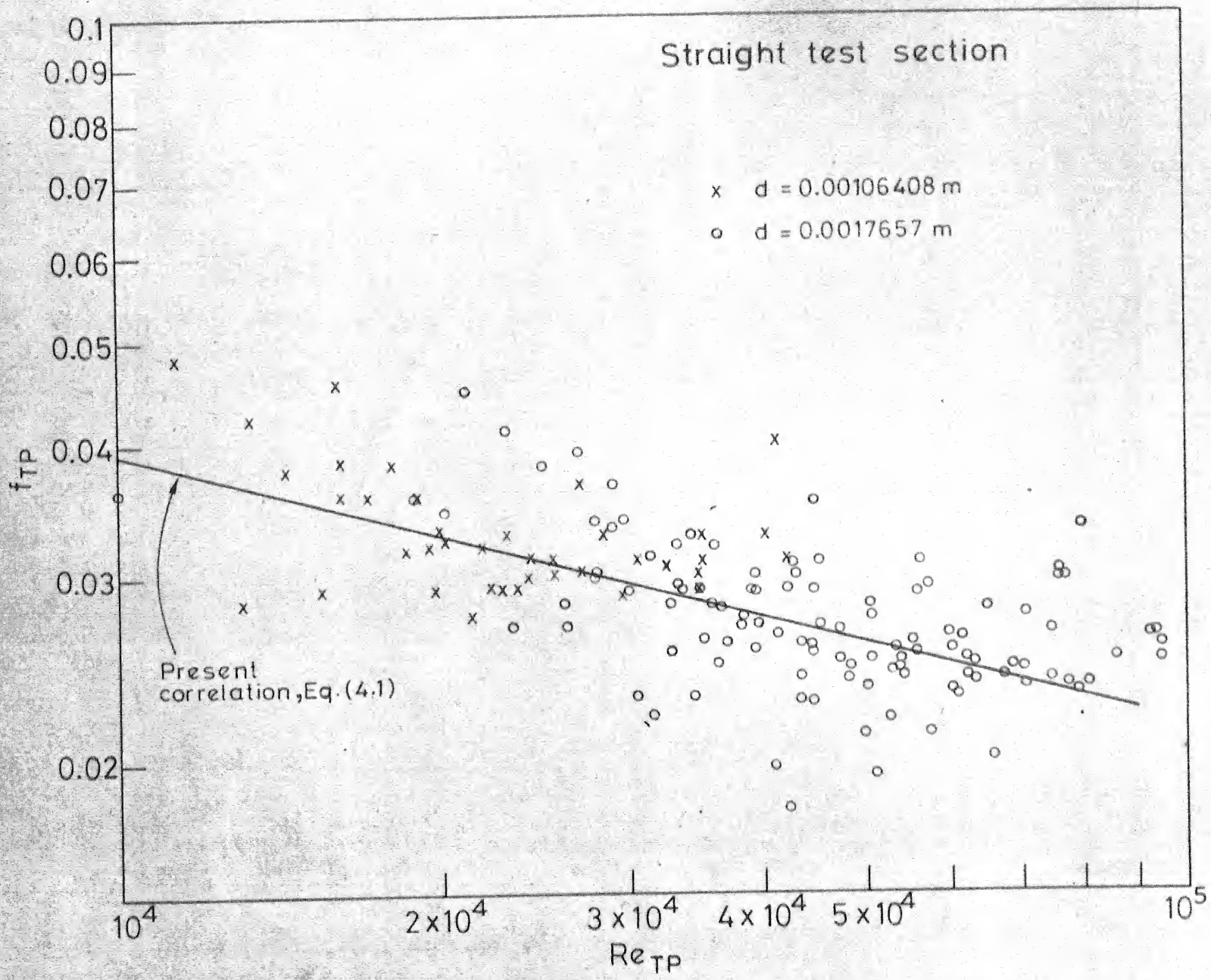

Fig. 4.5 Friction factor vs. Reynolds number for different sized capillary tubes

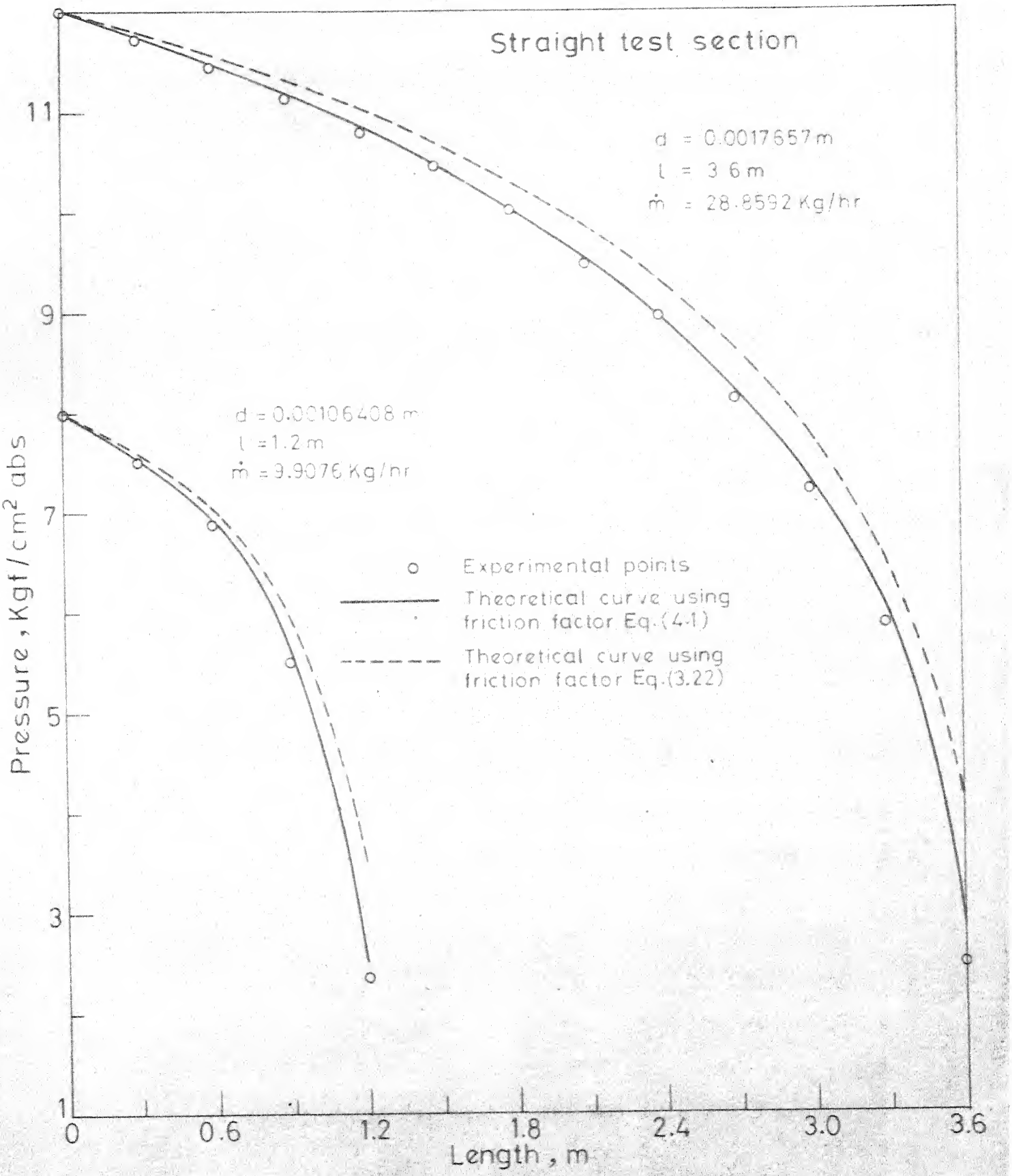

Fig. 4.6 Comparison of theoretical and experimental results

pressure drop is 3.36 m, for a 0.0017657 m diameter capillary tube.

Figure 4.5 gives the variation of local values of the two-phase flow friction factor, f_{TP}, with the two-phase Reynolds number, Re_{TP}, determined by the method described in Chapter III. Large scattering of the data for the local values of the friction factor is discerned due to the random character of the two-phase flow phenomenon. The two-phase flow Reynolds numbers for the above data, are seen to lie in the range 10^4 - 10^5. Figure 4.5 also shows the curve obtained by using the friction factor correlation :

$$f_{TP} = 0.412518 / R_{eTP}^{\,0.255611} . \qquad (4.1)$$

The above correlation is derived by substituting the values of the constants A and B in Eq. (3.26). The constants A and B are determined by the regression technique, employing the data gathered during the present investigation.

Figure 4.6 compares the present theoretical and experimental pressure values for the two different capillary tube sizes. The theoretical values have been obtained in two different ways by substituting relations (4.1) and (3.22) for the friction factor in the general Eq. (3.17) for (dp/dl). It is seen that the experimental points are in closer agreement with the theoretical curve obtained by using Eq. (3.17) and the friction factor

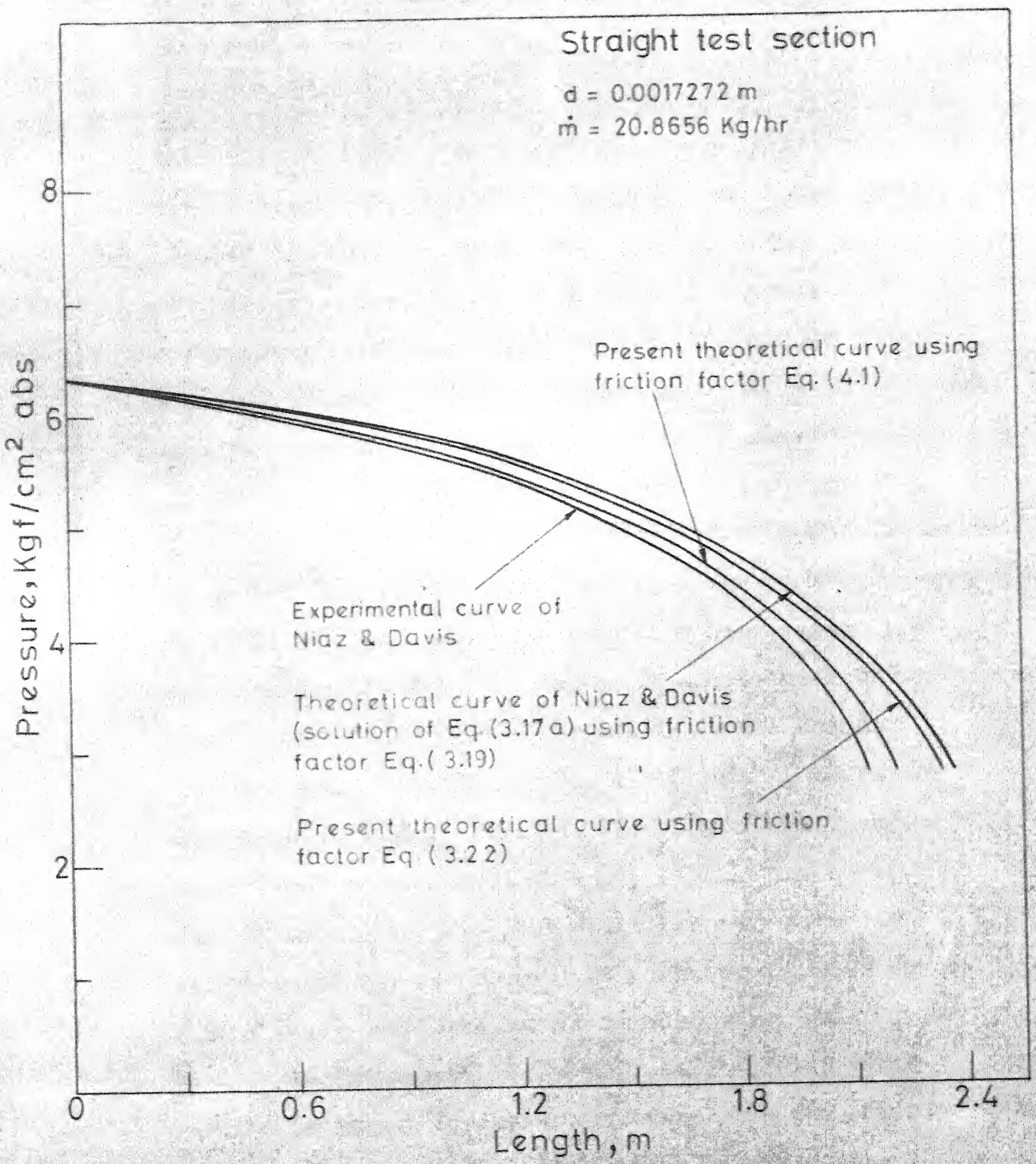

Fig. 4.7 Comparison of present theoretical result with the result of Niaz and Davis

relation (4.1). This proves the accuracy of the present developed correlation (4.1) for the friction factor.

Also, the present theoretical results for the variation of local pressure vs capillary length have been compared with both the theoretical and the experimental results of Niaz and Davis (18), in Fig. (4.7). It is obvious that there is too much deviation between the experimental and theoretical results of Niaz and Davis, specially towards higher capillary lengths. Niaz and Davis realized that in the derivation of their theoretical results, the friction factor used was too low. An attempt has, therefore, been made in the present investigation to improve their friction factor by developing a new curve-fit expression (3.20) for f_1. The resulting expression (3.22) obtained for the friction factor is substituted in the general expression (3.17) for (dp/dl). The theoretical pressure values yielded by Eq. (3.17) with (3.22) have also been plotted in Fig. (4.7). It is found that the theoretical curve, thus obtained, is slightly lower than that of Niaz and Davis, but still far away from their experimental curve. However, the friction factor correlation (4.1) developed in the present work, when substituted in the general Eq. (3.17) for (dp/dl), gives results which are in better agreement with the experimental findings of Niaz and Davis. Therefore, the theoretical [illegible] presented by Eqs. (3.17) and (4.1), are recommended for the design of straight capillary tubes for refrigeration systems in the temperature range -35 °C to 50 °C.

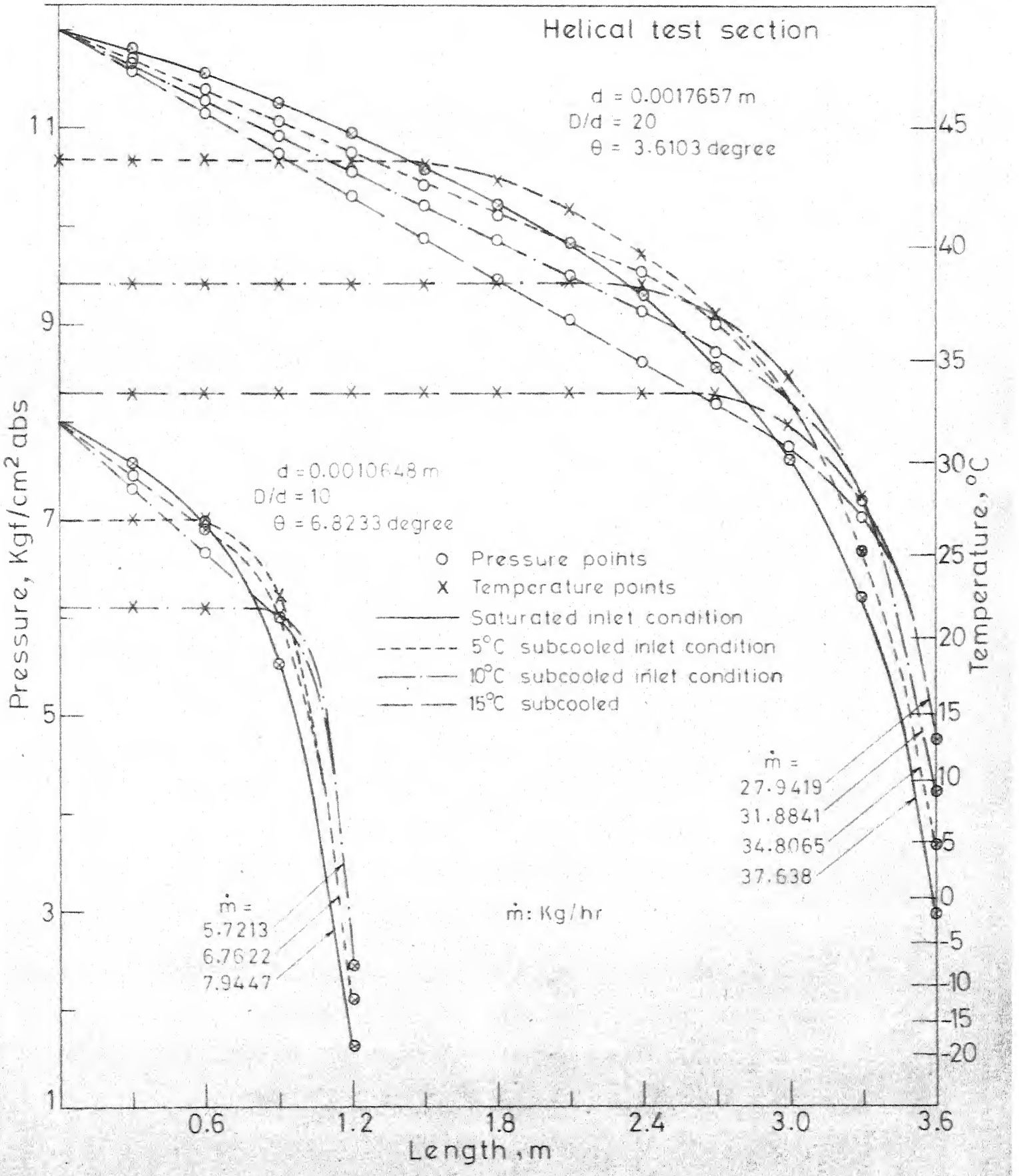

Fig. 4.8 Pressure-temperature variation with capillary length for different inlet temperatures at a particular inlet pressure

4.2 Helical Section

Fifteen helical test sections of various tube diameters, lengths and coil to tube diameter ratios (D/d) have been studied at saturated and subcooled inlet conditions as mentioned in Table 1.1. The variables associated with this test series are, therefore, the diameter, length, D/d ratio, the temperature and pressure at the inlet and the refrigerant mass-flow rate. The effect of helix angle has not been studied. It has, however, been assumed that its effect is negligible in comparison to other parameters.

All the data collected on helical test sections are analysed and plotted. Since, the trend of the curves is found similar to those of the straight section, only a few representative curves are presented for discussion.

Figure 4.8, shows the variation of pressure and temperature with the length of the capillary tube for various refrigerant inlet conditions and two sizes of the helical specimens. Mass flow rate corresponding to each test run is also shown in the figure. The following observations are made:

(i) metastability is found to occur for subcooled refrigerant flow through the capillary as observed in the case of the straight section. The metastable length is also seen to decrease with increased subcooling.

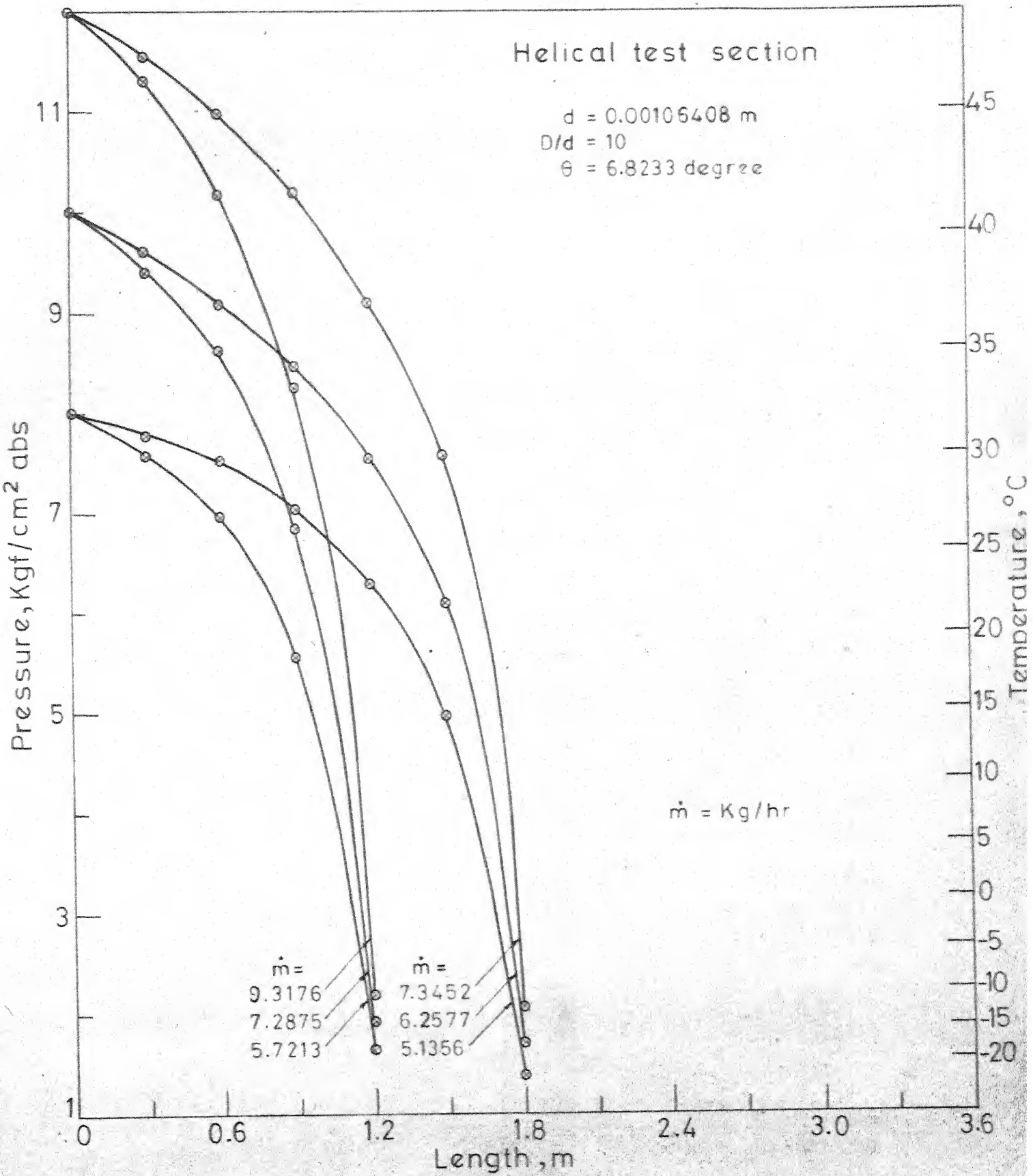

Fig.4.9(a) Pressure and temperature vs. capillary length for saturated liquid at different inlet pressures

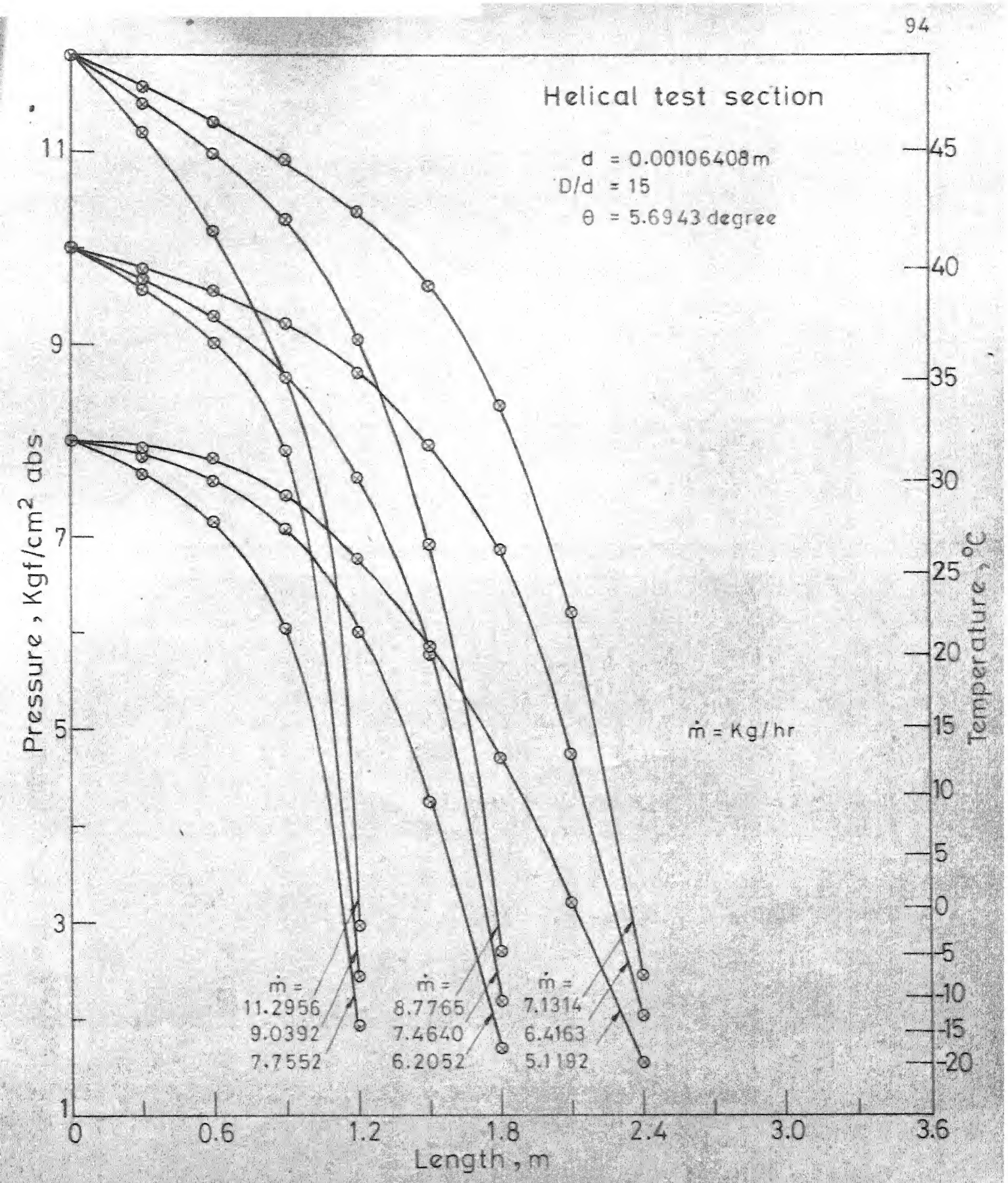

Fig.4.9(b) Pressure and temperature vs. capillary length for saturated liquid at different inlet pressures

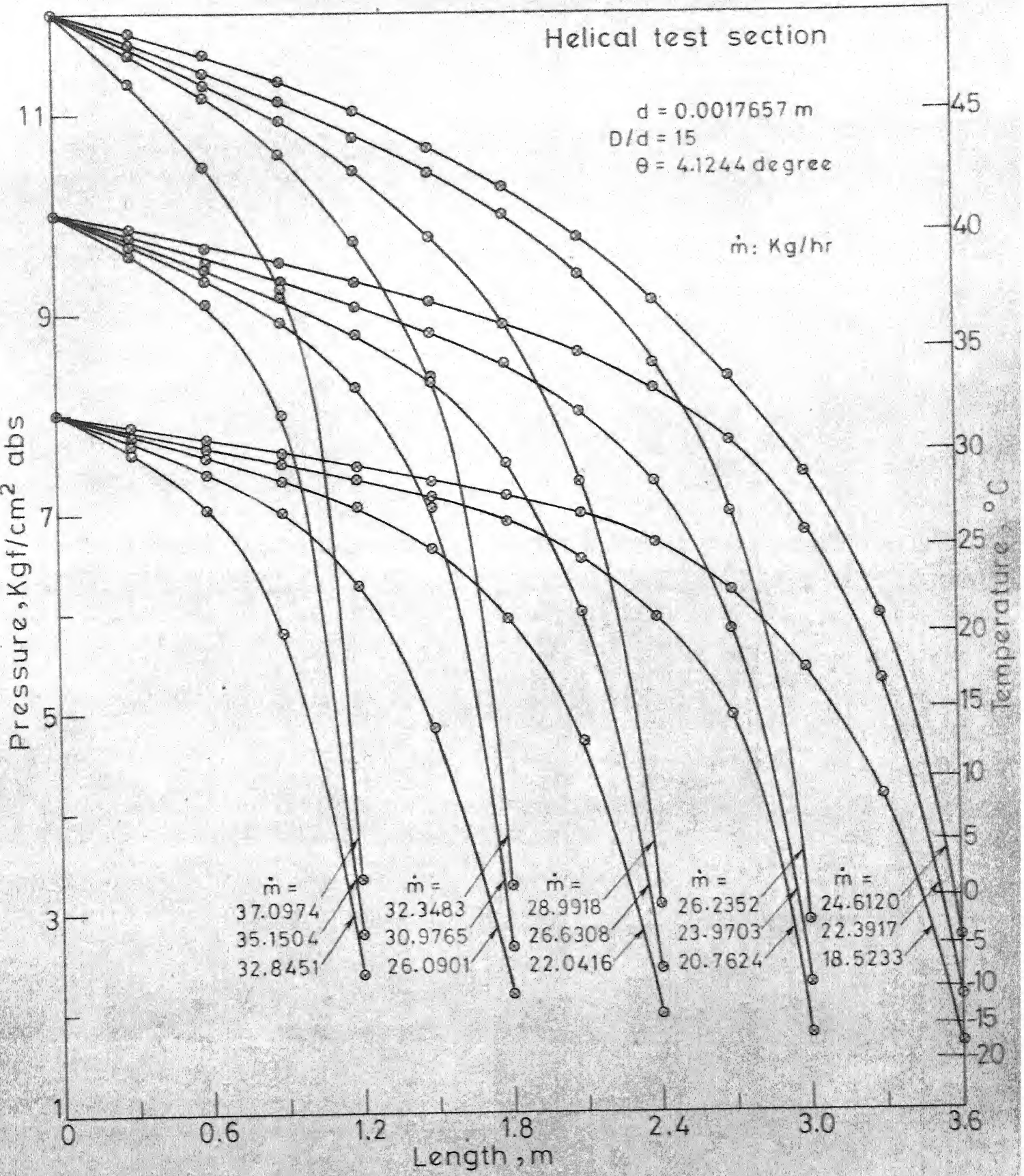

Fig. 4.9(c) Pressure and temperature vs. capillary length for saturated liquid at different inlet pressures

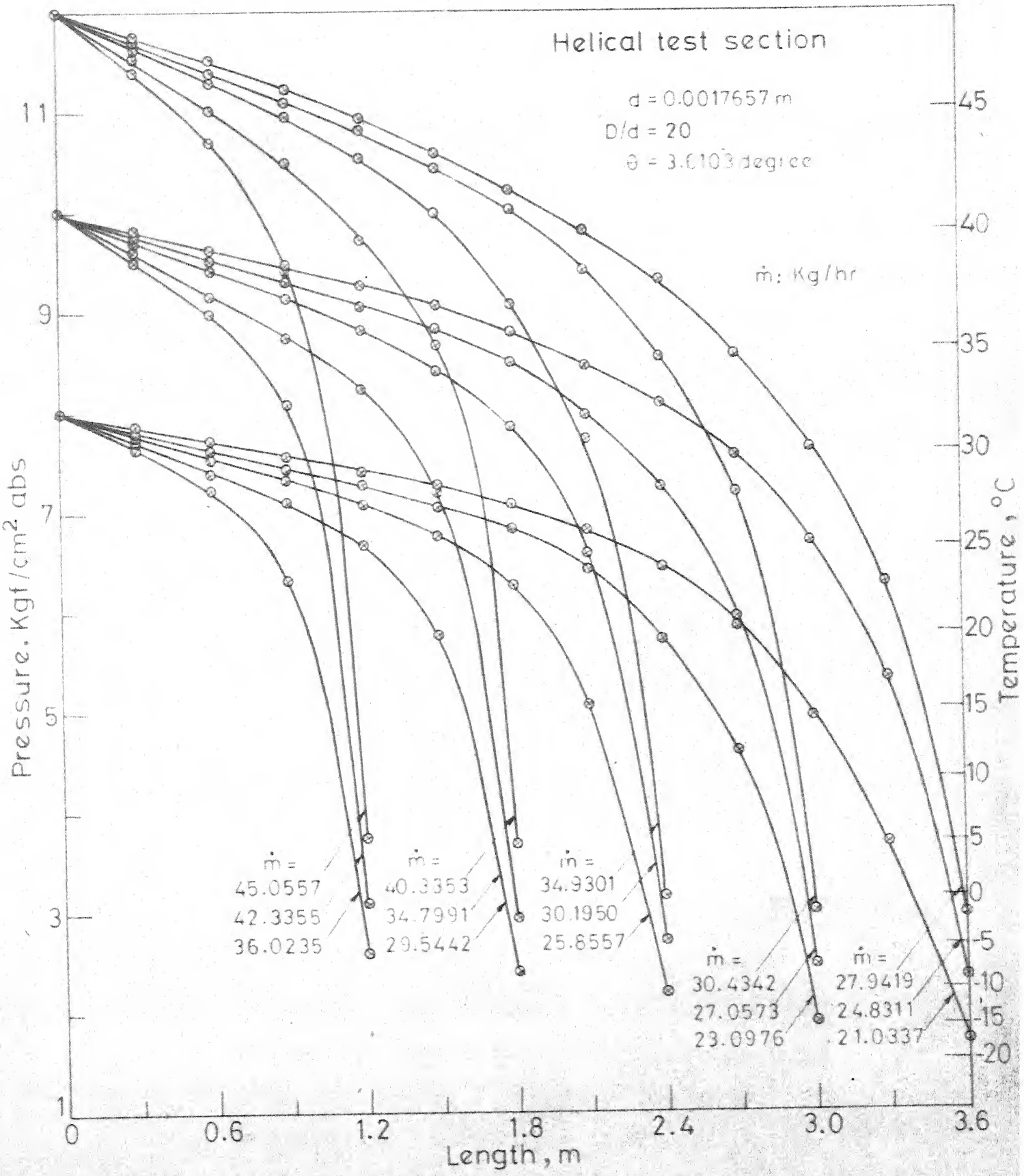

Fig. 4.9(d) Pressure and temperature vs. capillary length for saturated liquid at different inlet pressures

(ii) the exit pressure and the flow rate increase as the inlet temperature decreases from the saturated to the subcooled condition.

It is also observed that the greater the degree of subcooling, the lower the rise in the exit pressure.

The reasons for the above findings are the same as already explained for the straight section.

Figures 4.9 (a) through (d) demonstrate the pressure-temperature variation with the capillary length for various saturated refrigerant inlet conditions. As for the straight section, the pressure and temperature follow the saturation relationship. Also, the exit pressure and the flow rate decrease non-linearly with capillary length for the same initial temperature-pressure conditions. It is further observed that:

(i) the exit pressure and the flow rate decrease appreciably with decrease of the capillary diameter, for the same inlet conditions, length and D/d ratio, as can be seen from figures 4.9 (b) and 4.9 (c).

(ii) compared with the straight section, the exit pressure and the flow rate in the helical case, are relatively smaller in values, for identical inlet conditions and capillary tube sizes. This is because of the secondary flows developed in the helical section due to its curvature. The

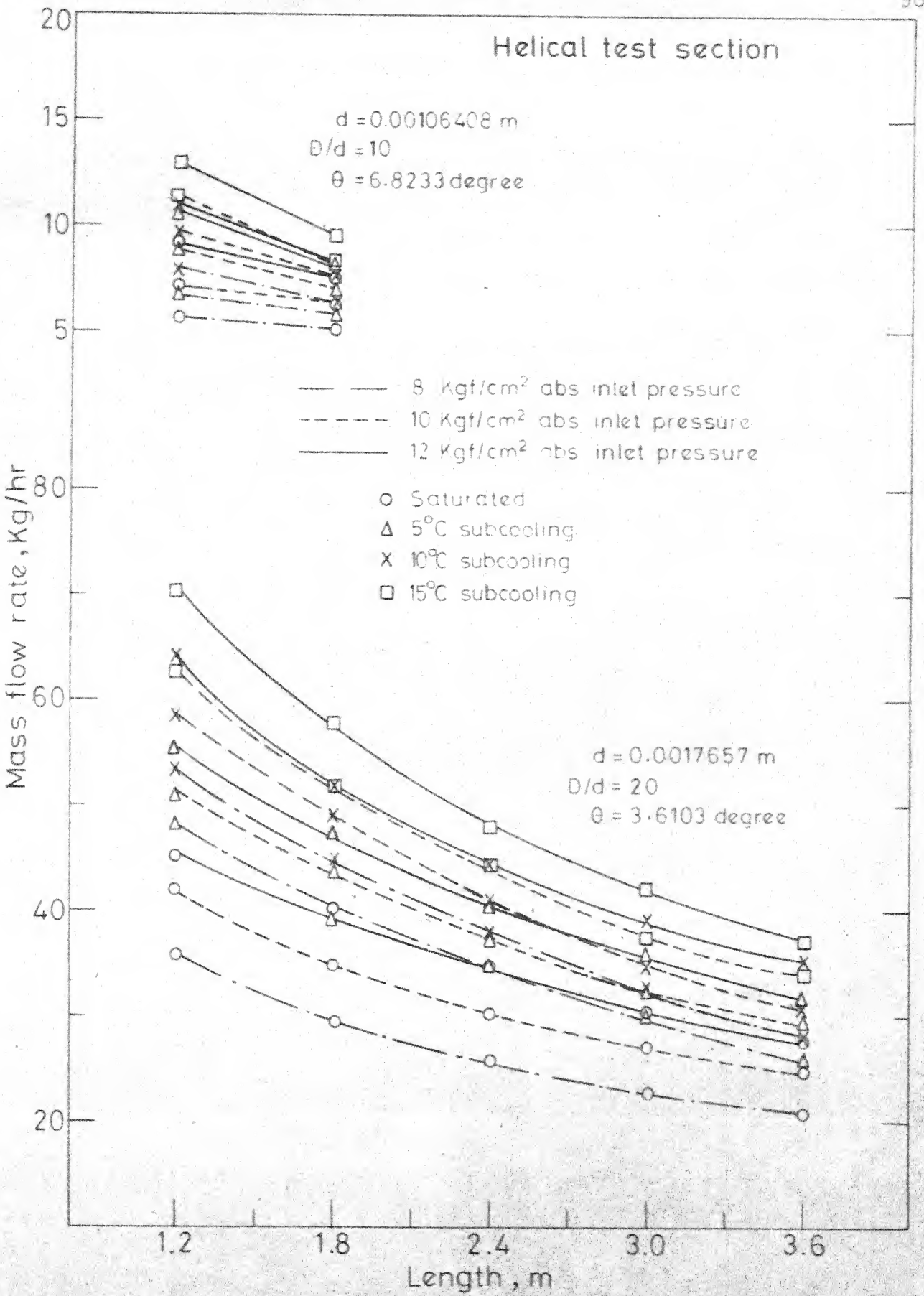

Fig. 4.10(a) Mass flow rate of R-12 vs. length of capillary tube for different inlet conditions and diameters

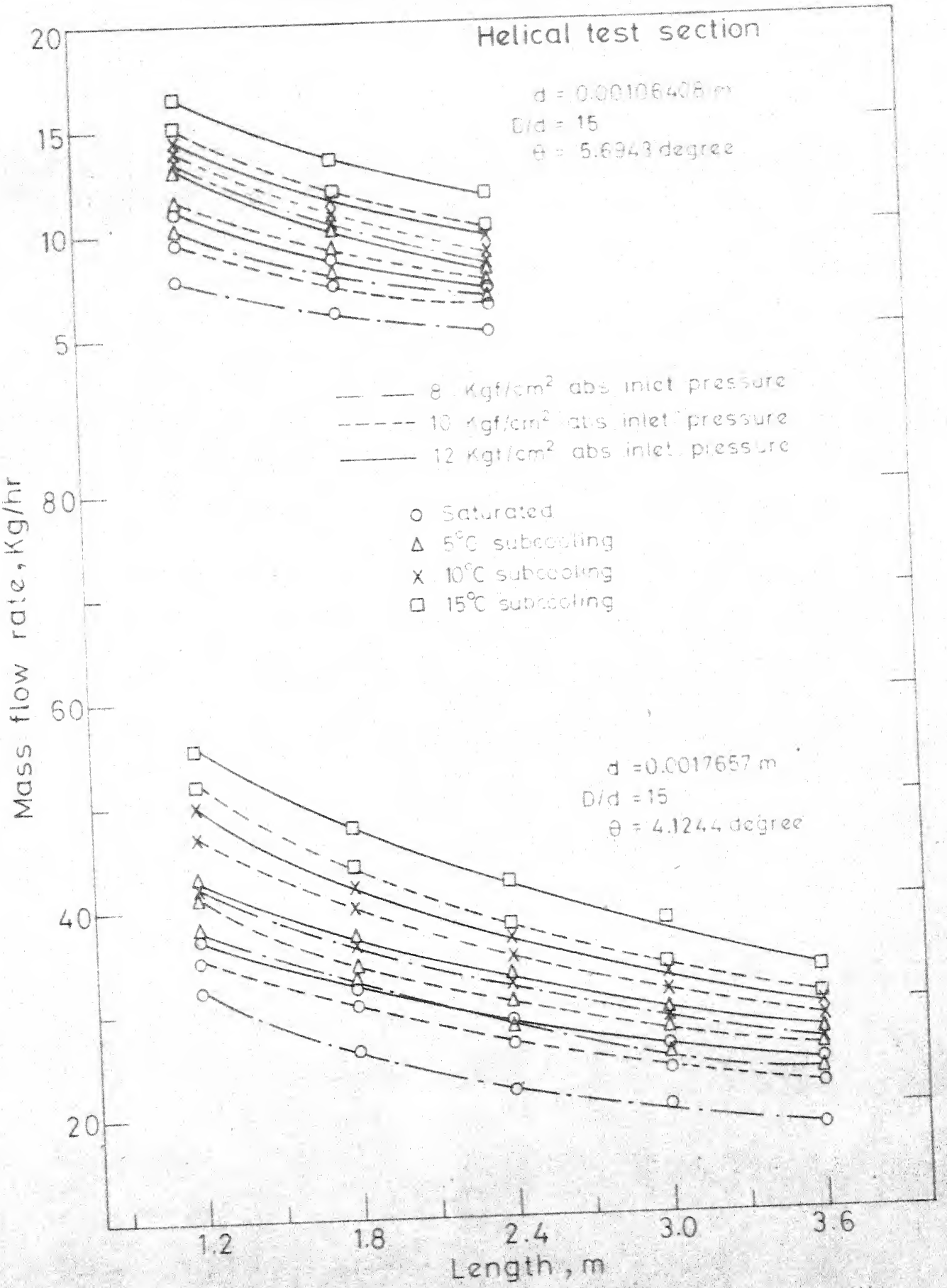

Fig. 4.10(b) Mass flow rate of R-12 vs. length of capillary tube for different inlet conditions and diameters

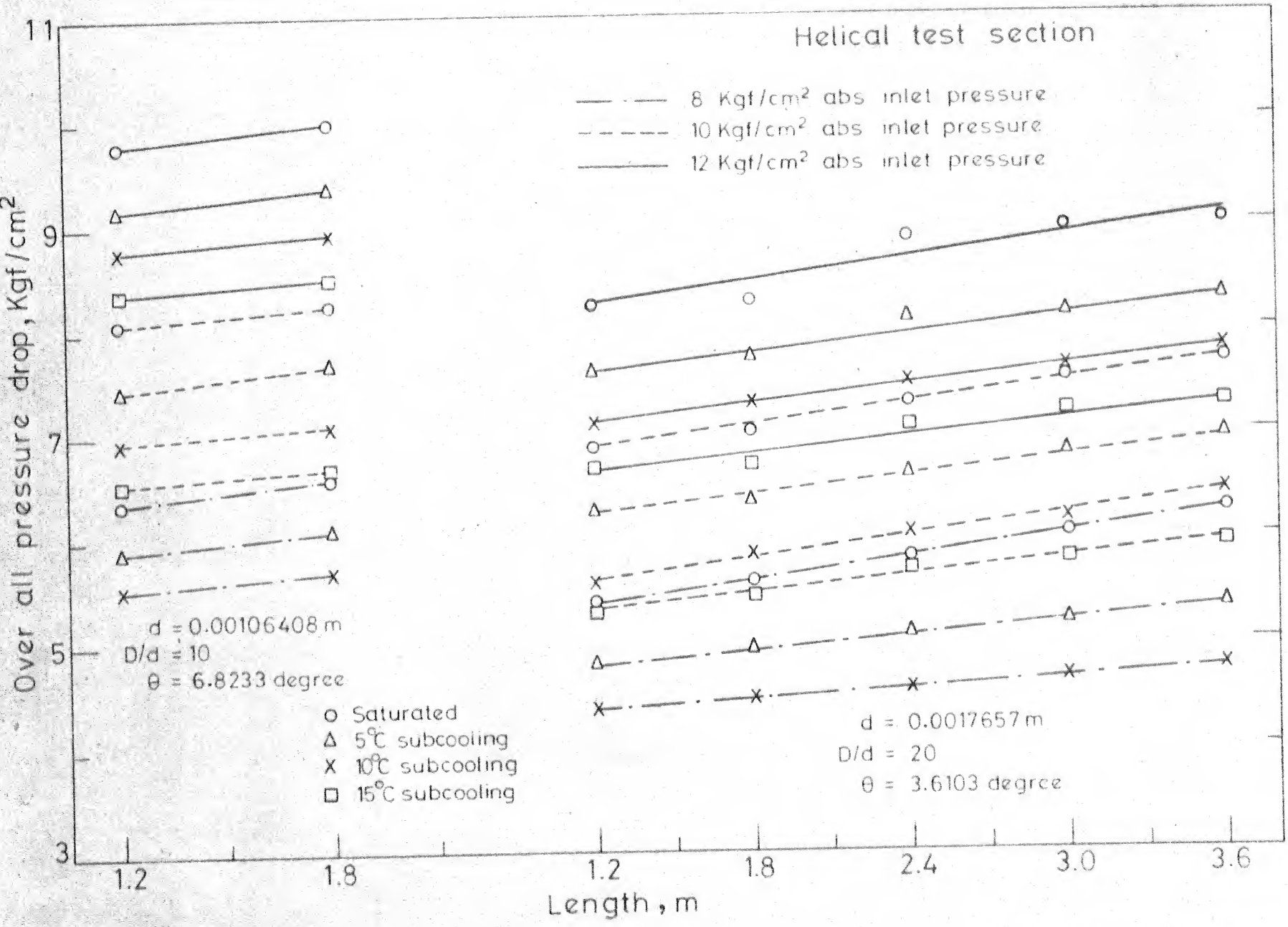

Fig. 4.11(a) Overall pressure drop vs. length of capillary tube for different inlet conditions and diameters

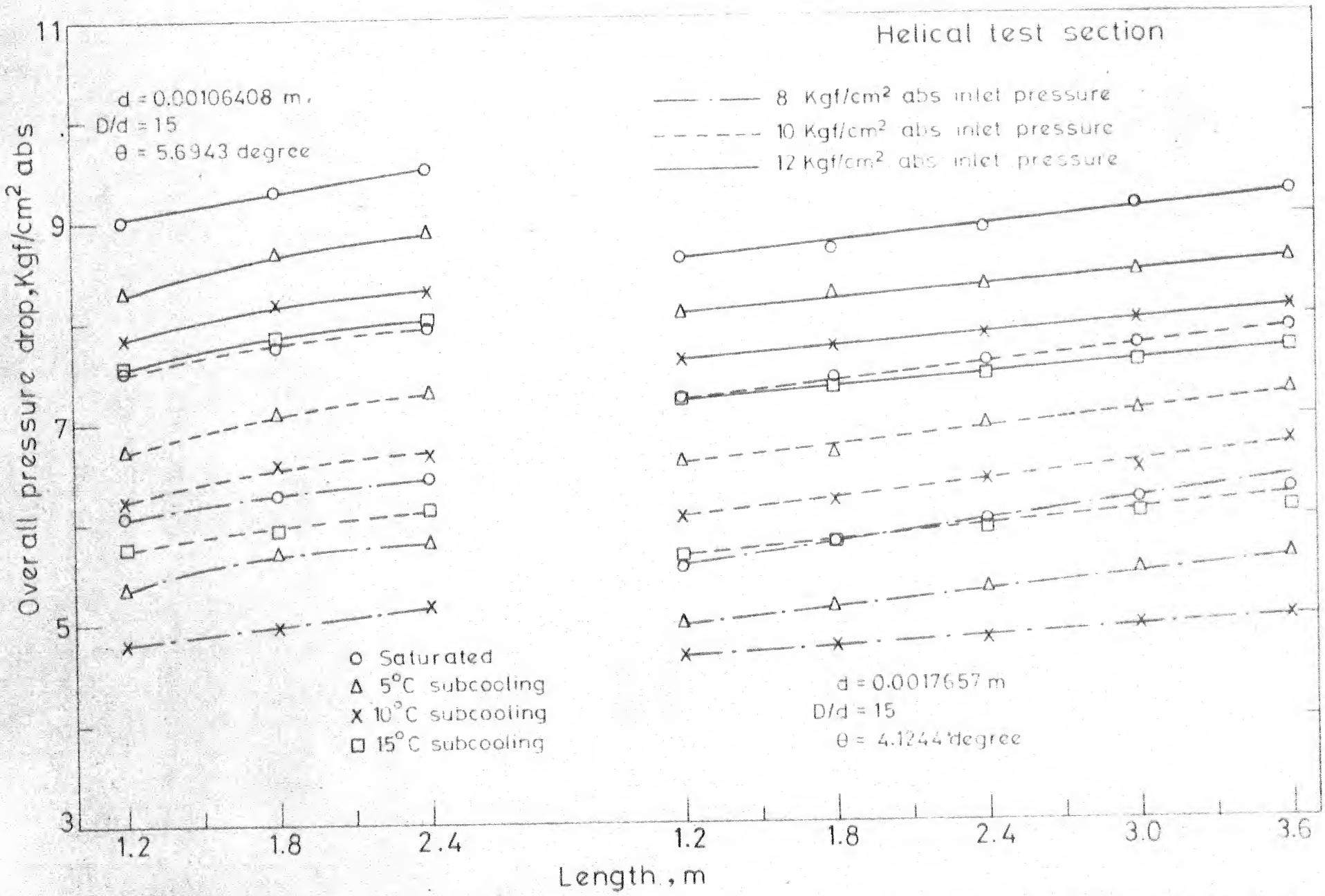

Fig. 4.11(b) Overall pressure drop vs. length of capillary tube for different inlet conditions and diameters

secondary flows tend to increase the resistance to the flow, thereby, resulting in higher pressure drops, and reduced flow rates and exit pressures.

(iii) the exit pressure and the flow rate also decrease gradually with a decrease in D/d ratio, as obvious from figures 4.9 (a), 4.9 (b) and 4.9 (c), 4.9 (d). As D/d ratio decreases, the curvature effect increases which further enhances the resistance to the flow; thereby, resulting in further decrease in the exit pressure and the flow rate.

In figures 4.10 (a) and (b), the refrigerant mass flow rate is plotted against the capillary length for different inlet conditions, capillary tube diameters and D/d ratios. As for the straight section, the flow rate decreases with increasing capillary length.

Figures 4.11 (a) and (b) present the variation of overall pressure-drop with the capillary length, for different inlet conditions, diameters and D/d ratios. The overall pressure-drop is seen to increase with the capillary tube length, because of the increased resistance to flow. Comparing the above figures with the corresponding figure for the straight section (Fig. 4.4), it is noticed that the overall pressure-drop is relatively higher for the helical configurations, due to the secondary flow effects introduced by the curvature.

Figures 4.10 and 4.11 present data in the form of charts which can be conveniently used to determine the helical capillary tube size for known overall pressure drop and refrigerant inlet conditions in the design of a cooling unit. This is discussed in detail, in Appendix - D, where it can be seen that for identical capillary tube diameters and lengths, the tonnage, coefficient of performance and the power input turn out to be less in the case of helical configuration as compared to the straight section by approximately 17%, 6.5% and 11.5%, respectively. If, on the other hand, comparison between the helical and straight sections is based on identical operating pressure limits and tube diameters for a D/d ratio of 15 for the helical configuration, it is found that about 28% saving in capillary length and 2% increase in the tonnage is achieved.

The above results clearly reveal that a capillary tube expansion device should not be used in the helical form without appropriate design considerations as, is the normal practice with the manufacturers of refrigerating devices. It has been shown above that such a practice results in the reduction of the coefficient of performance of the device. On the other hand, if the system using a helical capillary expansion device is properly designed, it can save a considerable length of the capillary tube and simultaneously increase the COP of the system.

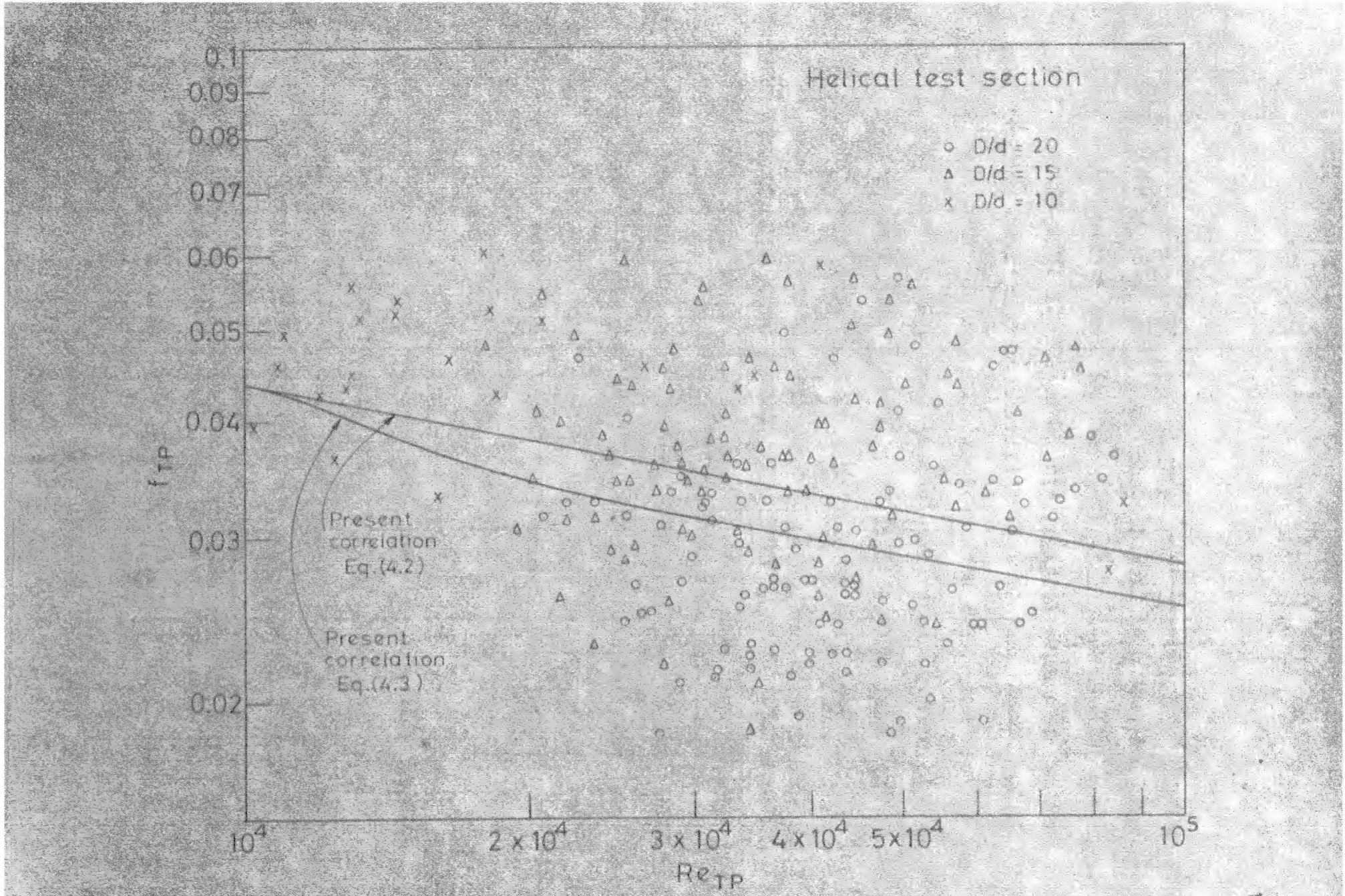

Fig.4.12 Friction factor vs. Reynolds number for different sized capillary tubes

The local values of the two phase friction factor, f_{TP} and the two phase Reynold's number Re_{TP} have also been determined for the helical case and are presented in Fig. 4.12. As expected, the local values of f_{TP} are relatively higher for helical configuration than for the straight, at a particular Reynold's number. It is further observed that these local values are more scattered than for the straight section. This is thought to be the effect of the secondary flows generated by the curvature of the helical section, superimposed on the random character of the two-phase flow phenomenon.

In Chapter III an expression of the form (3.29) has been assumed to develop a correlation for the two-phase flow friction factor. Using the present data for the helical configuration and employing the regression technique, the constants A', B' &C' are evaluated to give

$$f_{TP} = 1.1258 / (Re_{TP}^{0.1938} (D/d)^{0.5391}). \qquad (4.2)$$

Mori and Nakayama have also developed a single phase friction factor relation (3.27) in terms of single phase Reynolds number. The same has been modified in the present study by replacing the single phase Reynolds number by the two phase Reynolds number Re_{TP} and changing the constants 0.3 and 0.112 so as to furnish results conforming to the present data. The modified relation

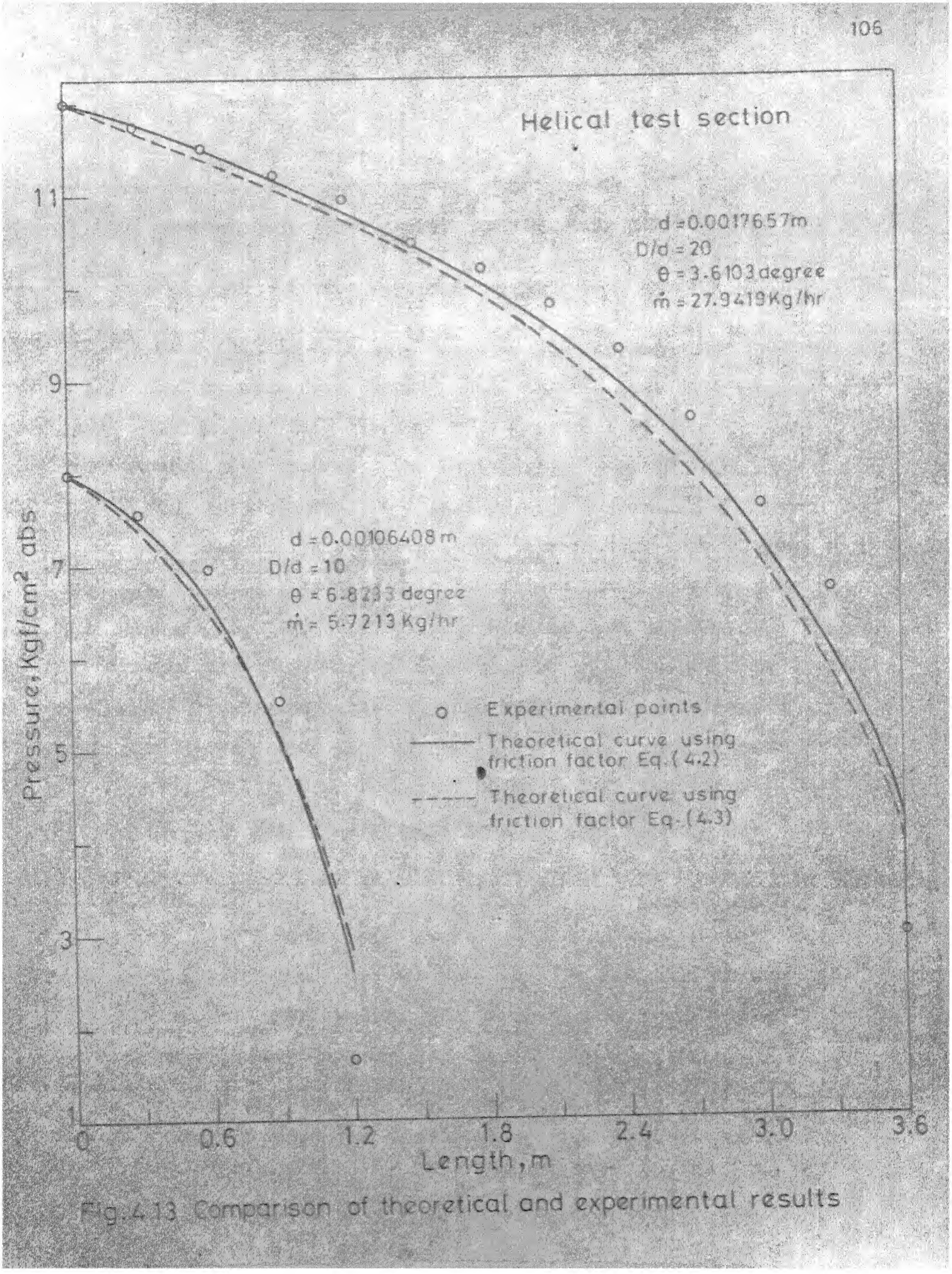

Fig. 4.13 Comparison of theoretical and experimental results

for f_{TP}, thus becomes:

$$f_{TP} = (0.3142\ (d/D)^{0.5} / (Re_{TP}\ (d/D)^{2})^{0.2}) * (1.0 + 0.1158 / (Re_{TP}\ (d/D)^{2})^{0.2}) \qquad (4.3)$$

The expressions (4.2) and (4.3), for the two-phase friction factor, are substituted in the general equation (3.16) for (dp/dl) to yield two sets of theoretical results for pressure variation with the capillary length. Both are plotted and compared with the experimental data for two different sizes of helical sections. The agreement, as seen from Fig. (4.13), is good. It is noticed that the expression (4.3) for f_{TP}, obtained by modifying Mori & Nakayama's expression (3.27) yields results which are more or less identical with those obtained by the simpler expression (4.2) developed in this study. Hence, the use of expression (4.2) for the estimation of helical section two-phase friction factor is recommended.

4.3 Spiral Section

Eight spiral test sections of different capillary sizes were tested at varying inlet conditions as given in Table 1.1. The parameters that are varied during these tests are the same as for the straight test sections. Pitch and minimum radius are kept constant while the outer radius which is dependent on the capillary

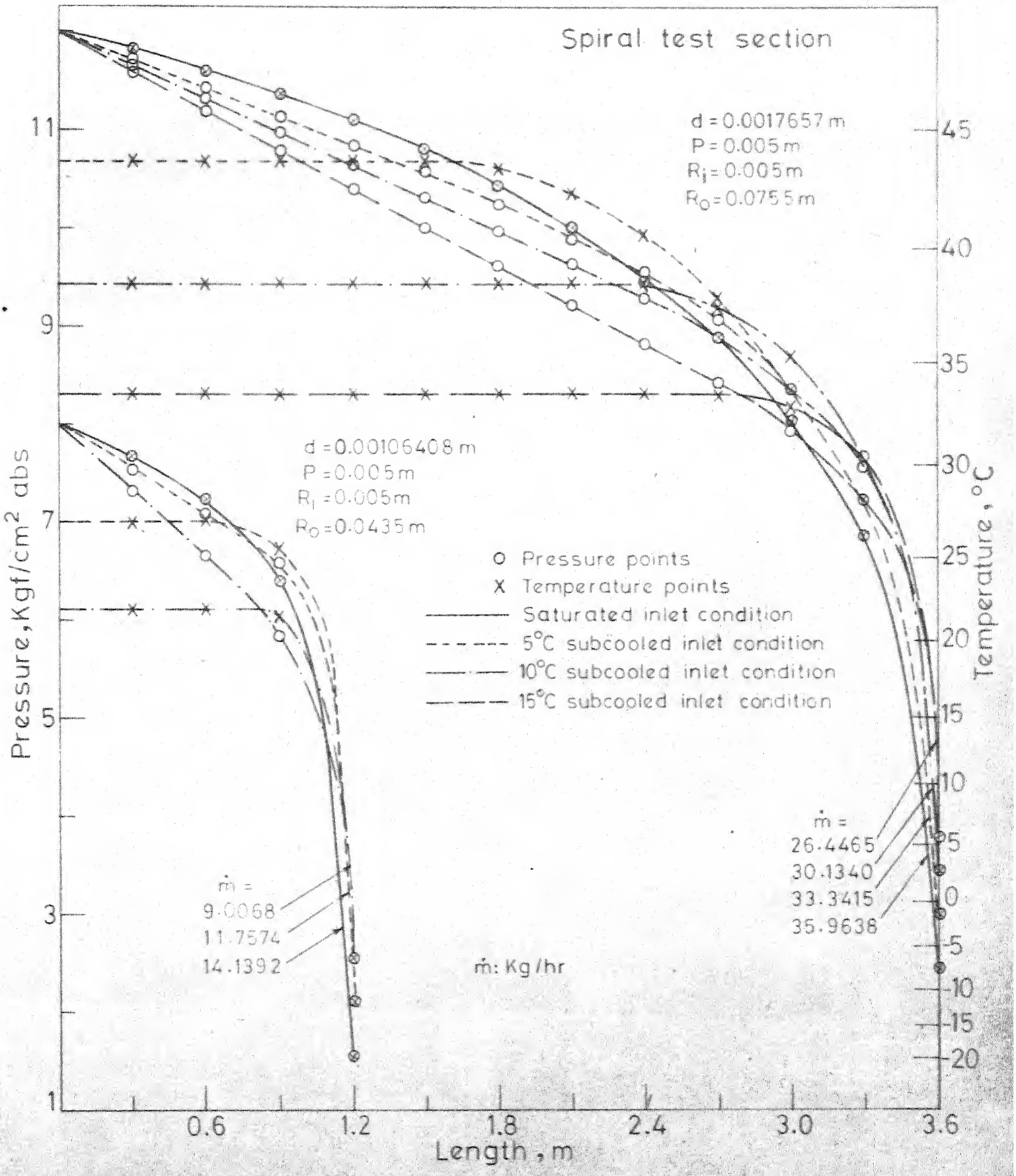

Fig. 4.14 Pressure-temperature variation with capillary length for different inlet temperature at a particular inlet pressure

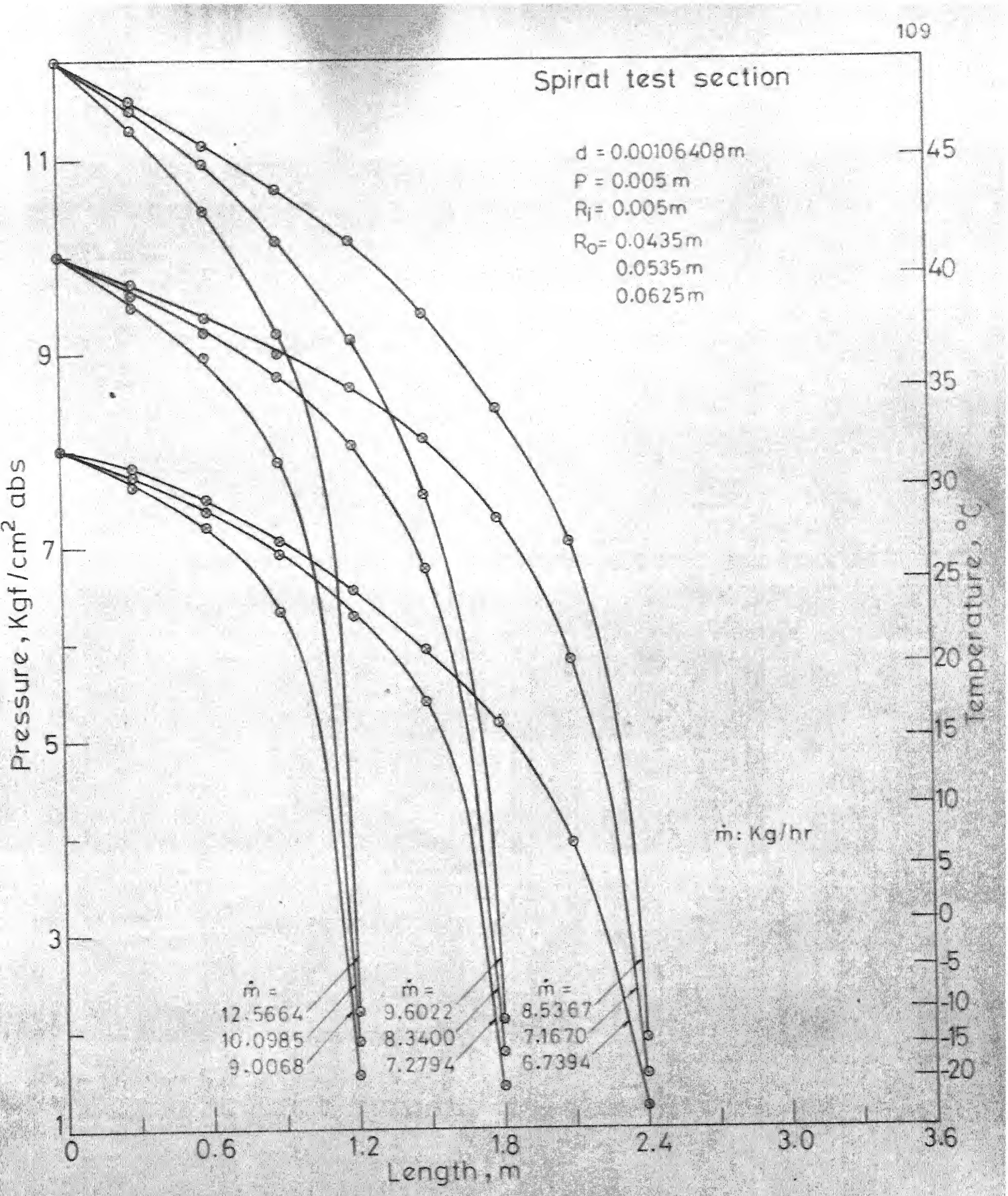

Fig. 4.15(a) Pressure and temperature vs. capillary length for saturated liquid at different inlet pressures

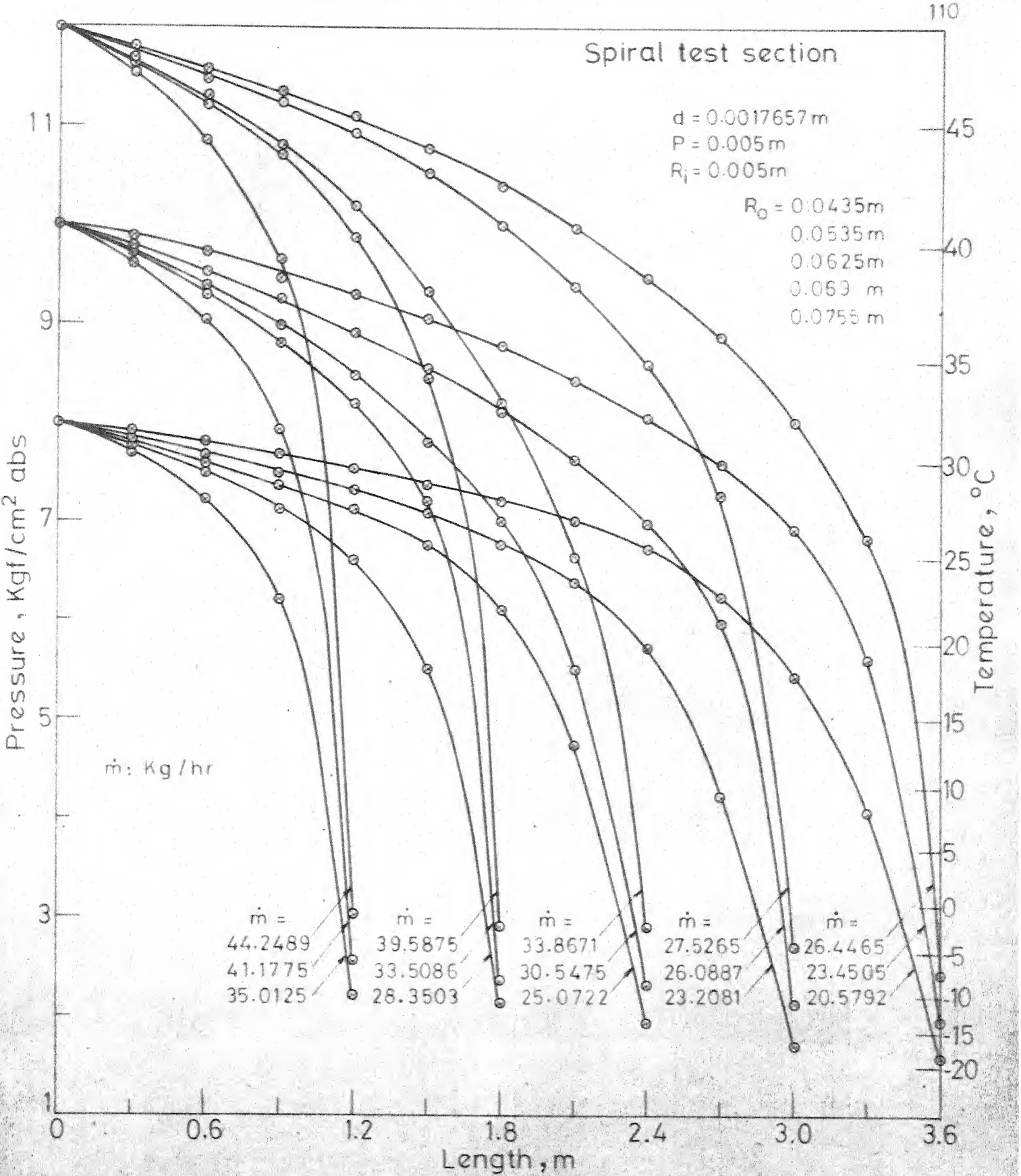

Fig 4.15(b) Pressure and temperature vs. capillary length for saturated liquid at different inlet pressures

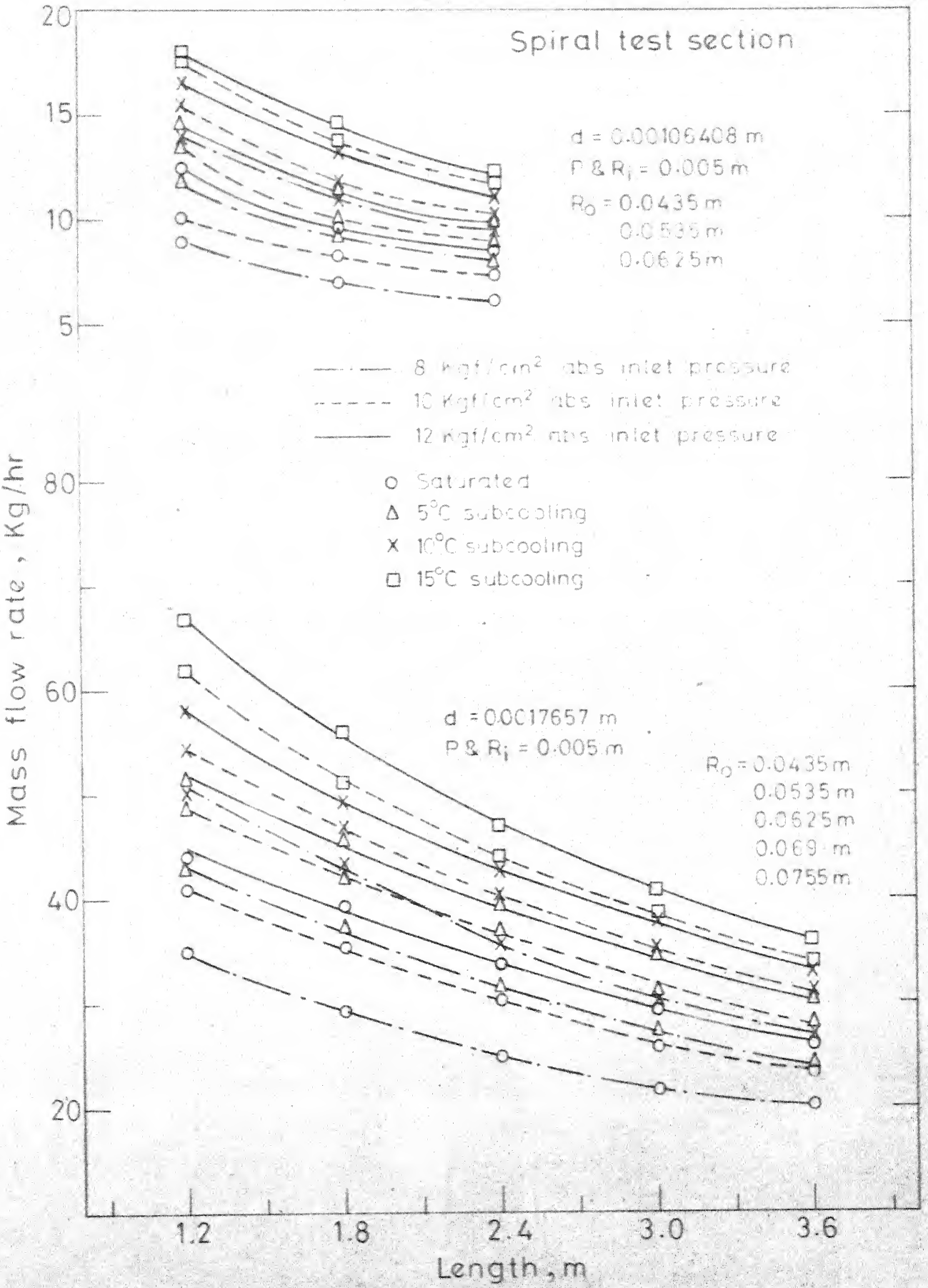

Fig.4.16 Mass flow rate of R-12 vs. length of capillary tube for different inlet conditions and diameters

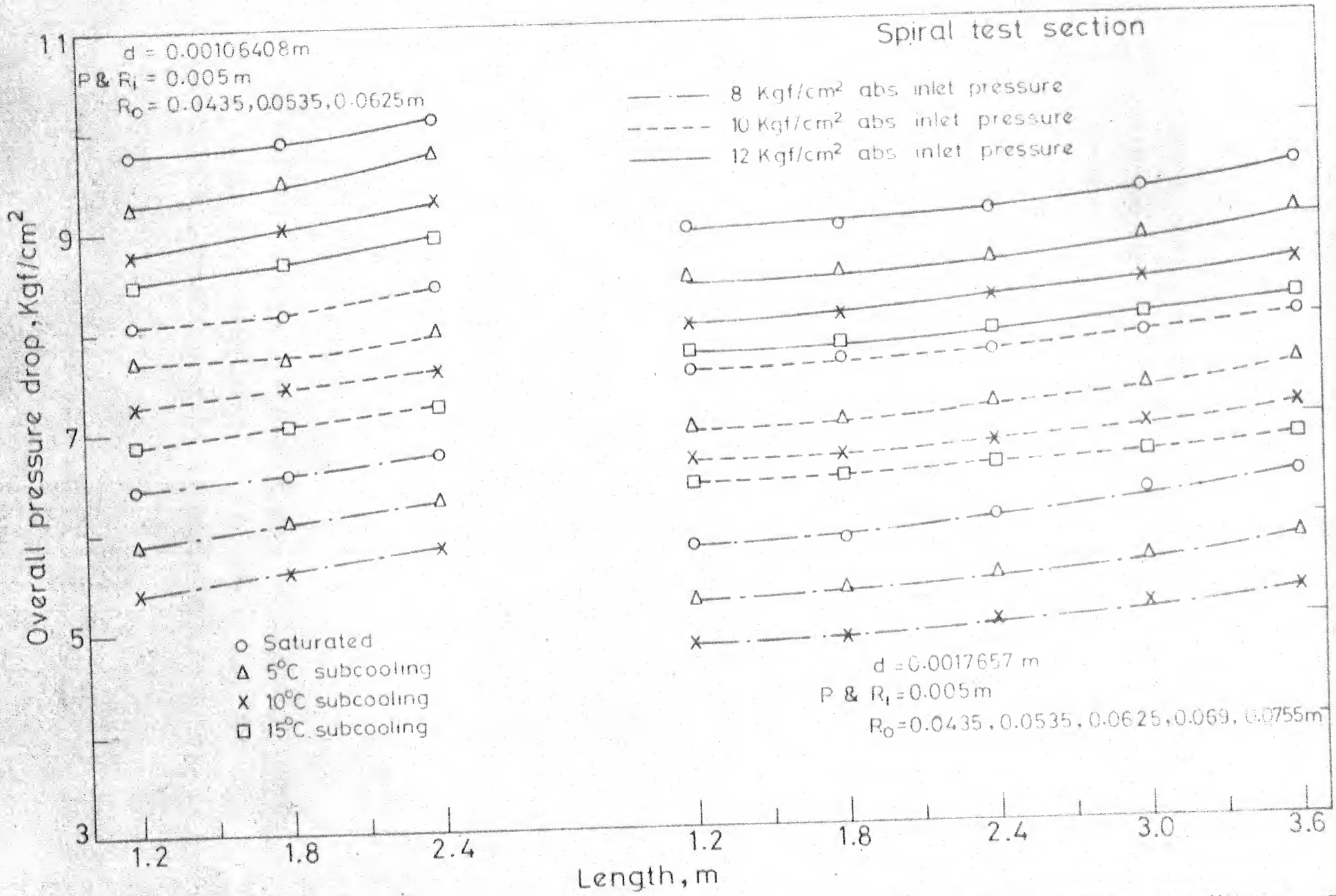

Fig. 4.17 Overall pressure drop vs. length of capillary for different inlet conditions and diameters

length is changed. All the test data gathered on the spiral sections are analysed and plotted in the same manner as for the straight and the helical configurations. Only the few representative plots are presented here for discussion.

Figures 4.14, 4.15(a) and (b), 4.16 and 4.17 for the spiral sections exhibit trends similar to those of figures 4.1, 4.2 (a) and (b), 4.3 and 4.4 for the straight and figures 4.8, 4.9 (a) and (b), 4.10 & 4.11 for the helical sections, respectively. The interpretation of these plots is the same as for the straight and the helical sections discussed previously. However, one noticeable exception to the above similarities between the curves, is as follows:

The exit pressures for the spiral sections are lower than those for the helical sections, thereby, causing higher pressure drops, while the flow rates for the spiral sections are higher than those for helical sections. This is caused by the fact that the curvature for the spiral section gradually decreases radially outwards. Since, the refrigerant flows from the periphery to the centre, it gets accelerated at each point along the spiral upto the exit point. This predominant accelerating behaviour in the spiral sections enhances the flow through the capillary and results in higher pressure drops.

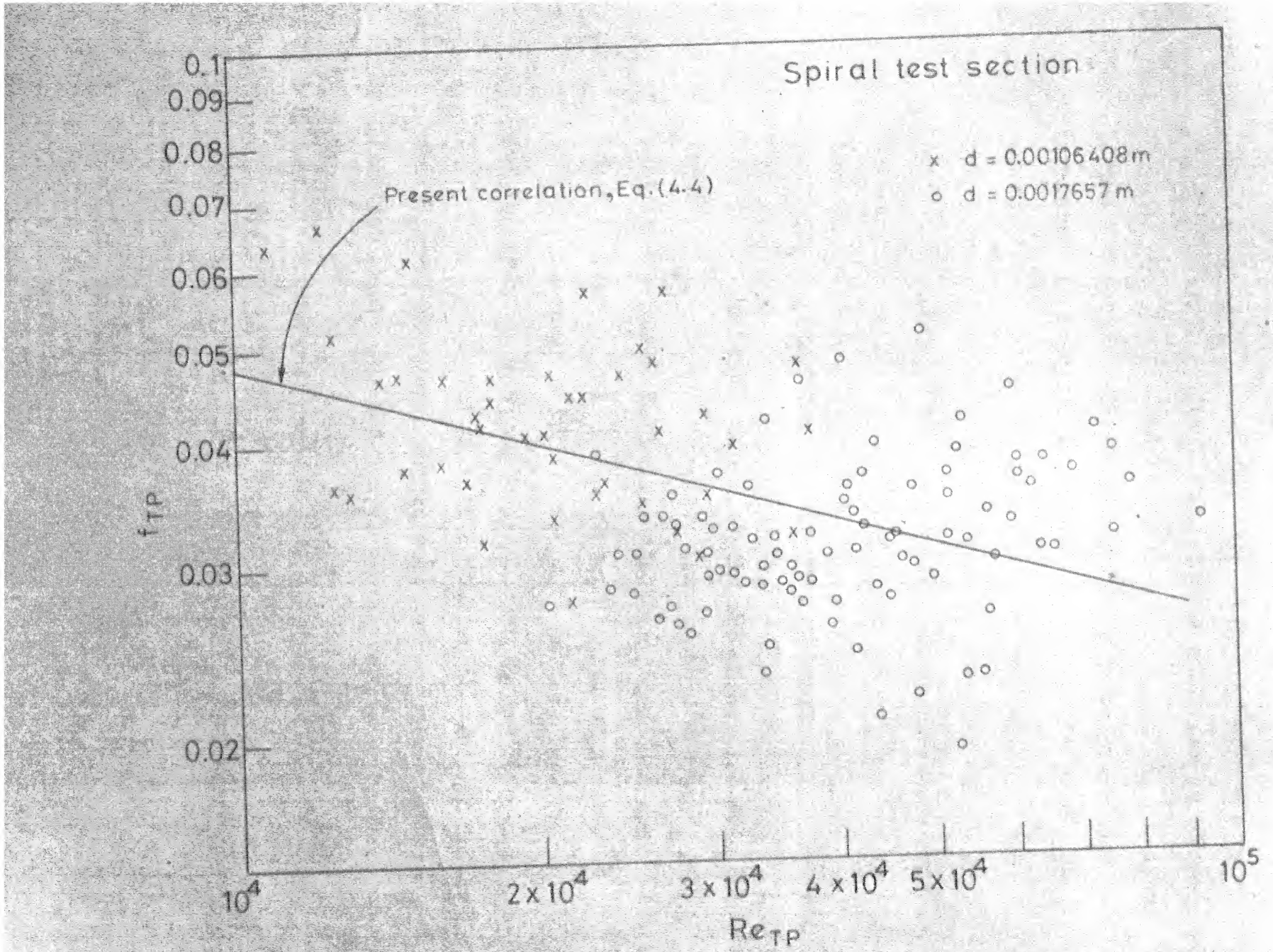

Fig. 4.18 Friction factor vs. Reynolds number for different sized capillary tubes.

Figures 4.16 and 4.17 present design data on spiral sections in the form of charts which can be conveniently used to predict the performance of spiral capillary expansion device. The method of using these charts is explained in Appendix - D through an example. The example demonstrates the merits of using a spiral capillary tube over straight and helical configurations. The design of capillary expansion tube in Archimedian spiral shape offers a saving in capillary length of about 58% as compared to the straight configuration and increase in the tonnage of approximately 48%.

The local values of the two-phase flow friction factor, f_{TP}, and the two-phase flow Reynold's number, Re_{TP}, have also been determined for the spiral case and are shown plotted in Fig. 4.18. The intensity of scattering in the data in this case is found to be less than that for the helical case. This is thought to be due to the predominant accelerating flow situation encountered in the spiral configuration. The correlation for the two-phase friction factor for the spiral configuration is represented by:

$$f_{TP} = (10.25271 / Re_{TP}^{0.24137}) * (d / (Pl)^{0.5})^{0.5132} * (R_o / (Pl)^{0.5})^{0.7539} * ((R_o - R_i) / (Pl)^{0.5})^{0.7517} \quad (4.4)$$

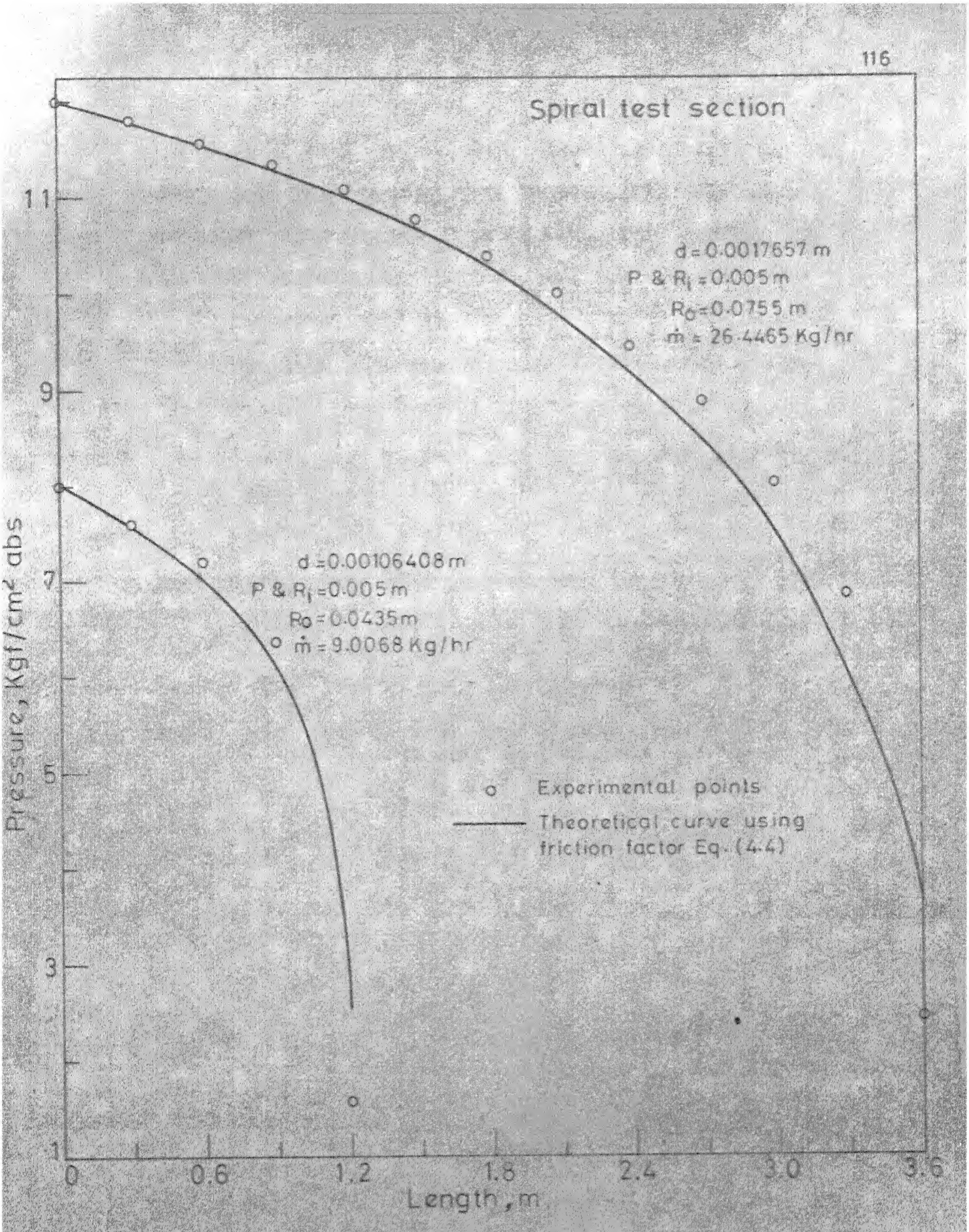

Fig. 4.19 Comparison of theoretical and experimental results

The above expression (4.4) is substituted in the Eq. (3.17) for (dp/dl) to determine the variation of pressure along the spiral shaped capillary length. The theoretical results, thus obtained, are plotted in Fig. 4.19 and compared with the data gathered from experiments on spiral sections of two different sizes. The agreement is satisfactory as shown by the figure.

CHAPTER V

CONCLUSIONS

The present work comprises both the experimental and the theoretical study of adiabatic, two-phase flow of R-12 through capillary tubes of straight, helical and Archimedian spiral configurations. Test specimens of different sizes, eight for the straight, fifteen for the helical and eight for the spiral shape, have been tested under various inlet conditions, as specified in Table 1.1 (Chapter I). The results, thus obtained, are analysed and discussed in Chapter IV. The following conclusions are drawn:

(i) For subcooled liquid inlet conditions to the capillary, the phenomenon of metastability is seen to occur invariably in all the configurations tested.

(ii) The exit pressure and the flow rate increase and the pressure drop decreases as the inlet temperature changes from saturated to subcooled conditions, for a particular sized specimen (i.e., fixed diameter and length) and a given inlet pressure. Further, it is noticed that the higher the degree of subcooling, the lower is the rise in the exit pressure.

(iii) For the same refrigerant inlet pressure and temperature conditions and for a particular diameter capillary tube, the exit pressure and the flow rate decrease, while the overall pressure drop increases with increased capillary length.

(iv) Under identical inlet conditions and for the same capillary length, the refrigerant flow rate is reduced appreciably, while the pressure drop increases for the case of the smaller diameter capillary.

(v) For a particular sized capillary, the overall pressure drop and the flow rate decrease with decreasing inlet pressures.

(vi) The overall pressure drop is seen to be the highest for the spiral configuration and higher for the helical compared to the straight configuration. However, the mass flow rate is higher for the spiral as compared to the helical and the highest for the straight sections.

(vii) Charts have been presented for each configuration which can be used conveniently for design applications. An example demonstrating the use of the charts has been included in Appendix - D. It is emphasized that capillary tube should not be shaped into either the helical or the spiral form

just for the sake of convenience to accommodate the long capillary lengths. They should, on the contrary, be suitably designed according to the given data. These precautions ensure an economic and a sound design of a refrigerating system. As shown in Appendix - D, considerable saving in capillary length is effected by using the spiral configuration as compared to the helical and the straight. It is, therefore, concluded that capillary tubes in the spiral form are most suitable and economical for systems employing capillary tube expansion devices.

The theoretical investigation carried out in the present work is summarized as follows:

(i) A theoretical equation based on the "homogeneous model" for the two phase flow has been developed to determine the capillary length for a given pressure drop, for each configuration. The equation is valid for the flow of R-12 within the temperature range - 35 °C to 50 °C.

(ii) Two-phase flow friction factor correlation has been obtained, separately, for each configuration using the present experimental data.

(iii) The results obtained by using the theoretical equation and the two-phase friction factor, appropriate to different configurations, show good

agreement with the corresponding experimental results.

The theoretical equations developed in this study for various capillary configurations and the correlations for the two-phase flow friction factors, seem to predict the experimental data reasonably, accurately and, hence, their use is recommended for the capillary restrictor design for the flow of refrigerant - 12 in the temperature range of - 35 °C to 50 °C.

SCOPE FOR FURTHER WORK

1. The present experimental investigation needs to be extended further to cover a greater range of capillary sizes and inlet conditions, appropriate to expansion devices of practical interest.
2. Combinations of different configurations may be studied, viz. straight with helical and spiral.
3. Experiments may be carried out for real non-adiabatic situations.
4. The validity of the present theoretical [redacted] be tested with the new experimental data.

REFERENCES

1. W.H. McAdams, W.K. Woods, and L.C. Heroman Jr., Vaporization Inside Horizontal Tubes - II, Benzene - Oil Mixture, Trans. ASME, 64, 193, 1942.

2. M.W. Benjamin and J.G. Miller, The Flow of a Flashing Mixture of Water and Steam Through Pipes, Trans. ASME, 64 (657 - 664), 1942.

3. George H. Clark, The When, Where, Why and How of Capillary Tube System, Refrig. Ind., February 1946.

4. L.A. Staebler, Theory and Use of a Capillary Tube for Liquid Refrigerant Control, Refrig. Eng., 55, 55, January 1948.

5. H.F. Lathrop, Application and Characteristics of Capillary Tubes, Refrig. Eng., 56, 129, August 1948.

6. Milo M. Bolstad, and Richard C. Jordon, Theory and Use of Capillary Tube Expansion Device, Refrig. Eng., 56, 519, December 1948.

7. General P. Marcy, Pressure Drop with Change of Phase in a Capillary Tube, Refrig. Eng., 57, 53, January 1949.

8. Milo M. Bolstad, and Richard C. Jordon, Theory and Use of Capillary Tube Expansion Device, Nonadiabatic Flow, Refrig. Eng., 57, 577, June, 1949.

9. Neil E. Hopkins, Rating the Restrictor Tubes, Refrig. Eng., 58, 1087, November 1950.

10. H.A. Whitesel, Capillary Two-phase Flow Part I, Refrig. Eng., 65, 42, April 1957.

11. L. Cooper, C.K. Chu, and W.R. Trusken, Simple Selection Method for Capillaries Deviced From Physical Flow Conditions, Refrig. Eng., 65, 37, July 1957.

12. H.A. Whitesel, Capillary Two-phase Flow Part II, Refrig. Eng., 65, 35, September 1957.

13. Thermodynamic Properties of R-12, General Chemical Division, New Jersy, 1958.

14. T.G. Beckwith and N. Lewis Buck, Mechanical Measurements, Addison-Wesley Publishing Company, Inc., London, 38, 1961.

15. Edward P. Mikol, Adiabatic Single and Two-phase Flow in Small Bore Tubes, University of Wisconsin, Eng. Expt. St., Reprint No. 665, 1963.

16. I.S.I. Steam Tables, Published by Indian Standards Institute, New Delhi, 1966.

17. ASHRAE Guide and Data Book (Fundamentals and Equipments), 615, 1966.

18. R.H. Niaz, and G. de Vahl Davis, Adiabatic Two-phase Flow in a Capillary Tube, M.E. Thesis, University of New South Wales, Australia, 1966.

19. Y. Mori, and W. Nakayama, Study on Forced Convective Heat Transfer in Curved Pipes (2nd Report, Turbulent Region), Int. J. Heat Mass Transfer, 10, 37, January 1967.

20. Indian Standard No. 5111, 1969.

21. Guy R. King, Modern Refrigeration Practice, McGraw-Hill Book Company, New York, 229, 1971.

22. Shaukat Ali and C.V. Seshadri, Pressure Drop in Archimedian Spiral Tubes, I & EC Process Design and Development, 10, 328, July 1971.

23. J.B. Collier, Convective Boiling and Condensation, McGraw-Hill Book Co. (U.K.) Ltd., England, 31, 1972.

24. K. Prasad, Fabrication of Compressor Test Rig, M.Tech. Thesis, I.I.T. Kanpur, India, January 1974.

25. V. Kadambi and Manohar Prasad, An Introduction to Energy Conversion, Vol. II, Wiley Eastern Private Ltd., New Delhi, 300, 1974.

APPENDIX - A

CALIBRATION OF INSTRUMENTS USED

(i) Flowmeter

Accurately measured volumes of double distilled water are poured into one of the flowmeter limbs and the gauge glass is graduated accordingly. The process is continued till it completely fills the flowmeter limb. Same procedure is repeated for the graduation of the second flowmeter limb. The graduations are marked in litres. Each limb of the flowmeter is found to have a capacity of 4.75 litres.

(ii) Pressure Gauges

The pressure gauges are calibrated using an Amthor dead weight tester and weights, standardised by the National Bureau of Standards, U.S.A. The gauges are found to be accurately calibrated as no difference in the readings of the gauge and the applied loads could be discerned.

(iii) Thermocouple

Copper-constantan thermocouples of 24 gauge have been calibrated by the comparison technique, against a Leeds and Northrup platinium resistance thermometer. The resistance - temperature relationship is provided with

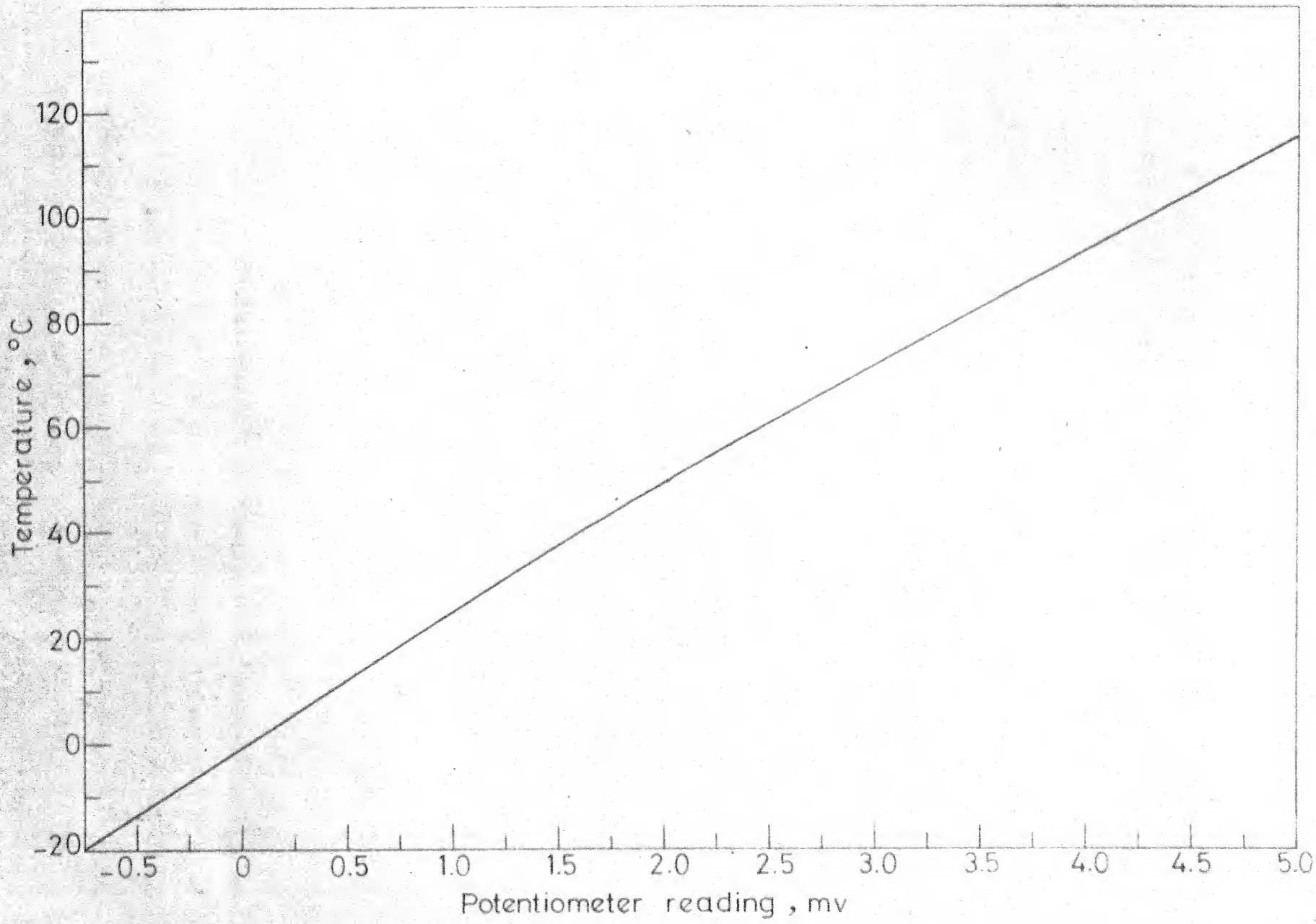

Fig. A-1 Calibration characteristic - thermocouple

the above thermometer for 0.005 °C temperature intervals in the range 0 - 300 °C. The resistance thermometer also uses a Leeds and Northrup Mueller's Bridge to measure the resistances. The e.m.f. generated in the thermocouple circuit is measured using a Leeds and Northrup millivolt potentiometer with the least count, 0.005 mv.

The calibration is carried out in an apparatus containing constant temperature vapour obtained by boiling a pure liquid, Bromobenzene, at a constant pressure under an inert atmosphere of N_2. By maintaining different pressures of N_2, vapours of Bromobenzene at various constant temperatures are obtained in the apparatus. Both the platinium-resistance thermometer and the thermocouples (four at a time) are inserted in their respective wells containing Silicon oil. The cold junction of the thermocouples is held in an ice bath. The calibration curve is given in Fig. A-1.

(iv) Calorimeter

The Calorimeter has been calibrated, as per Indian Standards Institute Specifications (20), as follows: The calorimeter is filled with R-12 upto the operating level and is then heavily insulated. The outlet and the inlet valves of the calorimeter are closed. The heater rods in the calorimeter are energized to maintain the refrigerant temperature at approximately 14 °C

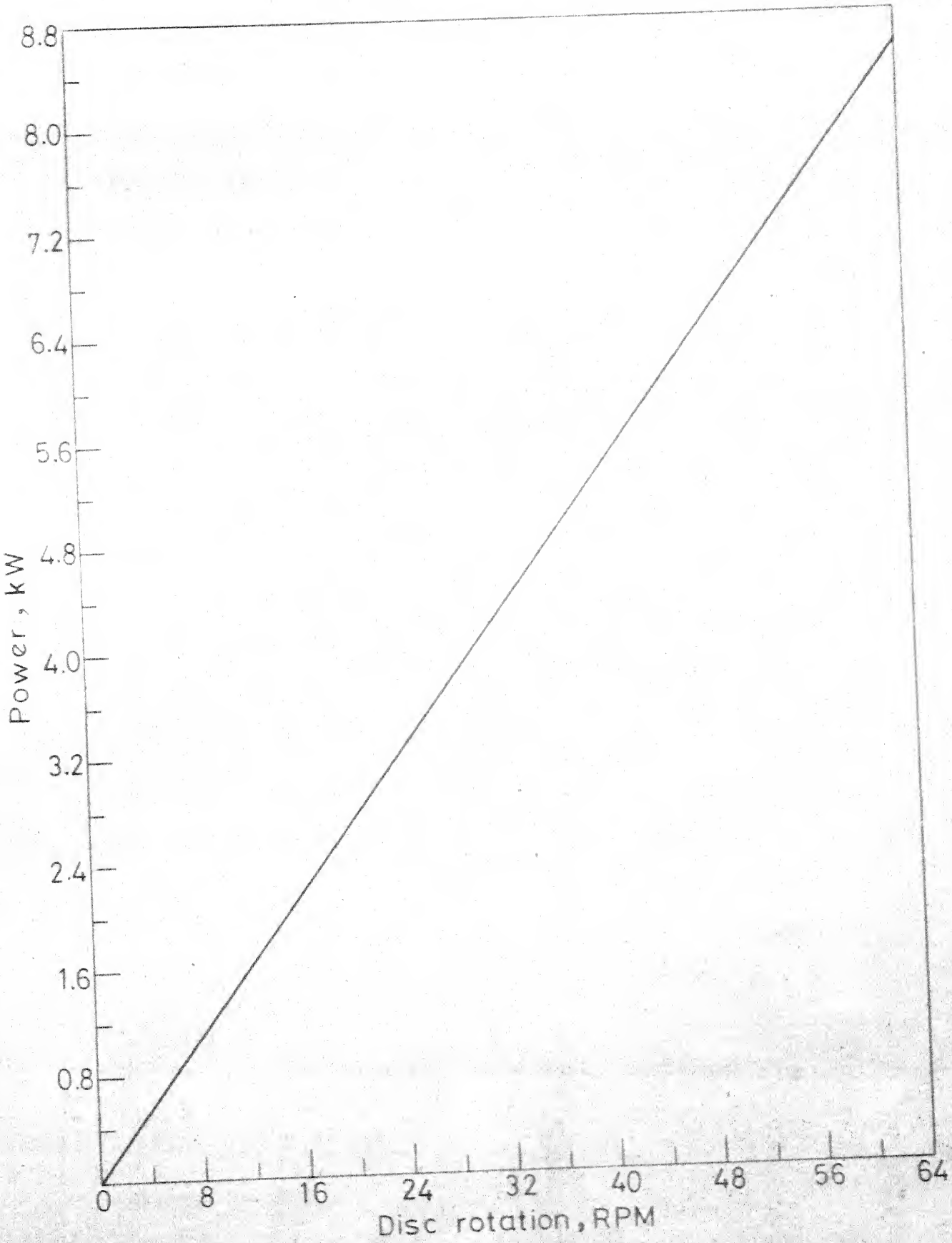

Fig. A-2 Calibration characteristic - single phase energy-meter

above the ambient. Steady-state is considered to have been attained when there is only 0.4 ^{o}C variation in the temperature in one hour. The electrical energy input is maintained constant to within 1 %. The heat leakage factor (HLF) is given by:

$$HLF = Q / (t_l - t_a), \text{ kcal / min } ^{o}C$$

where,

Q = heat equivalent of the electrical energy input, kcal / min.

t_l = liquid refrigerant temperature, ^{o}C.

t_a = ambient temperature, ^{o}C.

The HLF computed from the above relation comes out to be 0.45 kcal / min.

(v) Single-phase Energy-meter

The single-phase energy-meter is calibrated under a load with power factor nearly unity. The power factor is raised to near unity by inserting a capacitor of the required range in the circuit. An accurate voltmeter and an ammeter are employed to measure voltage and current respectively. The load is varied to get several readings. The calibration curve for the same is exhibited in Fig. A-2.

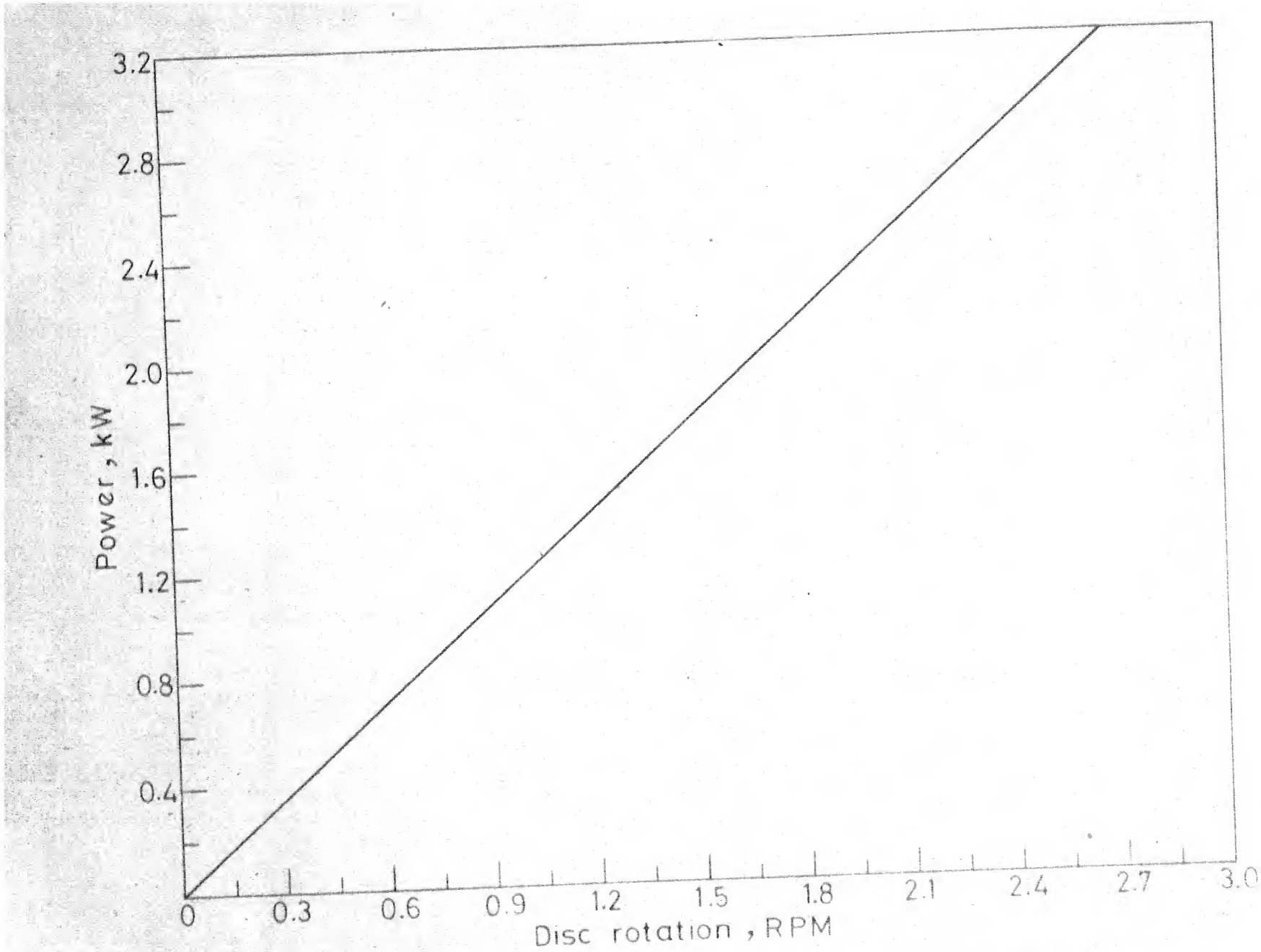

Fig. A-3 Calibration characteristic - three phase energy-meter

(vi) Three-phase Energy-meter

The three-phase energy-meter is also calibrated under a load, with power factor nearly unity. As before, a voltmeter and an ammeter are used.to indicate the voltage and the current readings respectively. The meter is tested similarly under a series of loads. The calibration curve is shown in Fig. A-3.

APPENDIX - B

DETERMINATION OF THE DIAMETER OF THE CAPILLARY TUBE

The Capillary tube bore is cleaned, first by tap water and then by double distilled water. The tube is, next, dried by passing hot air through it. The tube after drying is weighed in a chemical balance manufactured by the Scientific Products, U.S.A., with a least count of 0.1 gm. The length of the tube is measured by means of an accurate meter scale. The tube is then filled with double distilled water. Care is taken to remove all air bubbles from the tube. With water inside the capillary, both the ends of the tube are pressed and sealed. The weight of the tube with water inside is taken. The difference between the above two observations corresponds to the weight of the water required to fill the capillary tube. Next, the temperature of the water is measured and its density obtained from steam tables (16). Volume of the tube is given by, $v = w / \rho$. The diameter is found using the relation,

$$d = (4v / \pi l)^{0.5} ,$$

where,

w = weight of water, kg

ρ = density of water, kg/m^3

v = volume of tube, m^3/kg

l = length of tube, m

d = diameter of tube, m.

Diameters of the two different sized tubes used in this investigation are thus found to be 0.00106408 m and 0.0017657 m. These values are the average of three independent sets of readings taken for each size of the capillary tubing.

APPENDIX - C

ERROR ANALYSIS AND ESTIMATION

No measurement is ever free from error. Neither the value of the quantity being measured nor the error associated with the measurement can be determined exactly. Nevertheless, an error analysis must accompany an experiment so as to give an idea of the reliability of the results obtained and also to point out avenues for the improvement of the accuracy of the data. The errors estimated in this appendix are the extremum values and the actual errors lie in between the extrema.

(i) Length

The length of the test section is measured using an accurate meter scale graduated in mm. The random error in this measurement lies in the range,

$$\pm \left(\frac{1.0}{1200} * 100 * 2 \right) = \pm 0.16\ \% \ .$$

(ii) Diameter

The procedure adopted for determining the diameter of a capillary bore has already been presented in Appendix - B.

Errors involved in taking the weight of the capillary using a balance of 0.1 gm accuracy is

$$\pm \left(\frac{0.1}{20} * 100 \right) = \pm 0.5\% .$$

The temperature of distilled water is measured with the help of a mercury-in-glass thermometer graduated in 0.1 ^{o}F. The error introduced during this measurement is $\pm \left(\frac{0.1}{65} * 100 \right) = \pm 0.15\%$. This variation of temperature has negligible effect on the density of water. Assuming that there is no error in the values of density presented in the steam tables (16), the error involved in determining the diameter of the capillary tube is of the order,

$$\frac{\Delta d}{d} = 0.5 \left(\pm \frac{\Delta W}{W} \pm \frac{\Delta \rho}{\rho} \pm \frac{\Delta l}{l} \right)$$

$$= 0.5 \left(\pm 0.15\% \pm 0\% \pm 0.16\% \right)$$

$$= \pm 0.16\%.$$

(iii) Helical Section

(a) Diameter of Curvature: The error involved in making the pattern on a lathe machine of accuracy 0.1 mm is $\left(\pm \frac{0.1}{10} * 100 \right) = \pm 1.0\%$. The external diameter of the tube is measured using a micrometer with a least count of 0.01 mm. This involves an error of $\left(\pm \frac{0.01}{3} * 100 \right)$ $= \pm 0.33\%$.

Thus the maximum error introduced in the measurement of curvature would be of the order $(\pm 1.0\% \pm 0.33\%) = \pm 1.33\%$.

(b) Pitch of the Helix: The pitch is measured using a vernier with a least count of 0.05 mm. Thus, the maximum error possible is $(\pm \frac{0.05}{4} * 100) = \pm 1.25\%$.

(c) Helix Angle: This is given by

$$\theta = p / ((\pi D)^2 + p^2)^{0.5} \simeq p / \pi D$$

Therefore, the error can be

$$\frac{\Delta\theta}{\theta} = \pm \frac{\Delta p}{p} \pm \frac{\Delta D}{D} = \pm 1.25\ \% \pm 1.33\ \%$$

$$= \pm 2.58\ \%.$$

(iv) Spiral Section

(a) Pitch of the Spiral: Since the groove for the Archimedian spiral has been cut on a lathe machine having an accuracy of 0.1 mm, the maximum error introduced in the pitch would be $(\pm \frac{0.1}{5} * 100) = \pm 2\%$.

(b) Radius of Curvature: The minimum radius of the spiral is set on a lathe machine, giving an error of $(\pm \frac{0.1}{5} * 100) = \pm 2\%$ and the maximum radius is measured with the help of a vernier with a least count of 0.05 mm. The maximum error thus expected turns out to be,

$$(\pm \frac{0.05}{43.5} * 100) = \pm 0.11\ \%.$$

(v) Pressure Measurement

While discussing the calibration of pressure gauges, it has already been pointed out that there is

no systematic error associated with these gauges. The high pressure gauge having a least count of 0.5 psi, can introduce an error of $(\pm \frac{0.25}{100} * 100) = \pm 0.25\%$. The low pressure gauge has a least count of 0.1 psi. Only a few readings below 10 psi have been recorded using this gauge. The errors involved in pressure measurements are as follows:

No. of readings	% error
14	1 to 2%
119	0.4 to 1%
2686	< 0.4%

The error associated with the height of Hg, in the barometer is $\pm (\frac{0.05}{733} * 100) = \pm 0.0068\%$, which is quite negligible.

(vi) Temperature Measurement

The thermocouples have been calibrated, against platinum resistance thermometer, to 0.005 ^{o}C accuracy. The same millivolt potentiometer, least count 0.005 mv, has been used for both the calibration and the measurement purposes. The maximum error involved is estimated to be $\pm (\frac{0.0025}{0.1} * 100) = \pm 0.25\%$.

(vii) Measurement of Flow Rate

Assuming a negligible error in recording the time of fall of refrigerant using a stop watch, the error

associated with the measurement of volume flow is $\pm \left(\frac{1}{250} * 100 \right) = \pm 0.40\%$. As mentioned before, the error expected in the measurement of temperature is $\pm$ 0.25%. This error has a negligible effect on the density of a liquid refrigerant as obtained from the refrigerant table (13). However, the values of density reported in this table are accurate to within $\pm$ 0.15%. Therefore, the minimum error involved in computing the mass flow rate of a refrigerant is $(\pm 0.4\% \pm 0.15\%) = \pm 0.55\%$.

(viii) Quality

The expression of Whitesel (10) has been used to estimate quality, locally. This expression gives results within an accuracy of $\pm$ 1.0% (18).

(ix) Specific Volume

The values of v_g, v_f and p for R-12 reported by the General Chemical Division (13) have an accuracy of $\pm$ 0.2%, $\pm$ 0.15% and $\pm$ 0.2%, respectively. Taking account of the error involved in the above reported data and the curve-fit errors, the effective errors involved in v_g and v_f as evaluated from Eqs. (3.9) and (3.10) are

$$v_g = (\pm 0.2\% \pm 1.5521\% \pm 0.2\%) = \pm 1.9521\%$$

and $$v_f = (\pm 0.15\% \pm 0.2797\% \pm 0.2\%) = \pm 0.6297\%$$

Considering the error involved in the estimation of quality, x, the overall error introduced in v

according to Eq. (3.11) is

$$(\pm 1.9521\% \pm 1.0\%) = \pm 2.9521\%.$$

(x) Viscosity

The values of viscosities, μ_l and μ_g and the pressure, p for R-12, reported by the General Chemical Division (13) have accuracies of $\pm$ 0.3%, $\pm$ 0.5% and $\pm$ 0.2%, respectively. The curve fit expressions of Eqs. (3.20) and (3.21) have errors of $\pm$ 0.4064% and $\pm$ 0.8556% respectively. Therefore, the maximum effective errors involved in μ_l and μ_g are:

$$\mu_l = (\pm 0.3\% \pm 0.2\% \pm 0.4064\%) = \pm 0.9064\%$$

and $$\mu_g = (\pm 0.5\% \pm 0.2\% \pm 0.8556\%) = \pm 1.5556\%.$$

Estimated through Eq. (3.24), the maximum error in the two-phase flow viscosity comes out to be

$$(\pm 1.0\% \pm 1.5556\%) = \pm 2.5556\%.$$

(xi) Reynolds Number:

The error in mass velocity, G, is given by,

$$\frac{\Delta G}{G} = \pm \frac{\Delta \dot{m}}{\dot{m}} \pm 2 * \frac{\Delta A}{A}$$

$$= \pm 0.55\% \pm 2 * 0.16\%$$

$$= \pm 0.87\%.$$

Therefore, error in Re_{TP} , is

$$\frac{\Delta Re_{TP}}{Re_{TP}} = \pm \frac{\Delta G}{G} \pm \frac{\Delta d}{d} \pm \frac{\Delta \mu_{TP}}{\mu_{TP}}$$

$$= \pm 0.87\% \pm 0.16\% \pm 2.5556\%$$

$$= \pm 3.4856\%$$

(xii) Pressure Drop

The maximum error expected in pressure drop (dp / dl), is computed as,

$$\frac{\Delta(dp / dl)}{dp / dl} = \pm \frac{\Delta p}{p} \pm \frac{\Delta l}{l}$$

$$= \pm 0.4\% \pm 0.16\% = \pm 0.56\%.$$

(xiii) Friction Factor

For simplicity, the friction factor error is estimated using the expression for single phase friction factor,

$$f = (dp / dl) (2 dg_c / G^2 v)$$

instead of expressions (3.25) and (3.28).

Therefore, the maximum error involved in friction factor is;

$$\frac{\Delta f}{f} = \pm \frac{\Delta(dp / dl)}{dp/dl} \pm \frac{\Delta d}{d} \pm 2 \frac{\Delta G}{G} \pm \frac{\Delta v}{v}$$

$$= \pm 0.56\% \pm 0.16\% \pm 2 \times 0.87\% \pm 2.9521\%$$

$$= \pm 5.4121\%.$$

APPENDIX - D

APPLICATION OF DATA TO THE DESIGN OF A REFRIGERATION SYSTEM

To demonstrate the effect of capillary tube configuration and length on the design and performance of a refrigeration system with the help of data presented in this thesis, the following example has been chosen:

Consider a refrigeration system operating between the temperature limits of 41 ^{o}C and 0 ^{o}C, representing the condenser and evaporator temperatures, respectively. Assume that the refrigerant enters the capillary tube and the compressor in subcooled and superheated conditions of 5 ^{o}C and 15 ^{o}C, respectively, and that the efficiency of the compressor is 70%.

Solution Using Straight Section Data

The following thermodynamic properties of R-12 have been used, as reported in (25).

p, kgf/cm^2 abs	t_s, ^{o}C	h_l, kcal/kg 5^{o}C sub-cooling	h_g, kcal/kg 15^{o} super-heat	s, kcal/kg ^{o}K
3.145	0.0	-	47.4575	0.1756
10.044	41.0	17.2160	-	-

Therefore, the overall pressure drop from condenser to evaporator = 10.044 - 3.145 = 6.899 kgf/cm^2. Selecting a capillary tube of diameter 0.0017657 m and using Figs. 4.3 and 4.4, the mass flow rate of the refrigerant and the length of the capillary tube are obtained as 31.5 kg/hr and 3.36 m, respectively. The enthalpy and entropy at the inlet to the compressor as found from the superheated tables for R-12 (25) are 47.4575 kcal/kg and 0.1756 kcal/kg ^{o}K, respectively. The enthalpy at the end of the isentropic compression is again obtained from the superheated tables for R-12 as 53.13 kcal/kg. Using these values, the tonnage, coefficient of performance and the power input to the system are evaluated as follows:

Tonnage = 31.5 (47.457 - 17.216) / 3000

= 0.3175 ton

COP = 0.7 (47.457 - 17.216) / (53.13 - 47.457)

= 3.7259

Power Input = 31.5 (53.13 - 47.457) 1000 / (0.7 * 860)

= 296.84 W

Solution Using Helical Section Data:

(a) Assuming the capillary tube length and diameter the same as for the straight section, considered above, the values of the tonnage, COP and power input will be determined for the helical coil of

D/d ratio 15. Using Figs. 4.10 and 4.11, the mass flow rate and the overall pressure drop are found to be 26.2 kg/hr and 7.15 kgf/cm^2, respectively. Further, taking the condenser pressure to be same as for the straight section i.e. 10.044 ata, the evaporator pressure comes out to be (10.044 - 7.150) = 2.894 ata. The enthalpy and entropy at the compressor inlet are 47.3432 kcal/kg and 0.1764 kcal/kg ^oK, respectively. Enthalpy at the end of the isentropic compression is found to be 53.3814 kcal/kg. Thus,

Tonnage = 26.2 (47.3432 - 17.216)/ 3000

= 0.2631 ton

COP = 0.7 (47.3432 - 17.216) / (53.3814 - 47.3432)

= 3.4926

Power Input = 26.2 (53.3814 - 47.343) 1000 / (0.7 * 860)

= 262.79 W

Comparing the above results with those obtained for the straight section of the same diameter and length, it is observed that the tonnage, COP and power input decrease for the helical case by 17.13%, 6.26% and 11.47% respectively.

(b) If, however, the refrigeration system is designed for the same capillary diameter and pressure limits as those for the straight section (i.e. 10.044 and 3.145 ata), with D/d ratio again assumed to be equal

to 15, the capillary tube length in the helical form will have to be determined. From Figs. 4.10 and 4.11, for the above mentioned conditions, the length of the capillary tube and the flow rate are found to be 2.4 m and 32.2 kg/hr, respectively. The enthalpy at the inlet and the outlet of the compressor, assuming isentropic compression, are the same as for the straight section (i.e. 47.457 and 53.13 kcal/kg). Hence,

$$\text{Tonnage} = 32.2\ (47.457 - 17.216) / 3000$$
$$= 0.3246 \text{ ton}$$
$$\text{COP} = 0.7\ (47.457 - 17.216) / (53.13 - 47.457)$$
$$= 3.7259$$
$$\text{Power Input} = 32.2\ (53.13 - 47.457)\ 1000 / (0.7 * 860)$$
$$= 303.436 \text{ W}$$

Comparing these values again with those of the straight section, it is seen that the length of the capillary in the helical form decreases by 28.6%, tonnage and power input increase by 2.23% while COP remains unaffected. This demonstrates the obvious advantage of using a helical configuration for the capillary expansion device as compared to the straight one.

Solution Using Spiral Section Data:

(a) Consider now the capillary tube in the spiral form having the same length and diameter as for the straight section (i.e. 3.36 m and 0.0017657 m). Let the pitch and the minimum radius of the spiral be taken as 0.005 m. Using Figs. 4.16 and 4.17, the flow rate and the pressure drop are read as 29.2 kg/hr and 7.4 kgf/cm^2, respectively. Assuming the condenser pressure to be 10.044 kgf/cm^2 abs., the suction pressure becomes (10.044 - 7.4) = 2.644 kgf/cm^2 abs. The enthalpy at the inlet and the outlet of the compressor, assuming isentropic compression, are found to be 46.848 and 53.6533 kcal/kg, respectively. Thus,

Tonnage = 29.2 (46.848 - 17.216) / 3000
= 0.2884 ton

COP = 0.7 (46.848 - 17.216) / (53.6533 - 46.848)
= 3.0480

Power Input = 29.2 (53.6533 - 46.848) 1000 / (0.7 * 860)
= 330 W

Comparing these results with those for the straight section of the same diameter and length, the tonnage and COP for the spiral section are seen to decrease by 9.16% and 13.19%, respectively, while the power input increases by 11.17%.

(b) On the other hand, the systen may be designed using spiral capillary tube of diameter 0.0017657 m, operating between the pressure limits of 10.044 and 3.145 ata, as for the straight section. The flow rate of the refrigerant and the length of the capillary tube are obtained, from Figs. 4.16 and 4.17, as 46.5 kg/hr and 1.42 m, respectively. This gives

Tonnage = 46.5 (47.457 - 17.216) / 3000

= 0.4687 ton

COP = 0.7 (47.457 - 17.216) / (53.13 - 47.457)

= 3.7259

Power Input = 46.5 (53.13 - 47.457) 1000 / (0.7 * 860)

= 438.1778 W

Comparing the results as before with those of the straight section, it is found that the capillary length in the spiral form is reduced by 57.74%, tonnage and power input increase by 47.52% and COP remains the same.